EVALUATION OF NOBLE GAS EXTRACTION METHODS FOR INTER- AND INTRAGRANULAR POREWATER IN ARGILLACEOUS ROCKS

by

Harry Barnes

uOttawa

Supervisor: Dr. Oliver Warr

A thesis submitted to the University of Ottawa in partial fulfilment of the requirements for Master of Science degree in Earth Science

Department of Earth and Environmental Sciences

Faculty of Science

University of Ottawa

EXAMINING COMMITTEE

The following served on the Examining Committee for this thesis:

Internal Examiner: Tom Al

Professor, Department of Earth and Environmental Sciences,

University of Ottawa

Richard Amos

Associate Professor, Institute for Environmental and Interdisciplinary

Sciences, Carleton University

Supervisor: Oliver Warr

Assistant Professor, Department of Earth and Environmental Sciences,

University of Ottawa

DECLARATION OF AUTHORSHIP

I hereby certify that this thesis is entirely my own original work except where otherwise indicated. I am aware of the University's regulations concerning plagiarism, including those concerning consequent disciplinary actions. Any use of the works of any other author, in any form, is properly acknowledged at their point of use.

ABSTRACT

The long-term, safe storage of nuclear waste within deep geological formations represents a critical focus of contemporary research and public interest. As nuclear energy continues to be an essential component of sustainable energy strategies – particularly within Canada – the use of noble gases as tracers of physico-chemical processes for the site characterisation of prospective Deep Geological Repositories (DGRs) is a promising yet technically challenging approach. This study develops and evaluates methodologies for extracting and quantifying isotopic noble gases from the porewater of the Opalinus Clay (OPA) formation in northwest Switzerland, a well-established analogue for argillaceous DGR settings (Bossart and Thury, 2008). The first study (Chapter 2) examines the traditional encapsulation of cores for porewater analysis within stainless-steel cylinders and evaluates three normalization techniques for estimating initial porewater concentrations from headspace noble gas measurements. A second study (Chapter 3) explores a more cost-effective encapsulation method involving core samples stored in vacuum-sealed PE/Al-foil bags, similar to Zuo et al. (2021). However, this method presented challenges due to limited degassing. Consequently, this required low-temperature baking to promote outgassing to form a headspace over a period of six weeks, although this process may have introduced isotopic fractionation associated with He, and elemental fractionation in Ne and Ar. Consequently, additional preparation, storage, and extraction refinements may be needed to realise the potential of this technique. Collectively, these findings highlight key methodological considerations in sampling and analysing argillaceous cores for noble gases, highlighting the need for further refinement towards establishing more comprehensive “best-practice” protocols.

ACKNOWLEDGEMENTS

Firstly, I would like to take this opportunity to acknowledge that the University of Ottawa is located on the traditional unceded territory of the Algonquin Anishinaabeg People.

I would like to now offer my sincerest thanks to my supervisor Dr. Oliver Warr for his ongoing support, guidance, and mentorship throughout my graduate studies here at the Department of Earth and Environmental Sciences. Without your knowledge and expertise, it is extremely unlikely that this project will have reached fruition. You have provided me with this opportunity to prove to myself that I have the drive and determination to be the first in my family to pursue an M.Sc. I am honoured to have been your first M.Sc. student, and with high hopes of being your first to graduate. I am eternally grateful for your reassurance, patience, and support throughout these previous two years.

I would also like to thank the countless others who have supported myself and this project during my time at the University of Ottawa. Namely, Anthony Lapp, for without your patience, supervision, and guidance in running my final Chapter 3 sample set under an extreme time crunch, this thesis would have been noticeably weaker. I sincerely appreciate the time you have devoted to training me within the AEL Noble Gas Laboratory over these past two years. I would also like to thank Dr. Daniele Pinti and Camila Paz Poblete Gonzalez, for providing me guidance, assistance, and in some cases, running my Chapter 2 samples at l'Université du Québec à Montréal (UQAM) last December during our downtime period at the University of Ottawa. In addition, it would be remiss of me to not thank those involved in the Mont Terri PC-D project, including our Principal Investigator (PI) Laura Kennell-Morrison, and our fellow collaborators Florian Eichinger (Hydroisotop GmbH) and Johanna Lippmann-Pipke (BGR).

Additional thanks are due to my fellow colleagues in the Warr Environmental Geochemistry Lab: Tanuj, Xuanqi, Matilda, Liam, Daisy,Zoe, and Medina – thanks to each of you for the

ongoing guidance, support, knowledge (and pints had together) throughout my time here. Your contributions to this work during our group discussions have been invaluable in shaping this thesis.

To my family and friends, I am so very thankful for the unwavering support also. To my parents and stepparents: Mam and Stephen, Dad and Emma – without each of you I would not have had the courage to make such a move to Canada and to persevere when times were tough. I am eternally grateful for all the support and encouragement throughout these two years. I would also specifically like to thank Jessica Adams, as for without our friendship I truly don't believe I would have been able to cope under the stress of putting this thesis together.

TABLE OF CONTENTS

LIST OF FIGURES

Figure 3.6b: Plot of normalized ^{22}Ne concentrations within the PE/Al-foil bag-encapsulated sample porewater with respect to their distance along the horizontal borehole. These concentrations are plotted alongside the corresponding concentrations from the stainless-steel cylinder encapsulated samples (SS).

Figure 3.7: Plot of $^{40}Ar/^{36}Ar$ values within the PE/Al-foil bag-encapsulated samples with respect to their distance along the horizontal borehole. Note the atmospheric ratio is 295.5 (Porcelli et al., 2002). These ratios are plotted alongside the corresponding ratios from the stainless-steel cylinder encapsulated samples (SS).

Figure 3.8a: Plot of normalized ^{36}Ar concentrations within the PE/Al-foil bag-encapsulated sample porewater with respect to their distance along the horizontal borehole. These concentrations are plotted alongside the corresponding concentrations from the stainless-steel cylinder encapsulated samples (SS).

Figure 3.8b: Plot of normalized ^{38}Ar concentrations within the PE/Al-foil bag-encapsulated sample porewater with respect to their distance along the horizontal borehole. These concentrations are plotted alongside the corresponding concentrations from the stainless-steel cylinder encapsulated samples (SS).

Figure 3.8c: Plot of normalized ^{40}Ar concentrations within the PE/Al-foil bag-encapsulated sample porewater with respect to their distance along the horizontal borehole. These concentrations are plotted alongside the corresponding concentrations from the stainless-steel cylinder encapsulated samples (SS).

Figure 3.9: Plot of $^{20}Ne/^{36}Ar$ values within the PE/Al-foil bag-encapsulated samples with respect to their distance along the horizontal borehole. Note the atmospheric ratio is 0.52 (Porcelli et al., 2002).

LIST OF TABLES

NOTATION

DGR: Deep Geological Repository

OPA: Opalinus Clay

LLW: Low-Level (Nuclear) Waste

ILW: Intermediate-Level (Nuclear) Waste

HLW: High-Level (Nuclear) Waste

URL: Underground Research Laboratory

ASW: Air-Saturated Water

Helix-MC: Multi-Collector Noble Gas Mass Spectrometer

SRG: Spinning Rotor Gauge

SS: Stainless-Steel

ACT: Activated Charcoal (Trap)

CHAPTER 1: INTRODUCTION

1.1 Introduction to nuclear power in Canada and globally

According to the Government of Canada's Provincial and Territorial Energy Profiles (Government of Canada, 2024), approximately 59% of the total 153 TWh energy generation of Ontario in 2019 was attributed to nuclear power. With the demand for energy ever increasing to match the growing global population, the considerable role and reliance on nuclear power represents a crucial component in Canada's ongoing decarbonization efforts with the stable and continuous energy demand ever-increasing (Crawley, 2023; Government of Canada, 2024). The continued development of nuclear energy is a controversial subject matter, particularly given the disasters at Chernobyl in 1986 and Fukushima in 2011. Gupta et al. (2019) evaluated the opinion towards nuclear power within the United States over time and identified that support often fluctuates with the timing of nuclear disasters. The disasters at Chernobyl and Fukushima were generally consistent with a decrease in public support, however when there have been variations in energy security risk – particularly when energy security has been low – public support for nuclear energy has increased.

However, a critical component of long-term dependency on nuclear power, and maintaining societal support depends on effective management and storage of the radioactive waste produced as a by-product, which remains an ongoing area of research, development and policy making in Canada and beyond (Ramana, 2013; Hall and Keech, 2017; Alwaeli and Mannheim, 2022; Drace et al., 2022; Fernández-Arias et al., 2023). In Canada, the Nuclear Waste Management Organization (NWMO) is the responsible non-profit organization dealing with the safe and effective long-term storage of nuclear waste.

1.2 Introduction to Deep Geological Repositories (DGRs)

A key challenge associated with nuclear resources lies in being able to effectively manage the generated waste. The most hazardous waste – used nuclear fuel and high-level radioactive

waste (HLW) – remains radiotoxic for well over tens of thousands of years, and often into geological timescales of up to a million years (or more), which is far beyond the lifespan of any conventionally engineered storage facility or contemporary human institution (World Nuclear Association, 2025). While spent fuel pools and dry casks have proven effective for short-term containment of nuclear waste, these methods are not considered viable for long-term safe storage over the timescales needed for the nuclear waste to decay safely (NWMO, 2024). Finding a longer-term solution is of direct and immediate importance. The Nuclear Waste Management Organisation (NWMO) has, while writing this thesis, recently concluded the site selection process for a potential nuclear waste repository, termed "Deep Geological Repository" (DGR), within Ontario. Thus, site characterisation is a critical priority. Specifically, any repository needs to be well-characterised in terms of the physico-chemical and biological processes that may occur over millions of years (or longer) to assess suitability for storing this hazardous waste. There is broad scientific agreement that a DGR, an engineered facility excavated hundreds of metres underground in a stable rock formation, offers the safest and most sustainable solution for isolating nuclear waste from the biosphere over geological timescales (Alexander et al., 2015; Apted and Ahn, 2017; Hall and Keech, 2017; NWMO, 2024; World Nuclear Association, 2025).

Unlike surface or near-surface storage, a DGR provides multiple layers of defence between the radioactive material and the environment. Engineered barriers (such as robust metal canisters and clay or cement backfill) and natural barriers (such as the host rock formation) work in unison to contain and isolate radionuclides (Apted and Ahn, 2017; Hall and Keech, 2017; NWMO, 2024). The repository should typically be located 500-800 m underground in a low-permeability, geologically stable formation, such as dense crystalline rock or clay-rich sedimentary rock. Groundwater flow should be minimal, and oxygen should be scarce, in order to reduce corrosion and radionuclide mobility (Apted and Ahn, 2017; Hall and Keech, 2017;

World Nuclear Association, 2024). These factors should significantly reduce the likelihood of radionuclides from mobilising and migrating away from the selected storage site.

The importance of DGRs extends beyond technical safety – there is an ethical and financial imperative to implement a permanent solution for nuclear waste. Specifically, until a more permanent solution is found, indefinite surface storage remains a burden on current and future generations with respect to maintenance, security, potential generation of secondary waste, and the risk of eventual containment failure. The United Nations Brundtland Commission of 1987 defined sustainability as "meeting the needs of the present without compromising the ability of future generations to meet their own needs" (World Commission on Environment and Development, 1987). Thus, if we compromise the ability of future generations to effectively and safely store nuclear waste, then the confidence that can be placed on nuclear energy as a sustainable alternative to fossil fuels is undermined.

Worldwide, significant progress has been made toward implementing DGRs for nuclear waste, although the process and progress varies by country. Finland is at the forefront, with its Onkalo repository at Olkiluoto – based on the KBS-3 engineered barrier system of copper canisters and bentonite clay (World Nuclear Association, 2024). It is hosted within a crystalline granite and received a construction license in 2015 and was planned to begin operations in 2024-25 as the world's first DGR for spent nuclear fuel, although there have been setbacks resulting in this date being delayed. Currently it is still in the trial stage (Siren, 2017; World Nuclear Association, 2024; Kraev, 2025).

Sweden has a similar KBS-3 repository planned at Forsmark, with the site selected in 2009 and after extensive safety reviews, the Swedish government approved the project in 2022. Construction is estimated to be completed by the mid-2030s, with the facility encapsulating ~12,000 tonnes of spent fuel in copper canisters 500 m underground in crystalline bedrock

(Neretnieks, 2013; Radwaste Solutions, 2024a; Johnson, 2025). Similarly, in France, the development of the Cigéo repository in a clay formation at Bure is underway, targeting operation by the 2030s for a pilot phase of disposal of vitrified high-level waste (HLW) from its reprocessing program (Nuclear Engineering International, 2025a; Dalton, 2025). Other nations are in earlier stages of this process, such as Germany which is conducting a renewed site search after abandoning a previous salt-based site, and the United Kingdom and Japan have launched siting processes focused on community consent for a DGR (World Nuclear Association, 2024). The United States has the greatest inventory of commercial spent fuel; and while it does currently operate the WIPP facility in New Mexico, one of the world's only current operating DGRs – which has entombed intermediate-level waste (ILW) from defence programmes in a deep salt formation since 1999 (World Nuclear Association, 2024), progress in finding additional prospective DGRs remains uncertain as the Yucca Mountain repository in Nevada was defunded after years of study, leaving the U.S. without a HLW repository site (Clifford, 2021). Most pertinent to this thesis, Switzerland has recently identified a preferred repository analogue in the Opalinus Clay (OPA) in the northwest, near the German border. This OPA formation is what will be examined closely within this thesis, in the context that the OPA material is a homogeneous, analogous, low-porosity, argillaceous rock type.

In Canada, the Nuclear Waste Management Organisation (NWMO) has undertaken a multi-decade, community-driven process to site a DGR for long-term containment of nuclear fuel. Beginning in 2020, an initial list of 22 interested communities across several provinces was gradually narrowed to two finalist areas, both within Ontario, by the early 2020s (Jones, 2023; Ketonen, 2024; NWMO, 2024). One candidate was in southern Ontario's Municipality of South Bruce (within Saugeen Ojibway Nation territory), underlain by Paleozoic sedimentary rock (NWMO, 2024). The other was identified in northwestern Ontario near the Township of Ignace (within Wabigoon Lake Ojibway Nation territory), underlain by ancient crystalline rock

of the Canadian Shield (Szewczyk and West, 1976). Extensive technical evaluations confirmed that both sites met the NWMO's initial screening safety criteria, including the presence of a thick, stable host rock formation at ~500-800 m depth and viable transport routes. In parallel, the NWMO engaged in years of public consultation and Indigenous outreach in each area, upholding the principle that a DGR would only proceed at a site with an informed and willing host community (municipal and Indigenous) working in partnership (NWMO, 2024; Law, 2024; Nuclear Engineering International, 2025b).

The South Bruce area lies on the southeastern flank of the Michigan Basin and is characterized by a sequence of flat-lying Palaeozoic sedimentary formations (Raven et al., 2011; Zuo et al., 2021). Geological investigations (including deep boreholes and 3D modelling) identified the Ordovician Cobourg Limestone as the proposed repository horizon, at roughly 500-700 m below ground surface. This limestone is an argillaceous carbonate rock with extremely low permeability (Raven et al., 2011; Zuo et al., 2022). Notably, the Cobourg layer in South Bruce is overlain by approximately 200 m of lower-permeability Ordovician shale, which serves as a confining layer above the repository horizon (Jensen et al., 2009). These sedimentary strata form a stable and ancient groundwater system: the porewaters are highly saline and stagnant, indicating isolation from surface water for millions of years (Jensen et al., 2009). Such geological characteristics are favourable for a DGR, as they provide multiple natural barriers for radionuclide migration.

Alternatively, the Ignace-Wabigoon area is situated on the Canadian Shield and features Precambrian crystalline basement rock. The focus of study there is the Revell Batholith – a low-porosity large biotite-granodiorite-tonaliteintrusion with a history of tectonic stability spanning billions of years (Villamizar et al., 2023; Higgins et al., 2025). Crystalline rock formations are noted for their strength and structural stability; they lack the stratified pore space of sedimentary rocks, though they commonly contain natural fractures. Site characterization in

the Ignace area has concentrated on identifying sufficient rock volume with sparsely fractured crystalline rock at depth, where any fractures are old, sealed, or of limited connectivity (Hooper, 2010). Regardless of the specific lithology though, the repository concept relies on the combination of engineered and natural barriers: the waste fuel would be sealed in copper-coated cylinders surrounded by bentonite clay buffers, emplaced in tunnels excavated ~500 m deep in the rock (Noronha, 2016). The host rock provides a stable mechanical environment and long-term chemical reducing conditions, which together with a swelling clay buffer, would inhibit groundwater flow, and hence radionuclide mobilisation.

International experience underpins the viability of crystalline host rock DGRs. For example, Finland's Onkalo and Sweden's Forsmark repositories are sited in granitic bedrock – just as sedimentary formations have been successfully selected elsewhere (e.g., France, (Nuclear Engineering International, 2025a; Dalton, 2025)). It is important to design a plan to adopt a DGR approach that would be adaptable to either major geologic setting (both crystalline and sedimentary), ensuring that whichever site is chosen meets all technical safety requirements regardless of rocktype. Indeed, a current consensus has emerged that both types of formations, if properly selected and characterized, can provide effective isolation of HLW over geological timescales (IAEA, 2009; NWMO, 2019). This siting process conducted by the NWMO concluded in 2024 and selected the site local to the Township of Ignace, within Wabigoon Lake Ojibway Nation territory, which voted in favour of the construction of the repository (Ketonen, 2024; NWMO, 2024).

This global effort reflects both the urgency and the complexity of implementing DGRs. Many programs have faced delays due to regulatory scrutiny, funding, and especially public and local community acceptance issues. However, successful examples in consent-based siting – such as Finland, Sweden, and now Canada – indicate that with transparent process and community involvement, it is possible to gain the social license needed for these projects (Radwaste

Solutions, 2024b). International organizations like the IAEA and OECD-NEA facilitate knowledge-sharing so countries can leverage best practices and lessons learned from each other (NWMO, 2025). As of the mid-2020s, the clear trend is that DGRs are transitioning from concept to reality, marking a major milestone in the future sustainability of nuclear energy.

1.3 Principles and production of noble gases

Noble gases: helium(He), neon (Ne), argon (Ar), krypton (Kr), xenon (Xe), and radon (Rn), are colourless, odourless, and chemically-inert – notably characterised as non-reactive due to their filled valence electron shells. With the exception of Rn, all noble gases have several stable isotopes. These characteristics and long-term stability make noble gases excellent tracers, since they do not readily participate in chemical reactions, so their distribution is principally governed by physical processes such as diffusion, mixing, and degassing, as well as production via radioactive decay (Cook, 2020). Generally, the chemically inert behaviour of naturally occurring noble gases, and their low abundances, permits them to be used as effective tracers to understand the origin, evolution, and mixing of fluids in various geochemical settings (Lu et al., 2014; Brennwald et al., 2013; Althaus et al., 2009; Warr et al., 2022).

Generally, the 23 stable noble gas isotopes of He through Xe can be divided into two groups;

1. Those isotopes which are not produced in meaningful quantities in the subsurface (primordial).
2. Isotopes which have a primordial component but also have additional production in terrestrial settings directly and indirectly via radioactive decay processes (radiogenic).

The production rates of these stable noble gas isotopes are given in Table 1.1. In the case of the second group, among the most significant are ^{4}He (produced via α decay of U and Th) and ^{40}Ar (produced via ^{40}K electron capture). Additional noble gases of note in this second group

include ^{3}He, produced via thermal neutron capture, ^{21,22}Ne from oxygen and fluorine α capture, and $^{131\text{-}136}$Xe via ^{238}U-based fisson (Ballentine and Burnard, 2002).

Consequently, depending on production rates and residence times, concentrations of these radiogenic isotopes, and ratios made of these with their non-radiogenic counterparts, can far exceed those found in in the atmosphere (Ballentine and Burnard, 2002; Cook, 2020). The present-day production rates of the noble gases examined in this thesis are presented in Table 1.1.

Table 1.1: Present day production rates of He, Ne, Ar, Kr, and Xe in cm^{3}STP/yr within oceanic and different types of continental crust.

(Ballentine and Burnard, 2002)

Crust	Oceanic	Lower	Middle	Upper	Total	Relative Abundance (%)
^{3}He	-	3.30E+03	1.42E+04	4.26E+04	6.00E+04	99.99986
^{4}He	4.55E+10	4.88E+11	3.54E+12	2.95E+12	7.68E+12	0.000140
^{20}Ne	-	1.96E+03	1.60E+04	1.74E+04	3.53E+04	90.50
^{21}Ne	2.28E+03	2.04E+04	1.65E+05	1.79E+05	3.65E+05	0.268
^{22}Ne	-	4.09E+04	3.30E+05	3.58E+05	7.29E+05	9.230
^{36}Ar	-	2.64E+03	9.70E+03	4.49E+04	5.73E+04	0.3364
^{38}Ar	-	1.47E+03	1.19E+04	1.29E+04	2.63E+04	0.0632
^{40}Ar	1.17E+10	1.61E+11	6.24E+11	6.72E+11	1.46E+12	99.60
^{83}Kr	9.69E-01	6.87E+00	6.35E+01	7.08E+01	1.41E+02	11.477
^{84}Kr	3.51E+00	2.49E+01	2.30E+02	2.56E+02	5.11E+02	57.00
^{86}Kr	2.31E+01	1.64E+02	1.51E+03	1.68E+03	3.36E+03	17.398
^{131}Xe	1.30E+01	9.25E+01	8.55E+02	9.53E+02	1.90E+03	21.22
^{132}Xe	8.67E+01	6.14E+02	5.68E+03	6.33E+03	1.26E+04	26.89
^{134}Xe	1.24E+02	8.79E+02	8.13E+03	9.06E+03	1.81E+04	10.430
^{136}Xe	1.50E+02	1.06E+03	9.83E+03	1.10E+04	2.18E+04	8.857

1.4 Applications of noble gases in the geosciences

Due to the conservative nature of the naturally abundant noble gases, their isotopic compositions and concentrations are widely used to trace environmental processes. Stable and radioactive noble gas isotopes both serve a purpose as complementary tracers in geological,

hydrogeological, and geochemical studies. In this section, the most commonly studied isotopes and their tracer applications will be outlined.

1.4.1 Helium

Helium has two stable isotopes, ^{3}He and ^{4}He. Overall, helium represents a very minor component within the atmosphere, at 5.24 ppm (NOAA, 2024) with ^{4}He representing the overwhelmingly dominant isotope (atmospheric $^{3}He/^{4}He$ is equal to 1.399×10^{-6}, Porcelli et al., 2002). In noble gas geochemistry, the observed ratio of $^{3}He/^{4}He$ relative to the atmospheric ratio is termed R_a and is a commonly used fingerprint for identifying the presence of crustal fluids where the crustal end member is significantly lower (~0.02 R_a or below) (Clark and Phillips, 2000; Ballentine and Burnard, 2002; Yamamoto et al., 2004). Similarly, these isotopes are also commonly used to identify the presence of mantle-derived fluids, which are commonly enriched in ^{3}He relative to the atmosphere (~6-40 R_a) (Hilton et al., 1999; Ballentine and Burnard, 2002; Jackson et al., 2007). ^{4}He is a radiogenic isotope with a production rate significantly greater than that of ^{3}He (which is produced in very minor quantities via thermal neutron capture of ^{6}Li within the crust), although ^{3}He is generally considered primordial. The mantle generally has retained primordial ^{3}He from the Earth's formation, while the crust tends to have lost its ^{3}He through degassing (Ballentine and Burnard, 2002). Thus, helium isotopic ratios can be used to discern mantle versus crustal contributions in geothermal fluids and gas emissions.

In hydrogeology, the concentration of radiogenic ^{4}He in groundwater increases with time as rocks continuously release helium through U and Th decay processes (Ballentine and Burnard, 2002). In turn, this makes helium a powerful groundwater age dating tool. Even without a precise "helium age", an excess in ^{4}He qualitatively indicates, old, long-residence-time water, or isolated pore fluids (Torgesen and Clarke, 1985; Holland et al., 2013; Warr et al., 2018). In fact, helium accumulation has been used in conjunction with other similarly in-situ produced

noble gas isotopes to date groundwater on scales of tens of thousands to millions, or even billions, of years (Warr et al., 2022). In addition, the same principle can be applied to model ^{4}He age estimates of hydrocarbon-associated groundwater, by incorporating factors such as known end-member compositions and mass fractionation during noble gas partitioning between oil and water phases (Zhou and Ballentine, 2006). At the other end of the spectrum, for relatively young groundwaters, residence times can be calculated via ^{3}H-^{3}He dating, whereby ingrowth of ^{3}He from ^{3}H (tritium) is used to date young waters, on a scale of years to decades (Solomon et al., 1993; Aeschbach-Hertig et al., 1998).

Helium's mobility (due to its small molecular size and sparingly soluble behaviour) means it can diffuse out of rocks and upward (Torgersen et al., 2004; Torgersen, 2010; Cheng et al., 2021). In tectonic contexts, ^{4}He anomalies in soil gas have even been used to locate deep faults or degassing zones (Aggarwal et al., 2015; Oxburgh and O'Nions, 1987), and their potential role in helium resource generation (Halford et al., 2024a; Halford et al., 2024b). Overall, helium's inertness and the sensitivity of the ^{3}He/^{4}He ratio make it a uniquely versatile tracer for both identifying fluid origin as well as quantifying residence times.

1.4.2 Neon

Neon, much like helium, forms a very minor component within the atmosphere, at 18.182 ppm, just over triple the concentration of helium (NOAA, 2024). Isotopes of neon include ^{20}Ne, ^{21}Ne, and ^{22}Ne, all of which are stable. As discussed, ^{20}Ne is the dominant isotope, which is atmospheric and primordial in nature, whereas ^{21}Ne is nucleogenic, from reactions such as ^{18}O(α,n)^{21}Ne, or even through small-scale cosmogenic production. Finally, ^{22}Ne is mostly atmospheric, with minor nucleogenic production (Ballentine and Burnard, 2002).

The majority of elemental neon within the atmosphere is composed of ^{20}Ne, which is the dominant isotope by a significant margin (at 90.5% of atmospheric neon) whereby ^{22}Ne and, in particular, ^{21}Ne are less abundant, (9.23% and 0.268%, respectively) (Ballentine and

Burnard, 2002). As noble gases have well-known temperature-dependent solubilities, the concentrations of Ne (often in conjunction with other noble gases, such as Ar, Kr, and Xe) can be used to to reveal the temperature and excess air conditions during recharge (Wilson and McNeill, 1997; Cey, 2009; Cook, 2020; Seltzer et al., 2021).

In the atmosphere and crust, the dominant isotope, ^{20}Ne, is primordial in nature, whereas ^{21}Ne and ^{22}Ne are additionally produced via nucleogenic reactions in crustal settings from reactions such as ^{18}O(α,n)^{21}Ne, ^{19}F(α,n)^{22}Na(β+)^{22}Ne and ^{19}F(α,p)^{22}Ne (Wetherill, 1954; Ballentine and Burnard, 2002; Warr et al., 2018).Consequently, neon in crustal fluids tends to show an excess of both ^{21}Ne and ^{22}Ne relative to air, reflecting this nucleogenic production; studies have found that crustal fluids in post-Archean settings worldwide usually have a relatively uniform ^{21}Ne/^{22}Ne production ratio based on the local O/F ratio adjacent to U-bearing mineralogies (Kennedy et al., 1990; Ballentine, 1997, Lippmann-Pipke et al., 2011).

1.4.3 Argon

Argon forms the third-most significant component of the atmosphere, at approximately 0.934% (9340 ppm) of its chemical makeup excluding water vapour (NOAA, 2024), making it a far more significant component of the atmosphere than helium and neon. Argon has three stable isotopes: ^{36}Ar, ^{38}Ar, and ^{40}Ar. Of these, ^{40}Ar is by far the most abundant (atmospheric Ar is ~99.6% ^{40}Ar), followed by ^{36}Ar and ^{38}Ar: 0.3364% and 0.0632%, respectively (Ballentine and Burnard, 2002). Argon makes for a very useful tracer, as ^{40}Ar is typically enriched in the crust, due to ^{40}K decay (McDougall and Harrison, 1999). In young groundwaters, dissolved argon tends to be primarily atmospheric, reflected by air-like ^{40}Ar/^{36}Ar and ^{38}Ar/^{36}Ar isotopic ratios. As with ^{4}He, groundwaters that have been isolated for long timescales can accumulate radiogenic ^{40}Ar from constituent ^{40}K in the surrounding rock. Detecting excess ^{40}Ar, or higher ^{40}Ar/^{36}Ar ratio than air (~295.5, Porcelli et al., 2002) in groundwaters and fluids therefore indicates a crustal contribution of ^{40}Ar (Ballentine and Burnard, 2002). As a result, much like

^{4}He, ^{40}Ar can also be used as a powerful, groundwater age dating tool, useful for dating waters on the scale of tens of thousands to millions (or sometimes billions) of years (Lippmann et al., 2003; Seltzer et al., 2021; Warr et al., 2022).

Beyond the stable argon isotopes, the isotope ^{39}Ar has emerged as an important environmental tracer and is produced by neutron activation of ^{40}Ar (^{40}Ar (n, 2n) ^{39}Ar), or through cosmic ray interactions in the atmosphere (Corcho Alvarado et al., 2013; Lu et al., 2014; Purtschert et al., 2021). Once water is isolated from the atmosphere, ^{39}Ar decays with a half-life of 269 years, making it an ideal tracer for 50–1000-year timescales. In practice, ^{39}Ar has filled a critical dating gap between the reach of tritium (<60 years) and radiocarbon (~500-30,000 years), as outlined in Lu et al. (2014). However, its detection requires large samples and sensitive methods (either low-level counting, such as Resonance-Ionization Mass Spectrometry – RIMS – or modern Atom Trap Trace Analysis – ATTA). Recent advances in ATTA have made ^{39}Ar measurements more feasible on smaller samples, greatly enhancing its usability (Lu et al., 2014; Jia et al., 2025).

Another argon isotope, ^{37}Ar, is noteworthy in the context of nuclear monitoring. ^{37}Ar is produced by neutron activation of calcium within rocks, e.g., during a nuclear explosion, and has a 35-day half-life (Loosli, 1992). Its natural presence within soil gas is miniscule and generally only trace concentrations, unless there are recurring neutron fluxes in the vicinity of target ^{40}Ar or ^{40}Ca (Riedmann and Purtschert, 2011), so detection of ^{37}Ar above background tends to be indicative of an underground nuclear test or reactor operation. Although an unconventional tracer, ^{37}Ar exemplifies the sensitivity of argon isotopes as environmental indicators in specialized scenarios (Loosli, 1992; Musy et al., 2022; Musy and Purtschert, 2023).

1.4.4 Krypton

Krypton, like helium and neon, exists in very low quantities naturally within the atmosphere, on a scale of approximately 1.14 ppm (NOAA, 2024). Krypton has six stable isotopes: ^{78}Kr, ^{80}Kr, ^{82}Kr, ^{83}Kr, ^{84}Kr, and ^{86}Kr. In addition to these, krypton also has two useful radioactive isotopes: ^{85}Kr and ^{81}Kr. The stable isotopes of krypton can be used alongside Ar and Xe for paleoclimate reconstruction and excess air corrections (Severinghaus et al., 2003; Grachev and Severinghaus, 2003), however by themselves carry little unique fingerprint due to the limited natural variability in krypton isotopic ratios, primarily due to no significant radiogenic or nucleogenic krypton isotopes produced in the crust or the mantle (Ballentine and Burnard, 2002).

While several of these stable isotopes can be produced in crustal settings via U, Th decay, the production rates are typically so low so as to only have a marginal effect on the initial air-like ratios (Ballentine and Burnard, 2002; Warr et al., 2022). Instead, with respect to noble gas geochronology, the primary utility of krypton here lies in two of its radioisotopes – ^{85}Kr and ^{81}Kr. ^{85}Kr is a fission product released from anthropogenic nuclear activities; its presence in young groundwater is an unambiguous sign of post-1950 recharge. Due to the 10.74-year half-life and continuous replenishment via industrial releases, it can effectively function as a “bomb tracer” analogous to tritium or CFCs, but with the advantage of being chemically inert and unaffected by degradation, as tritium can enter water as HTO (tritiated water) and participate in the hydrological cycle, and CFCs (chlorofluorocarbons) can degrade or experience microbial consumption or oxidation processes (Lu et al., 2014; Musy et al., 2021). It is ideal for dating of ground- and pore-waters in the range of ~1-40 years and has been successfully applied to identify very recent infiltration and to calibrate young groundwater flow models (Lu et al., 2014; Musy et al., 2021).

Alternatively, ^{81}Kr (with a half-life of 229 ka) is a rare cosmogenic isotope that has become a breakthrough tracer for older groundwater. ^{81}Kr is chemically inert and uniformly mixed within the atmosphere, making it conceptually ideal for dating water in the 10^4-to-10^6-year range (Collon, 2004). Its long half-life means that fossil groundwater from the Pleistocene or earlier can be dated by measuring the residual ^{81}Kr fraction. This dating technique has been successfully applied to ancient aquifers and even to old ice cores (Collon et al., 2000; Collon, 2004; Buizert et al., 2014). The challenge lies with its extremely low abundance – on the order of 10^{-12} of natural Kr. However, recent advances in ATTA technology within the past 20 years has enabled routine ^{81}Kr measurements (Jiang et al., 2012; Yang et al., 2013). As of 2013, ATTA technology matured to allow ^{85}Kr or ^{81}Kr analyses on samples of few tens of litres of water (Jiang et al., 2012; Yang et al., 2013).

1.4.5 Xenon

Xenon has the greatest number of stable isotopes of any noble gas (nine stable isotopes from ^{124}Xe, ^{126}Xe, ^{128}Xe, ^{129}Xe,^{130}Xe, ^{131}Xe, ^{132}Xe, ^{134}Xe, and ^{136}Xe), however it is the least naturally abundant within the atmosphere, at approximately 0.09 ppm (NOAA, 2024). Dissolved xenon, along with krypton (see section 1.3.4) can yield unique information, and can be measured to deduce paleoclimate characteristics (Peeters et al., 2003). Xenon is the most soluble noble gas and is thus the most sensitive to fluctuations in temperature, which in turn increases the noble gas palaeothermometry resolution (Peeters et al., 2003; Aeschbach-Hertig and Solomon, 2013; Bekaert et al., 2023). Isotopically, natural xenon in the atmosphere has a distinct signature, whereas xenon that has been produced via spontaneous fission or decay in the subsurface has elevated concentrations of $^{131\text{-}136}$Xe (Reynolds, 1960; Staudacher and Allègre, 1982; Moreira, 2007). Detecting such anomalies in ground- or pore-waters or gas can suggest long-term isolation (allowing Xe from fission to accumulate) or input from a nuclear source (Moreira, 2007). In the context of nuclear safety, radioactive xenon (^{133}Xe, ^{135}Xe) in the atmosphere is

primary evidence of an underground nuclear test venting gases as these isotopes are short-lived and not naturally present (Galan et al., 2018; Bowyer, 2021). While those short-lived isotopes decay before reaching a far-field environment around a geological repository, the stable fission Xe inventory in spent nuclear fuel is very large. If a repository were to lose integrity, one might identify isotopically distinctive xenon in the surrounding environment (e.g., a shift in $^{136}Xe/^{130}Xe$ ratio) as a fingerprint of released fission gases and leaking fuel elements (Palcsu et al., 2001; Dresel and Waichler, 2004). This is analogous to how ^{85}Kr is used, however xenon would carry a more source-specific isotopic signature. Notably, one field experiment injected a radioxenon tracer (^{127}Xe) in situ along with ^{37}Ar. These tracers were successfully detected and modelled to understand gas migration, demonstrating their transport through rock (Johnson et al., 2019).

1.5 Noble gases as tracers of DGR processes

Prior literature regarding noble gases as tracers for DGR integrity is somewhat sparse, although being an emerging tracer and gaining momentum within the scientific community, this is beginning to change. In argillaceous host rocks, studies have measured noble gas concentrations in porewaters as a way to determine transport rates and past flow conditions. For example, radiogenic ^{4}He, produced via the decay of U and Th, is released from the solid phase and accumulates within the rock porewater (Lavielle et al., 2012). These formations are very low-permeability (diffusive transport dominates) and have often retained their porewater since deposition. Consequently, radiogenic noble gases produced in situ have accumulated over multi-million-year timescales, rather than migrating out, which is a strong indication of overall long-term isolation with minimal external exchange with adjacent lithological units. For example, many studies such as those documented in Osenbrück et al. (1998), Bensenouci et al. (2011), Lavielle et al. (2012), Neretnieks (2013), and Tsang et al. (2015) identify the potential for noble gases (particularly ^{4}He) measured within the porewater of fresh core samples

extracted from boreholes to serve as effective tracers for the investigation of diffusion transport in low porosity rock formations, and assist in the estimation of porewater residence times.

Notably, a lot of work has already been conducted at the Mont Terri rock laboratory in Switzerland, whereby the Opalinus Clay (OPA) has been closely studied. Much of this work has sought to characterize the OPA formation and its porewater (Van Loon, et al., 2004; Appelo and Wersin, 2007; Corkum and Martin, 2007; Joseph et al., 2011; Keller et al., 2013; Tsang et al., 2015; Mazurek and De Haller, 2018), however, only a small number of studies have focussed primarily on pore-water noble gas concentrations (Mazurek et al., 2011; Maineult et al., 2013; Tomonaga et al., 2019), and fewer yet have delved into the details of noble gas isotopes. The most pivotal study on this topic, as it pertains to this thesis, was documented in Rübel et al. (2002) The foundation of the Rübel et al. (2002)project was based on the determination of water content, stable isotope composition (δD and $\delta^{18}O$), and dissolved noble gas contents of the OPA porewater. The primary aim of this experiment was to determine which of advection or diffusion were the dominant transport processes (Rübel et al., 2002). The findings of this experiment suggested that the helium profile measured across the full thickness of the undisturbed formation was in steady state between in situ production and diffusive loss of He (into neighbouring formations). The ^{4}He profile indicated that molecular diffusion was the only effective transport process within the formation. In terms of porewater age and solute transport, stable water isotopes yielded the most important information for determining this (Rübel et al., 2002). However, an important consideration to be made is that only ^{4}He and ^{40}Ar were examined, meaning that the low range of noble gas isotopes studied is a major limitation in this study, and examining the whole suite of noble gas isotopes from ^{4}He to ^{40}Ar could shed more light on this, and enable more effective interrogation of sampling techniques.

More generally, noble gases have additionally been used as tracers to explore structural conditions of repository analogues. For example, Maineult et al. (2013) characterises the noble

gas profile to identify the Excavation Damaged Zone (EDZ) whereby desaturation processes occur, in addition to geophysical self-potential investigations to detect anomalies in subsurface fluid circulation within pre-existing tectonic fractures. In contrast, Tomonaga et al. (2015) analysed noble gases (in addition to N_2, O_2, H_2, CH_4, and CO_2) in the free gas phase for rock laboratory operational safety purposes. Furthermore, Mazurek et al. (2011) builds upon the work undertaken in Rübel et al. (2002) to fit model calculations to the noble gas tracer distributions to constrain diffusion times and large-scale diffusion coefficients within the OPA.

1.6 The Mont Terri Rock Laboratory

The Mont Terri underground rock laboratory (URL) is located in northern Switzerland, northwest of Bern and nearby the town of St-Ursanne, in the Clos du Doubs region. The rock laboratory is approximately 300 m underground and runs parallel to a highway tunnel, which extends from the Ajoie region to beyond the district capital, Porrentruy, see Figure 1.1 (modified from Bossart et al., 2017a).

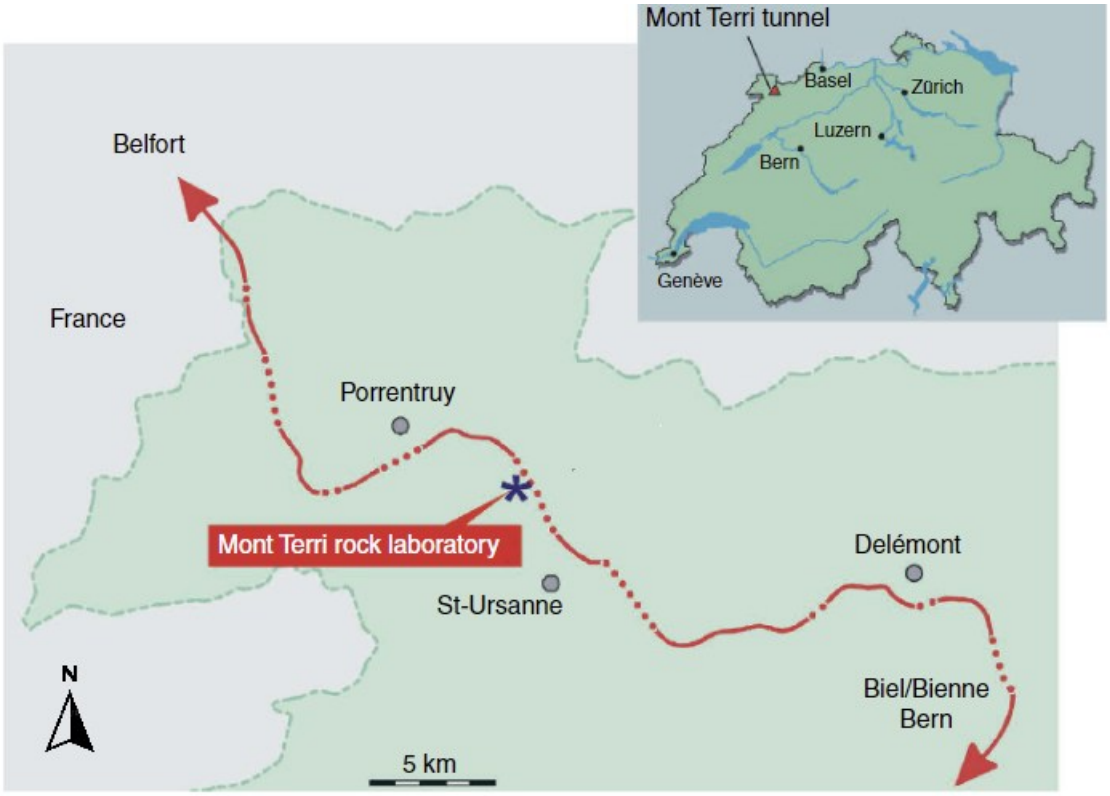

Figure 1.1: Map depicting the location of the Mont Terri rock laboratory in relation to the surrounding area in northwest Switzerland, the red line denoting the A16 Transjurane highway (modified from Nussbaum et al., 2011).

This research facility was established to investigate the surrounding clay formations as potential analogues of argillaceous host rocks for DGRs of intermediate (ILW) and high-level radioactive waste (HLW). It has been operated since 1996 under the management of the Swiss Federal Office of Topography (swisstopo) and collaborates with organisations from many countries worldwide.

Nussbaum et al. (2011) explains that the Jura mountains – in which the Mont Terri URL is located – were formed approximately 3-12 Ma before the present and comprise the Plateaujura (Freiberg and France), the Tafeljura (e.g. the Ajoie region) and the Faltenjura (Jura folds). The Mont Terri site specifically is located within the Faltenjura. The Mont Terri URL is located within the Opalinus Clay (OPA) formation and has been prospected as the preferred host rock for HLW (and potentially ILW) and is described as a marly argillaceous claystone with varying

proportions of sand and carbonates (Hostettler et al., 2017). The OPA formation specifically is composed of a sequence of grey, silty, micaceous clays and sandy shales that were originally deposited approximately 174 Ma before the present (Nussbaum et al., 2011). The URL is located entirely within the OPA formation, which has an apparent thickness of 160 meters and a true thickness of 90 meters. This formation is overlain by a sequence of sandy limestones, shales, and oolitic limestones from the early Bajocian stage of the Middle Jurassic period. Beneath the OPA formation lie 800 meters of Mesozoic limestones, marls, and shales, followed by 500 meters of Tertiary Molasse and, in some areas, Quaternary fluvio-glacial sediments. These layers rest unconformably on a basement composed of late Palaeozoic clastic sediments (Nussbaum et al., 2011). For a more comprehensive facies description and geologic history, see Appendix A.

While the goal of the Mont Terri URL is to assess the suitability of the OPA material for DGR applications, there are no plans to store waste at the site. Instead, due to the homogeneity of the OPA material, it is hoped that the work carried out at the URL will yield waste solutions in similar low-permeability argillaceous rocks (Rübel et al., 2002, Bossart and Thury, 2007; Bossart et al., 2017a)

1.7 Research rationale

As outlined in previous sections, noble gases are excellent tracers which enable greater approximations of residence times, and groundwater migration and mixing, with particular respect to site characterisation. However, a fundamental requirement for their application for prospective repositories is the ability to effectively sample groundwaters from core samples; extract, measure the noble gas isotopic content of pore fluids; and to consistently interpret the resulting data. To date, there is no definitive intercomparison of noble gas studies focusing on argillaceous cores to evaluate the various approaches to effectively sample, measure and

normalize the noble gas characteristics from core porewaters. There is no commonly applied standardisation when determining the porewater noble gas content. Consequently, in its absence, differing normalization approaches taken by different laboratories may result in different porewater concentrations and alternative interpretations of the same samples. Without a consensus, there is the potential for ambiguity and therefore an increased uncertainty in characterising deep crustal systems such as those being considered for DGRs.

The PC-D experiment was undertaken at the Mont Terri URL and consists of four project partners in the Mont Terri Consortium: NWMO (Canada), NWS (UK), BASE (Germany), and BGR (Germany). Three independent laboratories, with independent external-laboratory supports, participated in the noble gas program as part of PC-D: University of Ottawa, Hydroisotop GmbH, and BGR. Determining a 'best practices' approach for this purpose forms the basis of this work. Here, a series of OPA core samples were obtained from a common borehole at the Mont Terri site in Switzerland. This borehole was selected due to its homogeneity (NAGRA, 2024), an essential characteristic permitting an inter-laboratory comparison such as this.

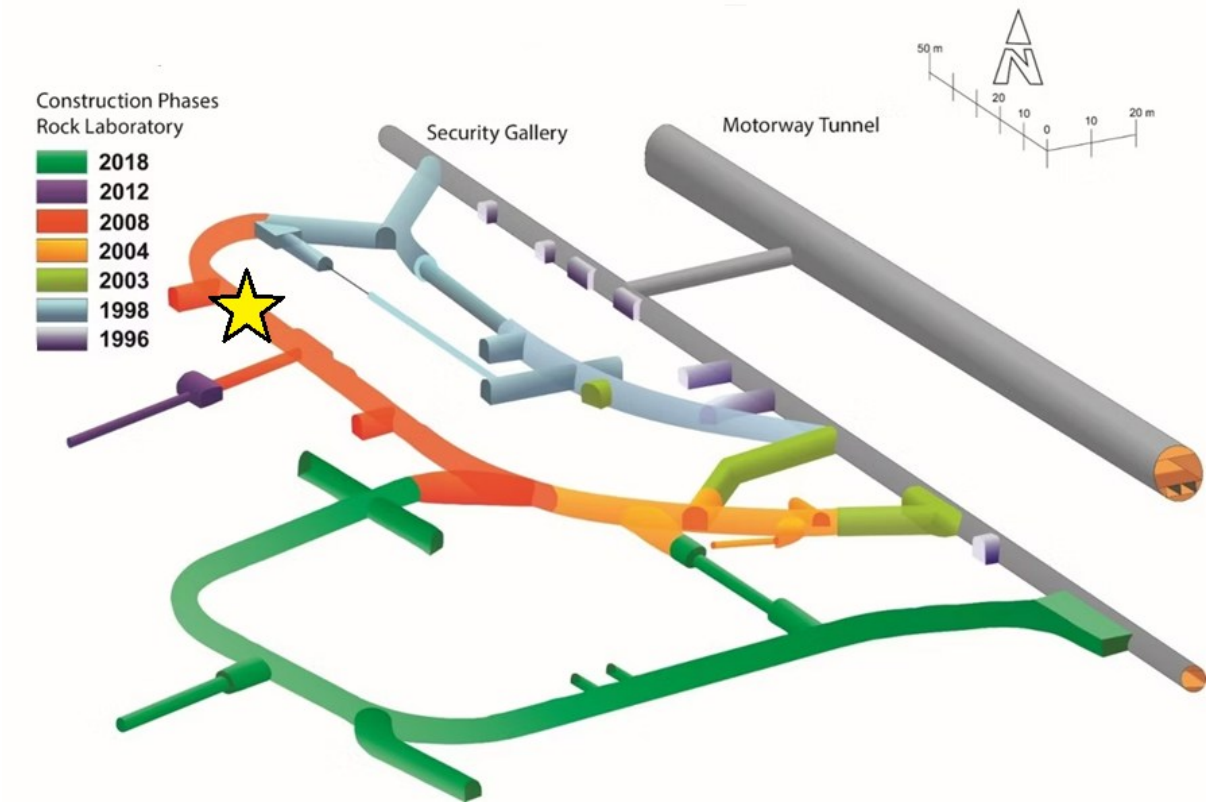

Figure 1.2: Schematic of the Mont Terri rock laboratory, with each construction phase noted. The BPCD-1 borehole from which the "PC-D" cores were obtained from is denoted with the yellow star (modified from Mont Terri, 2023).

A total of 20 core sections from varying intervals between 480 to 2060 cm along a horizontal profile were obtained from the horizontally drilled borehole (BPCD-1, starred) in Gallery 08 of the Mont Terri rock laboratory and is depicted in Figure 1.2 (modified from Mont Terri, 2023). In these studies, "sample depth" will refer to the distance of the centre point of the core along the horizontal borehole.

Once these core sections were recovered from the borehole, they were broken into lengths between 10 and 30 cm using a hammer and chisel, and the rim was brushed to remove excess powdered rock. Once sampled, they were then packed into PVC bags and vacuum-sealed using a vacuum device to minimise air contamination and porewater loss.

These sample cores were then subsequently packed in a second PVC bag, and finally in a laminated OPP/PE/Foil/PE Mil PRF-131K Class 1 vapour-barrier Al-foil bag. 5 of these 20 samples were prepared in the laboratory at BGR, however for the remaining 15, these were prepared at Hydroisotop and were divided into two groups. The first group of samples (5 of the 15) were left "as-is" inside of the evacuated Al-foil bag and were sent to the University of Ottawa. The second group of samples (the remaining 10 of the 15, half of these were shipped to the University of Ottawa after sample preparation) underwent additional preparations as discussed in section 2.2.1. These sample core sections were distributed amongst project partners so that each partner had adjacent samples from approximately the same sample depths along the core run.

The overarching aim for the research project based on the samples sent to the University of Ottawa is to discuss the strengths and weaknesses of core porewater analysis for future applications in the characterisation of potential Deep Geological Repositories (DGRs) for nuclear waste storage, and secondarily to compare the strengths and weaknesses between storage of cores within stainless-steel cylinders (the common sampling encapsulation approach for core samples in porewater studies) and to evaluate the viability of the vacuum-sealed Al-foil bags, which are a cheaper and quicker alternative to their stainless-steel counterparts. If the use of these Al-foil bags yields similar results with no significant disparities, it could potentially enable researchers to save a significant amount of money on resources and shipping costs, particularly for studies such as this in which an inter-laboratory comparison is conducted, and rock cores need to be exported internationally. Thus, an evaluation between the stainless-steel cylinders and Al-foil bags will provide additional insight into optimal sampling and storage practices for noble gas-based core samples.

1.8 Research objectives

The overarching aim of this study is to identify and evaluate different techniques for encapsulating, extracting, and analysing noble gases from the porewater of argillaceous rock cores. This was accomplished through two studies, with the following research objectives:

1. Identify and evaluate different techniques to normalise the sampled headspace concentrations from the stainless-steel cylinders to the rock porewater, and to explore the impact and effect of their associated assumptions.

2. Evaluate an alternative sample encapsulation technique (PE/Al-foil bag) with respect to its sampling and extraction efficacy, ability to effectively normalise headspace concentrations to the rock porewater, and robustness of the generated results.

1.9 References

Aeschbach-Hertig, W., Schlosser, P., Stute, M., Simpson, H. J., Ludin, A., & Clark, J. F. (1998). A 3H/3He study of ground water flow in a fractured bedrock aquifer. *Ground Water*, *36*(4), 661–670. https://doi.org/10.1111/J.1745-6584.1998.TB02841.X;WGROUP:STRING:PUBLICATION

Aeschbach-Hertig, W., & Solomon, D. K. (2013). Noble gas thermometry in groundwater hydrology. *Advances in Isotope Geochemistry*, 81–122. https://doi.org/10.1007/978-3-642-28836-4_5

Aggarwal, P. K., Matsumoto, T., Sturchio, N. C., Chang, H. K., Gastmans, D., Araguas-Araguas, L. J., Jiang, W., Lu, Z. T., Mueller, P., Yokochi, R., Purtschert, R., & Torgersen, T. (2015). Continental degassing of 4He by surficial discharge of deep groundwater. *Nature Geoscience*, *8*(1), 35–39.

https://doi.org/10.1038/NGEO2302;TECHMETA=125,127,140,144;SUBJMETA=209,2151,241,704;KWRD=GEOCHEMISTRY,HYDROGEOLOGY

Alexander, W. R., Reijonen, H. M., & McKinley, I. G. (2015). Natural analogues: studies of geological processes relevant to radioactive waste disposal in deep geological repositories. *Swiss Journal of Geosciences*, *108*(1), 75–100. https://doi.org/10.1007/S00015-015-0187-Y/FIGURES/13

Althaus, R., Klump, S., Onnis, A., Kipfer, R., Purtschert, R., Stauffer, F., & Kinzelbach, W. (2009). Noble gas tracers for characterisation of flow dynamics and origin of groundwater: A case study in Switzerland. *Journal of Hydrology*, *370*(1–4), 64–72. https://doi.org/10.1016/J.JHYDROL.2009.02.053

Alwaeli, M., & Mannheim, V. (2022). Investigation into the Current State of Nuclear Energy and Nuclear Waste Management—A State-of-the-Art Review. *Energies 2022, Vol. 15, Page 4275*, *15*(12), 4275. https://doi.org/10.3390/EN15124275

Appelo, C. A. J., & Wersin, P. (2007). Multicomponent Diffusion Modeling in Clay Systems with Application to the Diffusion of Tritium, Iodide, and Sodium in Opalinus Clay. *Environmental Science and Technology*, *41*(14), 5002–5007. https://doi.org/10.1021/ES0629256

Apted, M. J. ., & Ahn, Joonhong. (2017). *Geological repository systems for safe disposal of spent nuclear fuels and radioactive waste*. Woodhead Publishing.

Ballentine, C. J. (1997). Resolving the mantle He/Ne and crustal 21Ne/22Ne in well gases. *Earth and Planetary Science Letters*, *152*(1–4), 233–249. https://doi.org/10.1016/S0012-821X(97)00142-8

Ballentine, C. J., & Burnard, P. G. (2002). *Production, Release and Transport of Noble Gases in the Continental Crust* (Vol. 47, Issue 1, pp. 481–538). https://doi.org/10.2138/rmg.2002.47.12

Bekaert, D. v., Blard, P. H., Raoult, Y., Pik, R., Kipfer, R., Seltzer, A. M., Legrain, E., & Marty, B. (2023). Last glacial maximum cooling of 9 °C in continental Europe from a 40 kyr-long noble gas paleothermometry record. *Quaternary Science Reviews*, *310*, 108123. https://doi.org/10.1016/J.QUASCIREV.2023.108123

Bensenouci, F., Michelot, J. L., Matray, J. M., Savoye, S., Lavielle, B., Thomas, B., & Dick, P. (2011). A profile of helium-4 concentration in pore-water for assessing the transport phenomena through an argillaceous formation (Tournemire, France). *Physics and Chemistry of the Earth, Parts A/B/C*, *36*(17–18), 1521–1530. https://doi.org/10.1016/J.PCE.2011.10.016

Bossart, P., Bernier, F., Birkholzer, J., Bruggeman, C., Connolly, P., Dewonck, S., Fukaya, M., Herfort, M., Jensen, M., Matray, J. M., Mayor, J. C., Moeri, A., Oyama, T., Schuster, K., Shigeta, N., Vietor, T., & Wieczorek, K. (2017). Mont Terri rock laboratory, 20 years of research: introduction, site characteristics and overview of experiments. *Swiss Journal of Geosciences*, *110*(1), 3–22. https://doi.org/10.1007/S00015-016-0236-1/FIGURES/8

Bossart, P., Burrus, F., Jaeggi, D., & Nussbaum, C. (2017). The Mont Terri rock laboratory. In X.-T. Feng (Ed.), *Rock Mechanics and Engineering* (1st ed., Vol. 2, pp. 469–510). CRC Press. https://doi.org/10.1201/9781315364254-26

Bossart, P., & Thury, M. (2007). Research in the Mont Terri Rock laboratory: Quo vadis? *Physics and Chemistry of the Earth, Parts A/B/C*, *32*(1–7), 19–31. https://doi.org/10.1016/J.PCE.2006.04.031

Bossart, P., & Thury, M. (2008). *Mont Terri Rock Laboratory. Project, Programme 1997 to 2007 and results* (Issue 3).

Bowyer, T. W. (2021). A Review of Global Radioxenon Background Research and Issues. *Pure and Applied Geophysics*, *178*(7), 2665–2675. https://doi.org/10.1007/S00024-020-02440-0/FIGURES/6

Brennwald, M. S., Vogel, N., Scheidegger, Y., Tomonaga, Y., Livingstone, D. M., & Kipfer, R. (2013). Noble gases as environmental tracers in sediment porewaters and stalagmite fluid inclusions. *Advances in Isotope Geochemistry*, 123–153. https://doi.org/10.1007/978-3-642-28836-4_6/FIGURES/13

Buizert, C., Baggenstos, D., Jiang, W., Purtschert, R., Petrenko, V. v., Lu, Z. T., Müller, P., Kuhl, T., Lee, J., Severinghaus, J. P., & Brook, E. J. (2014). Radiometric 81Kr dating identifies 120,000-year-old ice at Taylor Glacier, Antarctica. *Proceedings of the National Academy of Sciences of the United States of America*, *111*(19), 6876–6881. https://doi.org/10.1073/PNAS.1320329111/SUPPL_FILE/PNAS.1320329111.SD01.XLS

Cey, B. D., Hudson, G. B., Moran, J. E., & Scanlon, B. R. (2009). Evaluation of Noble Gas Recharge Temperatures in a Shallow Unconfined Aquifer. *Groundwater*, *47*(5), 646–659. https://doi.org/10.1111/J.1745-6584.2009.00562.X

Cheng, A., Sherwood Lollar, B., Warr, O., Ferguson, G., Idiz, E., Mundle, S. O. C., Barry, P. H., Byrne, D. J., Mabry, J. C., & Ballentine, C. J. (2021). Determining the role of diffusion and basement flux in controlling 4He distribution in sedimentary basin fluids. *Earth and Planetary Science Letters*, *574*, 117175. https://doi.org/10.1016/J.EPSL.2021.117175

Clark, I. D., & Phillips, R. J. (2000). Geochemical and 3He/4He evidence for mantle and crustal contributions to geothermal fluids in the western Canadian continental margin. *Journal of Volcanology and Geothermal Research*, *104*(1–4), 261–276. https://doi.org/10.1016/S0377-0273(00)00209-2

Clifford, C. (2021). Nuclear waste: Why there's no permanent nuclear waste dump in U.S. *CNBC*. https://www.cnbc.com/2021/12/18/nuclear-waste-why-theres-no-permanent-nuclear-waste-dump-in-us.html

Collon, P., Antaya, T., Davids, B., Fauerbach, M., Harkewicz, R., Hellstrom, M., Kutschera, W., Morrissey, D., Pardo, R., Paul, M., Sherrill, B., & Steiner, M. (1997). Measurement of 81Kr in the atmosphere. *Nuclear Instruments and Methods in Physics Research Section B: Beam Interactions with Materials and Atoms*, *123*(1–4), 122–127. https://doi.org/10.1016/S0168-583X(96)00674-X

Collon, P., Kutschera, W., Loosli, H. H., Lehmann, B. E., Purtschert, R., Love, A., Sampson, L., Anthony, D., Cole, D., Davids, B., Morrissey, D. J., Sherrill, B. M., Steiner, M., Pardo, R. C., & Paul, M. (2000). 81Kr in the Great Artesian Basin, Australia: a new method for dating very old groundwater. *Earth and Planetary Science Letters*, *182*(1), 103–113. https://doi.org/10.1016/S0012-821X(00)00234-X

Collon, P., Kutschera, W., & Lu, Z. T. (2004). Tracing noble gas radionuclides in the environment. *Annual Review of Nuclear and Particle Science*, *54*, 39–67. https://doi.org/10.1146/ANNUREV.NUCL.53.041002.110622

Cook, P. (2020). *2.7 Noble Gases*. The Groundwater Project.

Corcho Alvarado, J. A., Pačes, T., & Purtschert, R. (2013). Dating groundwater in the Bohemian Cretaceous Basin: Understanding tracer variations in the subsurface.

Applied Geochemistry, *29*, 189–198. https://doi.org/10.1016/J.APGEOCHEM.2012.11.014

Corkum, A. G., & Martin, C. D. (2007). The mechanical behaviour of weak mudstone (Opalinus Clay) at low stresses. *International Journal of Rock Mechanics and Mining Sciences*, *44*(2), 196–209. https://doi.org/10.1016/J.IJRMMS.2006.06.004

Crawley, M. (2023, September 28). Ontario prepares to go big on nuclear, with demand for electricity poised to soar. *CBC News*.

Dalton, D. (2025). *French Nuclear Repository Project To Cost Up To €37 Billion, Says Andra*. https://www.nucnet.org/news/french-nuclear-repository-project-to-cost-up-to-eur37-billion-says-andra-5-2-2025

Drace, Z., Ojovan, M. I., & Samanta, S. K. (2022). Challenges in Planning of Integrated Nuclear Waste Management. *Sustainability 2022, Vol. 14, Page 14204*, *14*(21), 14204. https://doi.org/10.3390/SU142114204

Dresel, P. E., & Waichler, S. R. (2004). *Evaluation of Xenon Gas Detection as a Means for Identifying Buried Transuranic Waste at the Radioactive Waste Management Complex, Idaho National Environmental and Engineering Laboratory*. http://www.ntis.gov/ordering.htm

Fernández-Arias, P., Vergara, D., & Antón-Sancho, Á. (2023). Global Review of International Nuclear Waste Management. *Energies 2023, Vol. 16, Page 6215*, *16*(17), 6215. https://doi.org/10.3390/EN16176215

Galan, M., Kalinowski, M., Gheddou, A., & Yamba, K. (2018). New evaluated radioxenon decay data and its implications in nuclear explosion monitoring. *Journal of*

Environmental Radioactivity, *192*, 628–634. https://doi.org/10.1016/J.JENVRAD.2018.02.015

Gonzalez, R., & Wetzel, A. (1996). Stratigraphy and paleogeography of the Hauptrogenstein and Klingnau Formations (middle Bajocian to late Bathonian), northern Switzerland. *Eclogae Geologicae Helvetiae: Recueil Périodique de La Société Géologique Suisse= Mitteilungen Der Schweiz. Geologischen Gesellschaft*, *89*(1), 695–720.

Government of Canada. (2024). *CER – Provincial and Territorial Energy Profiles – Ontario*. https://www.cer-rec.gc.ca/en/data-analysis/energy-markets/provincial-territorial-energy-profiles/provincial-territorial-energy-profiles-ontario.html

Grachev, A. M., & Severinghaus, J. P. (2003). Determining the thermal diffusion factor for 40Ar/36Ar in air to aid paleoreconstruction of abrupt climate change. *Journal of Physical Chemistry A*, *107*(23), 4636–4642. https://doi.org/10.1021/JP027817U/ASSET/IMAGES/MEDIUM/JP027817UE00006.GIF

Gupta, K., Nowlin, M. C., Ripberger, J. T., Jenkins-Smith, H. C., & Silva, C. L. (2019). Tracking the nuclear 'mood' in the United States: Introducing a long term measure of public opinion about nuclear energy using aggregate survey data. *Energy Policy*, *133*, 110888. https://doi.org/10.1016/J.ENPOL.2019.110888

Halford, D. T., Karolytė, R., Andreason, M. W., Cathey, B., Cathey, M., Dellenbach, J. T., Cuzella, J. J., Sonnenberg, S. A., Cheng, A., McCaffrey, K. J. W., Gluyas, J. G., & Ballentine, C. J. (2024). Probabilistic Determination of the Role of Faults and Intrusions in Helium-Rich Gas Fields Formation. *Geochemistry, Geophysics, Geosystems*, *25*(6), e2024GC011522. https://doi.org/10.1029/2024GC011522;PAGEGROUP:STRING:PUBLICATION

Halford, D. T., Karolytė, R., Dellenbach, J. T., Cathey, B., Cathey, M., Balentine, D., Andreason, M. W., & Rice, G. K. (2024). Applications in utilizing soil gas geochemistry along with geological and geophysical data to construct helium exploration statistical models. *Frontiers in Earth Science*, *12*, 1434785. https://doi.org/10.3389/FEART.2024.1434785/BIBTEX

Hall, D. S., & Keech, P. G. (2017). An overview of the Canadian corrosion program for the long-term management of nuclear waste. *Corrosion Engineering Science and Technology*, *52*, 2–5. https://doi.org/10.1080/1478422X.2016.1275419/ASSET/9F40C875-91E3-4030-8458-AC4263F387CE/ASSETS/IMAGES/MEDIUM/10.1080_1478422X.2016.1275419-EQ3.GIF

Higgins, P. M., Song, M., Warr, O., & Sherwood Lollar, B. (2025). Natural H2 and Sulfate Production via Radiolysis in Low Porosity and Permeability Crystalline Rocks. *Journal of Geophysical Research: Biogeosciences*, *130*(6), e2025JG008863. https://doi.org/10.1029/2025JG008863

Hilton, D. R., Grönvold, K., Macpherson, C. G., & Castillo, P. R. (1999). Extreme 3He/4He ratios in northwest Iceland: constraining the common component in mantle plumes. *Earth and Planetary Science Letters*, *173*(1–2), 53–60. https://doi.org/10.1016/S0012-821X(99)00215-0

Holland, G., Lollar, B. S., Li, L., Lacrampe-Couloume, G., Slater, G. F., & Ballentine, C. J. (2013). Deep fracture fluids isolated in the crust since the Precambrian era. *Nature*, *497*(7449), 357–360.

https://doi.org/10.1038/NATURE12127;SUBJMETA=209,2151,704;KWRD=GEOCHEMISTRY

Hooper, A. J. (2010). Crystalline geological repository systems: characterisation, site surveying and construction technologies and techniques. *Geological Repository Systems for Safe Disposal of Spent Nuclear Fuels and Radioactive Waste*, 121–152. https://doi.org/10.1533/9781845699789.2.121

Hostettler, B., Reisdorf, A., Jaeggi, D., Deplazes, G., Bläsi, H., Morard, A., Feist-Burkhardt, S., Waltschew, A., Dietze, V., & Menkveld-Gfeller, U. (2017). Litho- and biostratigraphy of the Opalinus Clay and bounding formations in the Mont Terri rock laboratory (Switzerland). *Swiss Journal of Geosciences*, *110*. https://doi.org/10.1007/s00015-016-0250-3

IAEA. (2009). *Geological disposal of radioactive waste: technological implications for retrievability*.

Jackson, M. G., Kurz, M. D., Hart, S. R., & Workman, R. K. (2007). New Samoan lavas from Ofu Island reveal a hemispherically heterogeneous high 3He/4He mantle. *Earth and Planetary Science Letters*, *264*(3–4), 360–374. https://doi.org/10.1016/J.EPSL.2007.09.023

Jensen, M., Lam, T., Luhowy, D., McLay, J., Semec, B., & Frizzell, R. (2009). *Ontario Power Generation's proposed L and ILW deep geologic repository : an overview of geoscientific studies*. 1650.

Jia, Z. H., Zhang, P., Li, L. bin, Chen, Q. W., Liu, J. L., Liu, Y. G., Wu, Q., Yang, Y., Sun, L. T., Yang, G. M., Jiang, W., & Lu, Z. T. (2025). Stability and reliability study of an 39Ar enrichment system for accurate 39Ar dating. *Nuclear Instruments and Methods*

in Physics Research Section A: Accelerators, Spectrometers, Detectors and Associated Equipment, *1075*, 170438. https://doi.org/10.1016/J.NIMA.2025.170438

Jiang, W., Bailey, K., Lu, Z. T., Mueller, P., O'Connor, T. P., Cheng, C. F., Hu, S. M., Purtschert, R., Sturchio, N. C., Sun, Y. R., Williams, W. D., & Yang, G. M. (2012). An atom counter for measuring 81Kr and 85Kr in environmental samples. *Geochimica et Cosmochimica Acta*, *91*, 1–6. https://doi.org/10.1016/J.GCA.2012.05.019

Johnson, C., Aalseth, C. E., Alexander, T. R., Bowyer, T. W., Chipman, V., Day, A. R., Drellack, S., Fast, J. E., Fritz, B. G., Hayes, J. C., Huckins-Gang, H. E., Humble, P., Kirkham, R. R., Lowrey, J. D., Mace, E. K., Mayer, M. F., McIntyre, J. I., Milbrath, B. D., Panisko, M. E., … Zhong, L. (2019). Migration of noble gas tracers at the site of an underground nuclear explosion at the Nevada National Security Site. *Journal of Environmental Radioactivity*, *208–209*. https://doi.org/10.1016/J.JENVRAD.2019.106047

Johnson, S. (2025). *Sweden starts building 100,000 year storage site for spent nuclear fuel | Reuters*. https://www.reuters.com/business/energy/sweden-starts-building-100000-year-storage-site-spent-nuclear-fuel-2025-01-15/

Jones, A. (2023). *Site for Canada's underground nuclear waste repository to be selected next year | Globalnews.ca*. Global News. https://globalnews.ca/news/10191441/site-canada-nuclear-waste-ontario/

Jordan, P., Wetzel, A., & Reisdorf, A. G. (2008). Jurassic. Swiss Jura Mountains. *The Geology of Central Europe*, *2*, 880–889.

Joseph, C., Schmeide, K., Sachs, S., Brendler, V., Geipel, G., & Bernhard, G. (2011). Sorption of uranium(VI) onto Opalinus Clay in the absence and presence of humic

acid in Opalinus Clay pore water. *Chemical Geology*, *284*(3–4), 240–250. https://doi.org/10.1016/J.CHEMGEO.2011.03.001

Keller, L. M., Schuetz, P., Erni, R., Rossell, M. D., Lucas, F., Gasser, P., & Holzer, L. (2013). Characterization of multi-scale microstructural features in Opalinus Clay. *Microporous and Mesoporous Materials*, *170*, 83–94. https://doi.org/10.1016/J.MICROMESO.2012.11.029

Kennedy, B. M., Hiyagon, H., & Reynolds, J. H. (1990). Crustal neon: a striking uniformity. *Earth and Planetary Science Letters*, *98*(3–4), 277–286. https://doi.org/10.1016/0012-821X(90)90030-2

Ketonen, K. (2024). *Ignace council votes in favour of potential nuclear waste repository | CBC News*. CBC News. https://www.cbc.ca/news/canada/thunder-bay/ignace-nuclear-waste-vote-1.7259610

Kraev, K. (2025). *Finland Completes Key Trial For World's First Deep Geological Nuclear Waste Repository*. https://www.nucnet.org/news/finland-completes-key-trial-for-world-s-first-deep-geological-nuclear-waste-repository-3-2-2025?utm

Lavielle, B., Matray, J. M., Thomas, B., Dauzères, A., Bensenouci, F., & Gilabert, E. (2012). Stages of evolution of a Toarcian compacted claystone around galleries excavated between 1 and 124 years ago by the study of noble gases dissolved in pore water at the Tournemire Underground Research Laboratory (France). *Applied Geochemistry*, *27*(7), 1403–1416. https://doi.org/10.1016/J.APGEOCHEM.2012.01.006

Law, S. (2024). *Northwestern Ontario communities chosen for Canada's nuclear waste storage site | CBC News*. CBC News. https://www.cbc.ca/news/canada/thunder-bay/nuclear-waste-storage-site-chosen-1.7395660

Lippmann, J., Stute, M., Torgersen, T., Moser, D. P., Hall, J. A., Lin, L., Borcsik, M., Bellamy, R. E. S., & Onstott, T. C. (2003). Dating ultra-deep mine waters with noble gases and 36Cl, Witwatersrand Basin, South Africa. *Geochimica et Cosmochimica Acta*, *67*(23), 4597–4619. https://doi.org/10.1016/S0016-7037(03)00414-9

Lippmann-Pipke, J., Sherwood Lollar, B., Niedermann, S., Stroncik, N. A., Naumann, R., van Heerden, E., & Onstott, T. C. (2011). Neon identifies two billion year old fluid component in Kaapvaal Craton. *Chemical Geology*, *283*(3–4), 287–296. https://doi.org/10.1016/J.CHEMGEO.2011.01.028

Loosli, H. (1992). *Applications of 37Ar, 39Ar and 85Kr in hydrology, oceanography and atmospheric studies. Current state of the art*. https://inis.iaea.org/records/2yvnc-nb637

Lu, Z.-T., Schlosser, P., Smethie, W. M., Sturchio, N. C., Fischer, T. P., Kennedy, B. M., Purtschert, R., Severinghaus, J. P., Solomon, D. K., Tanhua, T., & Yokochi, R. (2014). Tracer applications of noble gas radionuclides in the geosciences. *Earth-Science Reviews*, *138*, 196–214. https://doi.org/10.1016/j.earscirev.2013.09.002

Maineult, A., Thomas, B., Nussbaum, C., Wieczorek, K., Gibert, D., Lavielle, B., Kergosien, B., Nicollin, F., Mahiouz, K., & Lesparre, N. (2013). Anomalies of noble gases and self-potential associated with fractures and fluid dynamics in a horizontal borehole, Mont Terri Underground Rock Laboratory. *Engineering Geology*, *156*, 46–57. https://doi.org/10.1016/J.ENGGEO.2013.01.010

Mazurek, M., Alt-Epping, P., Bath, A., Gimmi, T., Niklaus Waber, H., Buschaert, S., Cannière, P. de, Craen, M. de, Gautschi, A., Savoye, S., Vinsot, A., Wemaere, I., & Wouters, L. (2011). Natural tracer profiles across argillaceous formations. *Applied*

Geochemistry, *26*(7), 1035–1064. https://doi.org/10.1016/J.APGEOCHEM.2011.03.124

Mazurek, M., & Antoine De Haller, •. (2018). *Pore-water evolution and solute-transport mechanisms in Opalinus Clay at Mont Terri and Mont Russelin (Canton Jura, Switzerland)*. 131–151. https://doi.org/10.1007/978-3-319-70458-6_7

McDougall, Ian., & Harrison, T. Mark. (1999). *Geochronology and thermochronology by the 40AR* (2nd ed.). Oxford University Press; Clarendon Press.

Mont Terri. (2023). *Interior view*. Mont Terri Project. https://www.mont-terri.ch/en/interior-view

Moreira, M. (2007). Constraints on the origin of the 129Xe on Earth using the tellurium double beta decay. *Earth and Planetary Science Letters*, *264*(1–2), 114–122. https://doi.org/10.1016/J.EPSL.2007.09.014

Musy, S., Casolaro, P., Dellepiane, G., Berger, A., Braccini, S., & Purtschert, R. (2022). Quantification of 37Ar emanation fractions from irradiated natural rock samples and field applications. *Journal of Environmental Radioactivity*, *251–252*, 106966. https://doi.org/10.1016/J.JENVRAD.2022.106966

Musy, S., Meyzonnat, G., Barbecot, F., Hunkeler, D., Sültenfuss, J., Solomon, D. K., & Purtschert, R. (2021). In-situ sampling for krypton-85 groundwater dating. *Journal of Hydrology X*, *11*, 100075. https://doi.org/10.1016/J.HYDROA.2021.100075

Musy, S., & Purtschert, R. (2023). Reviewing 39Ar and 37Ar underground production in shallow depths with implications for groundwater dating. *Science of The Total Environment*, *884*, 163868. https://doi.org/10.1016/J.SCITOTENV.2023.163868

NAGRA. (2024). *Geosynthesis of Northern Switzerland (NTB 24-17)*. https://www.drbg.ch/rbg-gtl/zentrale-referenzberichte/geosynthesis-of-northern-switzerland-ntb-24-17/5-key-characteristics-of-the-host-rock-and-clay-mineral-rich-confining-units-as-geological-barriers-ntb-24-17/2738-5-10-overall-conclusions-on-key-characteristics-of-the-host-rock-and-confining-units-ntb-24-17

Neretnieks, I. (2013). Some aspects of release and transport of gases in deep granitic rocks: Possible implications for nuclear waste repositories. *Hydrogeology Journal*, *21*(8), 1701–1716. https://doi.org/10.1007/S10040-013-0986-Z/FIGURES/16

NOAA. (2024). *The Atmosphere | National Oceanic and Atmospheric Administration*. https://www.noaa.gov/jetstream/atmosphere

Noronha, J. (2016). *Deep Geological Repository Conceptual Design Report Crystalline / Sedimentary Rock Environment*. www.nwmo.ca

Nuclear Engineering International. (2025a). *French Cigéo HLW repository cost estimate - Nuclear Engineering International*. https://www.neimagazine.com/news/french-cigeo-hlw-repository-cost-estimate/?cf-view

Nuclear Engineering International. (2025b). *Special Report - Canada's GDF: Going far, together - Nuclear Engineering International*. https://www.neimagazine.com/analysis/special-report-canadas-gdf-going-far-together/?cf-view

Nussbaum, C., Bossart, P., Amann, F., & Aubourg, C. (2011). Analysis of tectonic structures and excavation induced fractures in the Opalinus Clay, Mont Terri underground rock laboratory (Switzerland). *Swiss Journal of Geosciences*, *104*(2), 187–210. https://doi.org/10.1007/s00015-011-0070-4

Nussbaum, C., Kloppenburg, A., Caër, T., & Bossart, P. (2017). Tectonic evolution around the Mont Terri rock laboratory, northwestern Swiss Jura: constraints from kinematic forward modelling. *Swiss Journal of Geosciences*, *110*(1), 39–66. https://doi.org/10.1007/S00015-016-0248-X/FIGURES/14

NWMO. (2019). *Postclosure Safety Assessment of a Used Fuel Repository in Sedimentary Rock*. Nuclear Waste Management Organization. https://iaac-aeic.gc.ca/050/documents/p17520/117100E.pdf

NWMO. (2024). *The Nuclear Waste Management Organization selects site for Canadas deep geological repository*. https://www.nwmo.ca/News/The-Nuclear-Waste-Management-Organization-selects-site-for-Canadas-deep-geological-repository

NWMO. (2025). *Canada's plan*. https://www.nwmo.ca/canadas-plan

Osenbrück, K., Lippmann, J., & Sonntag, C. (1998). Dating very old pore waters in impermeable rocks by noble gas isotopes. *Geochimica et Cosmochimica Acta*, *62*(18), 3041–3045. https://doi.org/10.1016/S0016-7037(98)00198-7

Oxburgh, E. R., & O'Nions, R. K. (1987). Helium Loss, Tectonics, and the Terrestrial Heat Budget. *Science*, *237*(4822), 1583–1588. https://doi.org/10.1126/SCIENCE.237.4822.1583

Palcsu, L., Molnar, M., Szanto, Zs., Svingor, E., Futo, I., & Pinter, T. (2001). Dissolved stable noble gas measurements from primary water of Paks NPP. *Proceedings of the International Conference Nuclear Energy in Central Europe 2001*, 7–7. https://inis.iaea.org/records/5c3ss-st528

Peeters, F., Beyerle, U., Aeschbach-Hertig, W., Holocher, J., Brennwald, M. S., & Kipfer, R. (2003). Improving noble gas based paleoclimate reconstruction and groundwater

dating using 20Ne/22Ne ratios. *Geochimica et Cosmochimica Acta*, *67*(4), 587–600. https://doi.org/10.1016/S0016-7037(02)00969-9

Porcelli, D., Ballentine, C., Chris, J., & Wieler, R. (2002). *Noble Gases in Geochemistry and Cosmochemistry*. De Gruyter.

Purtschert, R., Yokochi, R., Jiang, W., Lu, Z. T., Mueller, P., Zappala, J., van Heerden, E., Cason, E., Lau, M., Kieft, T. L., Gerber, C., Brennwald, M. S., & Onstott, T. C. (2021). Underground production of 81Kr detected in subsurface fluids. *Geochimica et Cosmochimica Acta*, *295*, 65–79. https://doi.org/10.1016/J.GCA.2020.11.024

Radwaste Solutions. (2024a). *Canada lands on spent fuel repository site -- ANS / Nuclear Newswire*. https://www.ans.org/news/article-6603/canada-lands-on-spent-fuel-repository-site/

Radwaste Solutions. (2024b). *Sweden's SKB approved to begin construction of spent fuel repository -- ANS / Nuclear Newswire*. https://www.ans.org/news/article-6520/swedens-skb-approved-to-begin-construction-of-spent-fuel-repository/

Ramana, M. v. (2013). Shifting strategies and precarious progress: Nuclear waste management in Canada. *Energy Policy*, *61*, 196–206. https://doi.org/10.1016/J.ENPOL.2013.05.085

Raven, K., McCreath, D., Jackson, R., Clark, I., Heagle, D., Sterling, S., & Melaney, M. (2011). Descriptive Geosphere Site Model. In *NWMO DGR-TR-2011-24*. https://ceaa-acee.gc.ca/050/documents_staticpost/17520/49820/site_model.pdf

Reynolds, J. H. (1960). Determination of the Age of the Elements. *Physical Review Letters*, *4*(1), 8. https://doi.org/10.1103/PhysRevLett.4.8

Riedmann, R. A., & Purtschert, R. (2011). Natural 37Ar concentrations in soil air: Implications for monitoring underground nuclear explosions. *Environmental Science and Technology*, *45*(20), 8656–8664. https://doi.org/10.1021/ES201192U

Rübel, A. P., Sonntag, C., Lippmann, J., Pearson, F. J., & Gautschi, A. (2002). Solute transport in formations of very low permeability: profiles of stable isotope and dissolved noble gas contents of pore water in the Opalinus Clay, Mont Terri, Switzerland. *Geochimica et Cosmochimica Acta*, *66*(8), 1311–1321. https://doi.org/10.1016/S0016-7037(01)00859-6

Seltzer, A. M., Krantz, J. A., Ng, J., Danskin, W. R., Bekaert, D. v., Barry, P. H., Kimbrough, D. L., Kulongoski, J. T., & Severinghaus, J. P. (2021). The triple argon isotope composition of groundwater on ten-thousand-year timescales. *Chemical Geology*, *583*, 120458. https://doi.org/10.1016/J.CHEMGEO.2021.120458

Severinghaus, J. P., Grachev, A., Luz, B., & Caillon, N. (2003). A method for precise measurement of argon 40/36 and krypton/argon ratios in trapped air in polar ice with applications to past firm thickness and abrupt climate change in Greenland and at Siple Dome, Antarctica. *Geochimica et Cosmochimica Acta*, *67*(3), 325–343. https://doi.org/10.1016/S0016-7037(02)00965-1

Siren, T. (2017). Overview of Finnish Spent Nuclear Fuel Disposal Programme. *Journal of the Korean Society of Mineral and Energy Resources Engineers 2017 54:4*, *54*(4), 367–376. https://doi.org/10.12972/KSMER.2017.54.4.367

Solomon, D. K., Schiff, S. L., Poreda, R. J., & Clarke, W. B. (1993). A validation of the 3H/3He method for determining groundwater recharge. *Water Resources Research*, *29*(9), 2951–2962. https://doi.org/10.1029/93WR00968

Staudacher, T., & Allègre, C. J. (1982). Terrestrial xenology. *Earth and Planetary Science Letters*, *60*(3), 389–406. https://doi.org/10.1016/0012-821X(82)90075-9

Szewczyk, Z. J., & West, G. F. (1976). Gravity study of an Archean granitic area northwest of Ignace, Ontario. *https://doi.org/10.1139/E76-114*, *13*(8), 1119–1130. https://doi.org/10.1139/E76-114

Tomonaga, Y., Giroud, N., Brennwald, M. S., Horstmann, E., Diomidis, N., Kipfer, R., & Wersin, P. (2019). On-line monitoring of the gas composition in the Full-scale Emplacement experiment at Mont Terri (Switzerland). *Applied Geochemistry*, *100*, 234–243. https://doi.org/10.1016/J.APGEOCHEM.2018.11.015

Torgersen, T. (2010). Continental degassing flux of 4He and its variability. *Geochemistry, Geophysics, Geosystems*, *11*(6), 6002. https://doi.org/10.1029/2009GC002930;PAGEGROUP:STRING:PUBLICATION

Torgersen, T., Kennedy, B. M., & van Soest, M. C. (2004). Diffusive separation of noble gases and noble gas abundance patterns in sedimentary rocks. *Earth and Planetary Science Letters*, *226*(3–4), 477–489. https://doi.org/10.1016/J.EPSL.2004.07.030

Tsang, C. F., Neretnieks, I., & Tsang, Y. (2015). Hydrologic issues associated with nuclear waste repositories. *Water Resources Research*, *51*(9), 6923–6972. https://doi.org/10.1002/2015WR017641

van Loon, L. R., Soler, J. M., Müller, W., & Bradbury, M. H. (2004). Anisotropic Diffusion in Layered Argillaceous Rocks: A Case Study with Opalinus Clay. *Environmental Science and Technology*, *38*(21), 5721–5728. https://doi.org/10.1021/ES049937G

Villamizar, B. J. G., DesRoches, A., Parmenter, A., & Sykes, E. (2023). Spatial Characterization of Shallow Structures in the Revell Batholith Integrating Seismic

Imaging Techniques. *Pure and Applied Geophysics*, *180*(12), 4081–4107. https://doi.org/10.1007/S00024-023-03382-Z/FIGURES/17

Warr, O., Ballentine, C. J., Onstott, T. C., Nisson, D. M., Kieft, T. L., Hillegonds, D. J., & Sherwood Lollar, B. (2022). 86Kr excess and other noble gases identify a billion-year-old radiogenically-enriched groundwater system. *Nature Communications*, *13*(1), 1–9. https://doi.org/10.1038/S41467-022-31412-2;TECHMETA=140,58;SUBJMETA=209,242,4112,445,47,704;KWRD=BIOGEOCHEMISTRY,ELEMENT+CYCLES,GEOCHEMISTRY,HYDROLOGY

Warr, O., Sherwood Lollar, B., Fellowes, J., Sutcliffe, C. N., McDermott, J. M., Holland, G., Mabry, J. C., & Ballentine, C. J. (2018). Tracing ancient hydrogeological fracture network age and compartmentalisation using noble gases. *Geochimica et Cosmochimica Acta*, *222*, 340–362. https://doi.org/10.1016/J.GCA.2017.10.022

Wermeille, S., & Bossart, P. (1999). *Paleohydrological Study on the Surroundings of the Mont Terri Rock Laboratory* (Issues 99–01).

Wetherill, G. W. (1954). Variations in the Isotopic Abundances of Neon and Argon Extracted from Radioactive Minerals. *Physical Review*, *96*(3), 679. https://doi.org/10.1103/PhysRev.96.679

Wilson, G. B., & McNeill, G. W. (1997). Noble gas recharge temperatures and the excess air component. *Applied Geochemistry*, *12*(6), 747–762. https://doi.org/10.1016/S0883-2927(97)00035-8

World Commission on Environment and Development. (1987). *Report of the World Commission on Environment and Development: Our Common Future Towards Sustainable Development 2. Part II. Common Challenges Population and Human Resources 4*.

World Nuclear Association. (2024). *Storage and Disposal of Radioactive Waste - World Nuclear Association*. https://world-nuclear.org/information-library/nuclear-fuel-cycle/nuclear-waste/storage-and-disposal-of-radioactive-waste

World Nuclear Association. (2025). *Radioactive Waste – Myths and Realities - World Nuclear Association*. https://world-nuclear.org/information-library/nuclear-fuel-cycle/nuclear-waste/radioactive-wastes-myths-and-realities

Yamamoto, J., Kaneoka, I., Nakai, S., Kagi, H., Prikhod'ko, V. S., & Arai, S. (2004). Evidence for subduction-related components in the subcontinental mantle from low 3He/4He and 40Ar/36Ar ratio in mantle xenoliths from Far Eastern Russia. *Chemical Geology*, *207*(3–4), 237–259. https://doi.org/10.1016/J.CHEMGEO.2004.03.007

Yang, G. M., Cheng, C. F., Jiang, W., Lu, Z. T., Purtschert, R., Sun, Y. R., Tu, L. Y., & Hu, S. M. (2013). Analysis of 85Kr: a comparison at the 10-14 level using micro-liter samples. *Scientific Reports 2013 3:1*, *3*(1), 1–5. https://doi.org/10.1038/srep01596

Zhou, Z., & Ballentine, C. J. (2006). 4He dating of groundwater associated with hydrocarbon reservoirs. *Chemical Geology*, *226*(3–4), 309–327. https://doi.org/10.1016/J.CHEMGEO.2005.09.030

Zuo, E., Lapp, A., Jautzy, J. J., & Clark, I. D. (2022). Crustal Noble Gas Isotopic Characteristics in Low-Permeability Ordovician Sedimentary Rock, Eastern Flank of the Michigan Basin. *ACS Earth and Space Chemistry*, *6*(1), 189–196. https://doi.org/10.1021/ACSEARTHSPACECHEM.1C00346

CHAPTER 2: EVALUATION OF APPROACHES TO DERIVE POREWATER NOBLE GAS CONCENTRATIONS

2.1 Introduction

The overarching PC-D project seeks to characterize cores of the Opalinus Clay (OPA) material (see section 1.6-8 and Appendix A) with respect to porewater noble gas content. This inter-laboratory comparison will evaluate the varying approaches posited by each laboratory to derive the noble gas isotopic concentrations of the porewater of the OPA from the raw isotopic concentrations within the stainless-steel cylinder headspace. Specifically, the project seeks to identify optimal sample collection, storage, extraction, and data processing to ensure standardisation in interpretations of porewater noble gases with respect to characterising crustal settings being prospected for future DGR sites. This will be accomplished by the study of a homogeneous, argillaceous-type setting as an analogue for potential future repositories (Rübel et al., 2002, Bossart and Thury, 2007; Bossart et al., 2017a,b).

Within the framework of the overall PC-D project, the University of Ottawa was tasked with the analysis and estimation of porewater noble gas concentrations for five cores stored in stainless-steel cylinders.

This chapter will focus on three different methods to reconstruct initial porewater noble gas content based on measured headspace data, with respect to the OPA material and its various characteristics, such as porosity, average water content, and porewater ^{20}Ne enrichment.

2.2 Materials and Methods

2.2.1 Sample preparation

First, the samples were removed from the evacuated bag (prepared per section 1.7), and the cores were dry cut with a diamond circular saw to remove the outer rim and were then each cubed such that each was the same size, shape, and volume. These cores were then sealed in stainless-steel cylinders (diameter = 8.49 cm, volume = 1115 cm^3) which were then nitrogen-

flushed and vacuum pumped. Following this, they were then nitrogen-flushed and then vacuum pumped once more, reaching a final pressure between 0.022 and 0.027 bar (i.e., vacuum-pumped twice). The time between the opening of the evacuated bags and sealing in the stainless-steel cylinders was between 8 and 12 minutes. A full list of samples (with both sample encapsulation methods) is provided in Table B.1 in Appendix B. The other two sets of samples collected in the stainless-steel cylinders were sent to Hydroisotop GmbH and BGR (Germany) where they were analysed independently and the data will be combined in an upcoming PC-D report combining the three datasets.

2.2.2 Sub-sample aliquoting procedure

Samples analysed as part of this study were prepared on-site at the Mont Terri rock laboratory per the procedures outlined in section 1.6. Samples were collected and prepared in September 2021; however, analysis was not conducted until December 2024, leading to over three years for diffusion of noble gases, water vapour, and other constituent gases into the headspace of the stainless-steel cylinders. Initially, the stainless-steel cylinders were planned to be interfaced directly to the existing noble gas sample extraction and purification line (hereby referred to as the "extraction line") inlet. However, based on calculations, it was anticipated that the stainless-steel cylinders would contain substantial concentrations of noble gases and water vapour, quantities too large for the current noble gas extraction and measurement system to purify, aliquot, and analyse effectively. To address this, the use of a drierite (desiccant) trap was considered, similar to the method employed by Zuo et al. (2022). However, there were significant concerns about this, given the unknown impact this may have on the noble gases being extracted and the lack of additional supporting literature validating its use in such applications.

Consequently, it was decided that the stainless-steel cylinder samples would be aliquoted into smaller sub-samples prior to introduction to the noble gas manifold using a length of ¼" copper

tubing. This approach is a standard protocol based on existing methodology currently applied in the University of Ottawa noble gas laboratory for inletting noble gas samples derived from gas or vacuum cylinders and required little adaptation for these solid-phase samples.

The aliquoting process was as follows, and the setup used to take the aliquots is depicted in Figure 2.1 First, a pre-configured ¼" Type-K copper tube of length 33 cm, was attached directly to the stainless-steel sample container. This length allowed triplicate 6 cm lengths (for aliquoting ~1.05cm^3) plus 7.5 cm of additional allowance at both ends of the copper tubing which accounted for tube bending and crimping. One end of the copper tube was bent 90° and the other end was bent 30°, a setup optimized for the angle of the sample inlet. A standard ¼" Swagelok tube connection was attached to each end, and the tube was interfaced to the canister and extraction line per Figure 2.1, below:

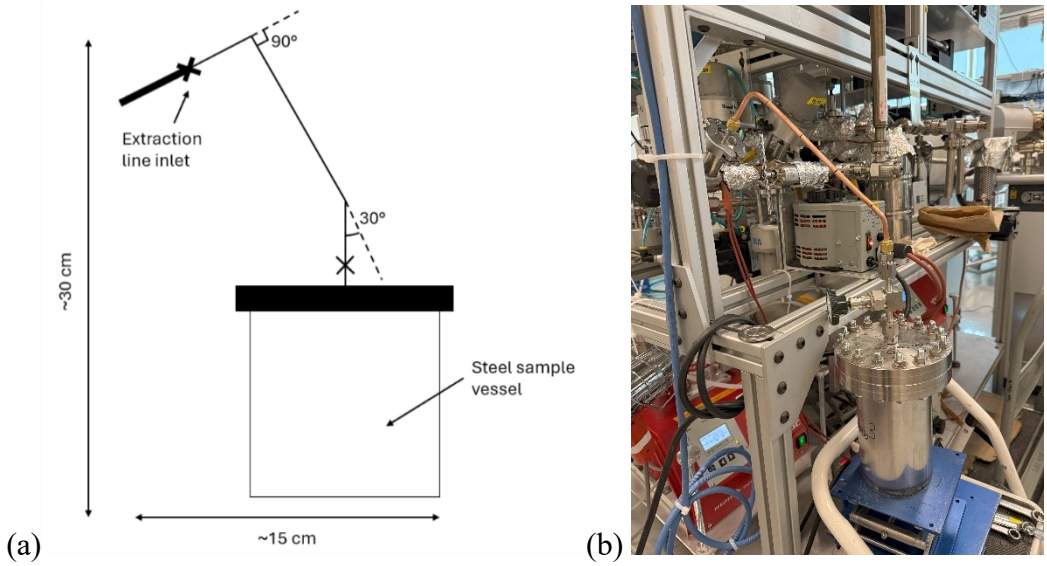

Figure 2.1a and Figure 2.1b: Schematic and photograph showing the setup of the stainless-steel cylinder interfaced with the inlet section of the noble gas extraction line.

Once the tube and cylinder were interfaced to the extraction line, the copper tubing was pumped down to baseline vacuum pressure overnight using the turbo pump, which is approximately 1 × 10^{-5} Torr or below (i.e., approximately below 1.33 × 10^{-5} mbar). The following day, the

integrity of the vacuum was confirmed via leak-checking by observing the baseline vacuum and then closing the turbo pump valve and observing the rate of pressure rise. Where the observed pressure was less than 1×10^{-4} Torr (i.e., approximately 1.33×10^{-4} mbar) or less over 15 minutes, the system was considered sufficiently isolated from the atmosphere and ready for extraction as follows. First, the turbo pump valve was reopened, the copper tube was crimped off at the pump end, ensuring a closed setup ready for expansion of the sample into the copper tube. As before, the pressure reading on the extraction line inlet side was observed to ensure no leaks occurred during this stage.

Next, the sample valve was then opened for 2 minutes to allow for equilibration of the copper tube volume with the sample headspace, after which it was then closed. Following this, as a final step, the copper tube was crimped at each of the four tick marks, starting at the lowermost tick mark (see Figure 2.1b) to create triplicate copper tube aliquots of 6 cm lengths containing the headspace gas, equivalent to an aliquot volume of ~1.05 cm^3.

2.2.3 UQAM-GEOTOP Noble Gas Extraction and Purification

Following the sample aliquoting carried out at the University of Ottawa, the copper tube samples (including a set of blanks) were measured at the UQAM-GEOTOP Noble Gas Laboratory in Montréal. The experimental setup consisted of a Helix-MC Plus Mass Spectrometer, equipped with a Faraday cup and a Compact Discrete Dynode (CDD) detector (multiplier), connected to a sample noble gas extraction and purification line, with an Advanced Research Systems (ARS) activated charcoal cryogenic trap. As per convention, all data was normalized to the atmospheric standard (1.399×10^{-6}, Porcelli et al., 2002). The air standards run utilised the "laboratory air" where pressure and temperature conditions are well monitored, before being purified on the getters for three hours.

Procedural blanks and standards were run prior to each sample for normalization and background corrections. These followed the same protocols as detailed here for samples with

the exception being that gettering would only take place for 10 minutes, with 5 minute "break" intervals between each gettering cycle due to the limited lifespan of the getters and the reduced gas load.

To analyse the copper tube sub-samples, a specialised device was used to open the copper tube under vacuum. This device used for inletting the copper tube aliquots is composed of a manual valve (used to push open the crimped end of the copper tube), a sapphire glass display port, and a soft-seal KF fitting to load the sample. This device was connected to the extraction line via a bellows with a VCR connection, mounted via clamp to the frame of the extraction line, see Figure 2.2a and 2.2b.

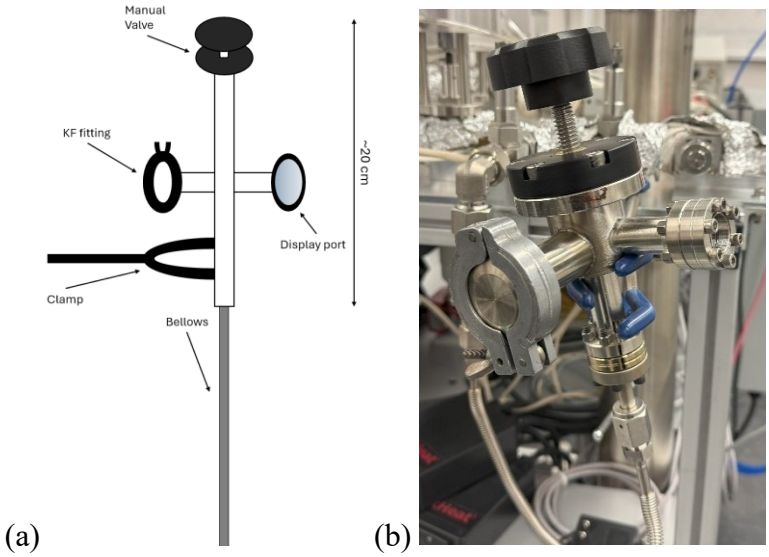

Figure 2.2a and Figure 2.2b: The custom inletting device used to open the copper tubes under vacuum, copper tube inlet into the KF fitting.

The isotopic sample purification and analysis from sections 2.2.3 through 2.2.5 were carried out per Poblete-Gonzáles et al. (2025). The copper tube inlet device was pumping overnight to a pressure of 1.27×10^{-7} mbar the following morning. The sample was then opened under vacuum via the manual valve, and the gas was expanded from the inlet device into a known and calibrated volume for 2 minutes. After this period, the calibrated volume was closed and

pressure reading taken. Following this, the gas in this calibrated volume was purified as follows. First, the contents of the inlet were purified to remove reactive (i.e., non-noble) gases from the sample using a series of three 99.8% pure Ti and ST-707 alloy (SAES) getters. The sample was first introduced to Getter 1 (G1) at 600°C for a 15-minute period. Afterwards, the getter was cooled to room temperature for 10 minutes, prior to introduction to Getter 2 (G2), also at 600°C for 15 minutes, after which the getter was cooled to room temperature for another 10 minutes. The sample was then introduced to Getter 3 (G3), at 125°C, for 15 minutes, and finally, the getter was then cooled once more for a 10-minute period.

After gettering, the sample was then opened to a cryogenic trap, set at 9 K for 15 minutes to allow all noble gases to be trapped. After this trapping stage was complete, the system was briefly opened to the turbo pump for 10 seconds to remove any final residual reactive gases.

2.2.4 Helium Analysis

The cryogenic trap temperature setpoint was raised to 40 K for 20 minutes to facilitate release of helium The temperature release profile of the UQAM-GEOTOP cryogenic trap is depicted in Figure 2.3.

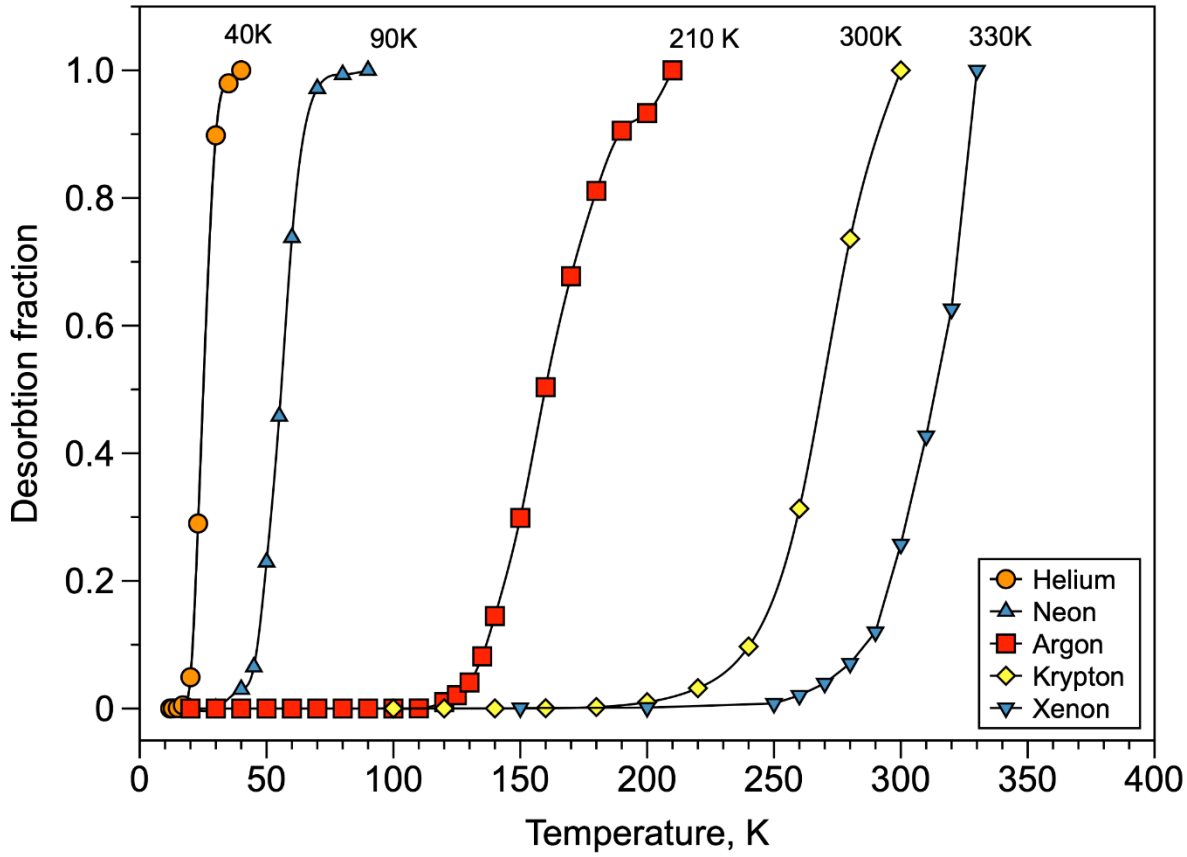

Figure 2.3: UQAM-GEOTOP cryogenic trap (ACT) temperature release profile by noble gas (Kambale Kavyavu et al., 2025).

After this 20-minute period, the ion pump on the mass spectrometer was closed, and the mass spectrometer inlet valve was opened for 1 minute to introduce helium into the mass spectrometer. ^{3}He was measured by ion counting on the axial Compact Discrete Dynode (CDD) detector due to its low abundance, and ^{4}He was measured on the Faraday cup. To promote equilibration, 30 seconds was given for the standard to inlet and fill the mass spectrometer, before the inlet valve was closed. Peak centring was then manually performed several times during analysis on the ^{3}He and ^{4}He peaks, before the sample was run for 60 measurement cycles. While running, the entire extraction line was opened to the turbo pump to clear helium from the line and from the cryogenic section. The mass spectrometer inlet and the cryogenic trap were then isolated again, and the temperature setpoint of the cryogenic trap was increased to 90 K for 20 minutes to release neon from the trap for analysis.

2.2.5 Neon Analysis

Following helium analysis, the mass spectrometer ion pump was opened for 10 seconds to fully pump any residual helium, after which it was then closed. As with helium analysis, the inlet valve was then opened for 1 minute equilibration time with the cryogenic trap for neon analysis, after which it was then closed. Peak centring was then run once again, following the same procedure as with the helium analysis. The purified neon was then analysed for each of the neon isotopes, ^{20}Ne, ^{21}Ne, and ^{22}Ne, taking 30 measurements of each. While ^{20}Ne and ^{22}Ne were measured on the Faraday cup, ^{21}Ne was measured by the axial CDD detector in ion counting mode due to its very low enrichment. While running, the entire extraction line was opened to the turbo pump to evacuate any residual neon before the cryogenic trap and mass spectrometer inlet were isolated again. The cryogenic trap was heated to 220 K for subsequent argon release.

2.2.6 Argon Analysis

Following neon analysis, the inlet process for argon is identical to neon, however, given the considerably higher natural abundance of argon, 3 dilutions were taken in a known volume on the extraction line. All argon isotopes (^{36}Ar, ^{38}Ar, and ^{40}Ar) were measured on the Faraday cup for 30 measurement cycles. Once argon had been measured, the mass spectrometer ion pump was opened to remove the residual argon and restore vacuum. During the analysis, the temperature of the cryogenic trap was set to 250 K to enable the release and pumping of any residual gases for 30 minutes. The extraction line was fully evacuated, removing all contaminants from all sections by opening the valves to all 3 getters and the known volume for dilutions. The cryogenic trap was then set back to 9 K for the next analyses.

2.2.6 Blank correction and normalization to air standards

Initially the raw data underwent a blank correction by subtracting the procedural blank values from the corresponding samples and standards. This step ensured that any and all background intensity was accounted for prior to further processing. Table 2.1 represents the concentrations

ascertained by running a procedural blank as a percentage of the measured sample concentrations. After the blank correction, the samples were normalized relative to air via the measured atmospheric standards.

Table 2.1: Results of running a blank, represented as a percentage of the corresponding sample, by noble gas isotope

Sample	^{3}He	^{4}He	^{20}Ne	^{21}Ne	^{22}Ne	^{36}Ar	^{38}Ar	^{40}Ar
1	0.00%	0.00%	2.44%	0.00%	0.00%	3.05%	2.91%	3.17%
2	0.00%	0.00%	0.00%	0.00%	0.00%	0.00%	0.00%	0.00%
3	0.00%	0.00%	0.00%	0.00%	0.00%	1.06%	1.03%	1.15%
4	0.00%	0.00%	0.00%	0.00%	0.00%	0.98%	1.73%	0.97%
5	0.00%	0.00%	0.00%	0.00%	0.00%	0.98%	1.78%	0.89%

2.3 Results

Blank-corrected and air-normalized results were calculated by the UQAM-GEOTOP laboratory in cm^3/cm^3 of sampled headspace gas (cc/cc) at Standard Temperature and Pressure (STP) and are given in Table C.1 (Appendix C) From this point onwards within this section, all concentrations represented in terms of cm^3/cm^3 and reflect the concentrations of each noble gas isotope within the headspace at the time of sampling. For context and comparison, both atmospheric ratios and concentrations are provided. Values for Air Saturated Water (ASW) are also provided and represent the concentration of noble gases in a water phase and is considered representative of initial porewater concentrations following the approaches of Holland et al., 2013; Warr et al., 2018; 2022; Heard et al., 2018. All ASW and air concentrations within this section are derived from Ballentine and Burnard (2002) unless stated otherwise, and ASW concentrations are relative to seawater at 10°C. In this section, each of the concentrations of ^{3}He, ^{4}He, ^{20}Ne, ^{21}Ne, ^{22}Ne, ^{36}Ar, ^{38}Ar, and ^{40}Ar, and the corresponding ratios between these noble gas isotopes will be outlined in turn. All analytical errors in this study were propagated using the standard addition in quadrature method as employed in Warr et al. (2015).

2.3.1 Helium

The most pivotal metric to examine in any noble gas geochemistry study involving the measurement of helium isotopes, is the R/R_a ratio. The R/R_a ratio refers to the ratio of ^3He to ^4He observed within the sample, relative to the atmospheric $^3He/^4He$ ratio (1.399 × 10-6, per Porcelli et al., 2002). Therefore, if our samples exhibited an atmospheric $^3He/^4He$ signature, the R/R_a would be equal to 1. Figure 2.4 represents the R/R_a metric for the porewater within each of the five cores, and how they correspond to the distance along the horizontally drilled borehole:

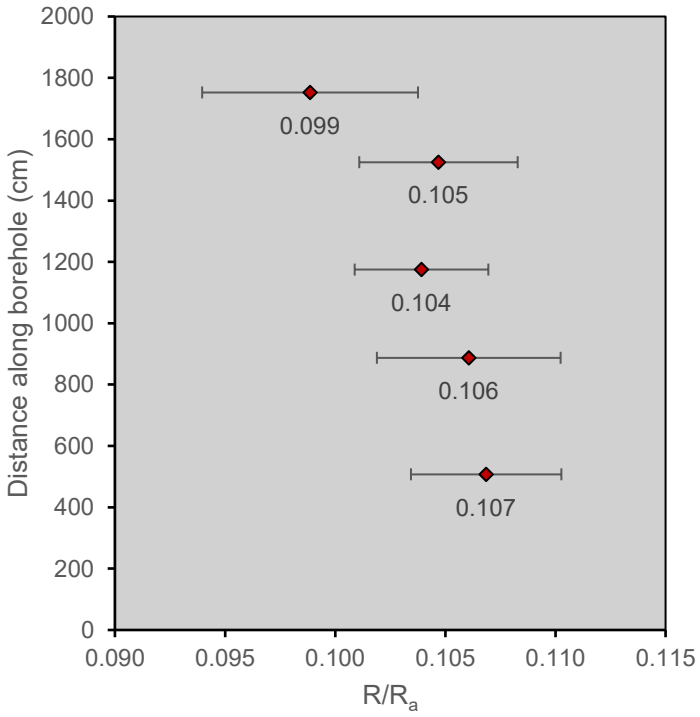

Figure 2.4: R/R_a plot of samples with respect to their core distance along the horizontal borehole.

Overall, there is general agreement across each of the cores, with all values falling within uncertainty of one another, and a mean R/R_a value of 0.104 ± 0.004 across all five cores examined as part of this study. Generally, the shallowest four cores exhibit the most agreement

between one another, with the fifth core at the most distant core interval along the borehole exhibiting a slightly lower R/R_a of 0.099 ± 0.005.

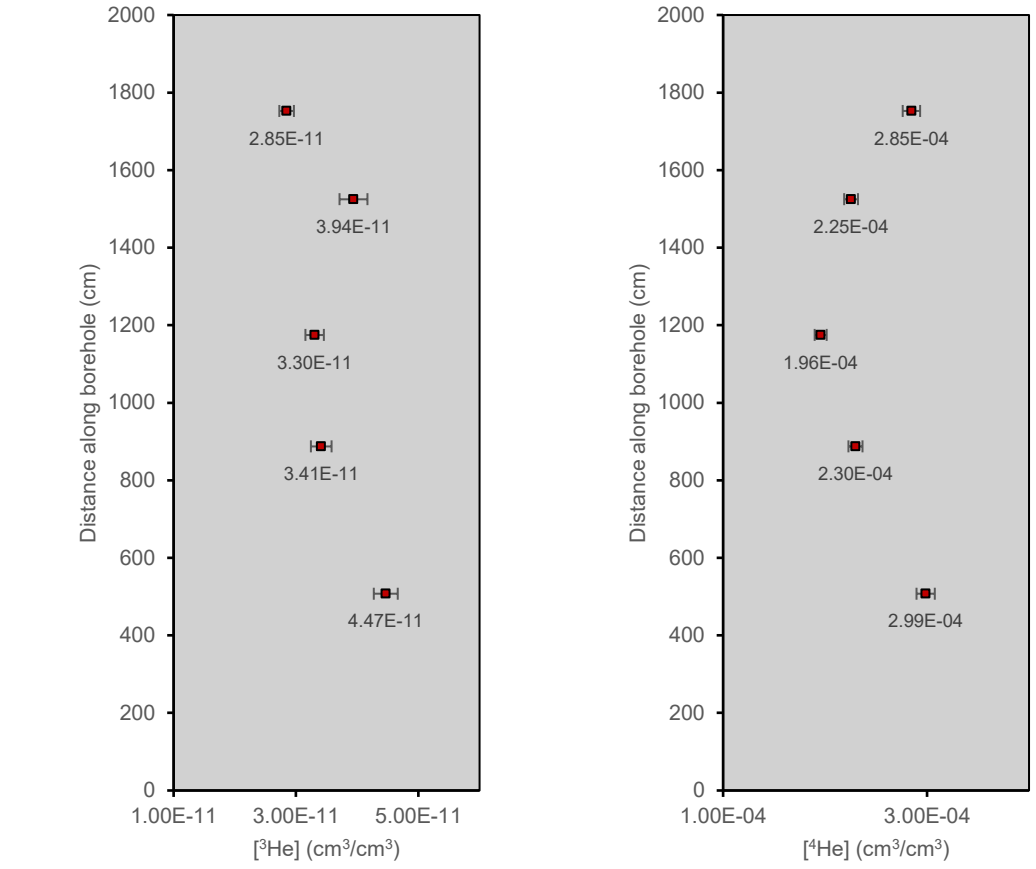

(a) (b)

Figure 2.5a and Figure 2.5b: Plot of ^3He (2.6a) and ^4He (2.6b) concentrations in cm^3STP/cm^3 within the sampled headspace gas with respect to their core distance along the horizontal borehole.

As for the ^3He and ^4He concentrations, these are represented in Figures 2.5a and 2.5b, respectively. With respect to ^3He, the mean concentration from all five samples is approximately $3.59 \times 10^{-11} \pm 5.58 \times 10^{-12}$ cm^3/cm^3. This is 4.9 times greater than the air concentration of ^3He (7.34×10^{-12} cm^3/cm^3). This minimal production of ^3He (relative to ^4He, as mentioned) is indicative of minor thermal neutron capture of ^6Li within the crust (Ballentine and Burnard, 2002). This is consistent with the observed R/R_a values as represented previously,

since the ^{3}He production rate is very minor, and the expected ^{4}He production rate through radiogenic processes is very high. Generally, variation between samples seems to be relatively minimal, with all samples falling within 2 standard deviations of the mean. The lowest ^{3}He concentrations are evident in the deepest sample (2.85×10^{-11} cm^3/cm^3), and the greatest ^{3}He values evident in the shallowest sample (4.47×10^{-11} cm^3/cm^3) – although there is no clear trend between the two.

The mean concentration of ^{4}He is approximately $2.47 \times 10^{-4} \pm 3.87 \times 10^{-5}$. This is 47.11 times greater than the air concentration of ^{4}He (5.24×10^{-6} cm^3/cm^3), which, as previously highlighted by the R_a values, indicate a significant crustal production of radiogenic ^{4}He. As with ^{3}He, variation between samples is fairly low, with all samples again falling within 2 standard deviations of the mean. The lowest ^{4}He concentrations are evident in the sample at depth 1175 cm (1.96×10^{-4} cm^3/cm^3), and the greatest ^{4}He enrichment evident in the sample at depth 507.5 cm (2.99×10^{-4} cm^3/cm^3). While there are too few samples to observe a clear trend, these samples suggest a possible relative decrease in ^{4}He enrichment with depth, from the sample at depth 507.5 to the sample at depth 1175 cm, then begin to increase in ^{4}He after this point, to the sample at depth 1752.5 cm.

2.3.2 Neon

Similar to the helium R/R_a ratio, the $^{20}Ne/^{22}Ne$ ratio can likewise reveal a crustal input via nucleogenic inputs. ^{22}Ne can be produced in small quantities in the crust (see Chapter 1), whereas ^{20}Ne is the dominant neon isotope that is non-radiogenic (Ballentine and Burnard, 2002; Ozima and Podosek, 2002; Warr et al., 2018) and, over time this ratio should decrease from an initial 9.81. The variation of the $^{20}Ne/^{22}Ne$ ratio by sample, plotted against core distance along the horizontally drilled borehole, is shown in Figure 2.6.

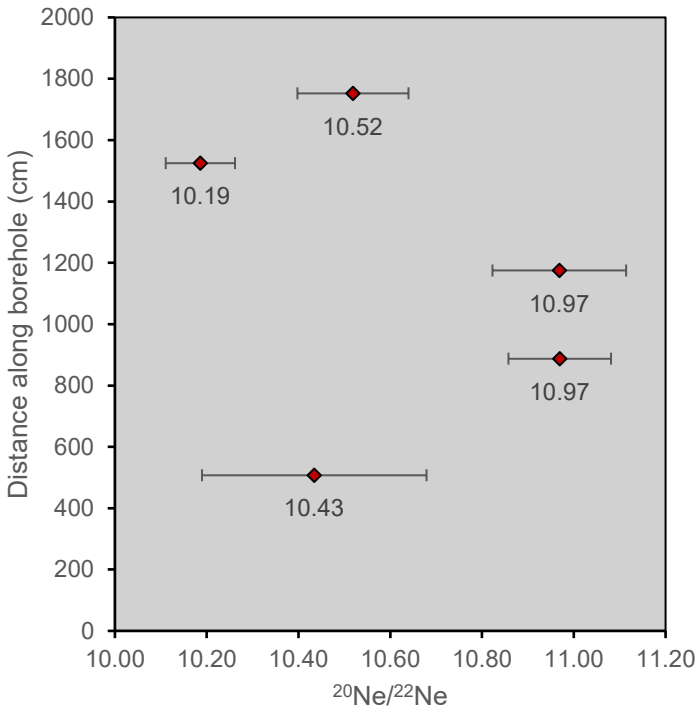

Figure 2.6: $^{20}Ne/^{22}Ne$ plot of samples with respect to their core distance along the horizontal borehole.

The $^{20}Ne/^{22}Ne$ ratio remains somewhat constant. However, the mean $^{20}Ne/^{22}Ne$ is 10.62, and all $^{20}Ne/^{22}Ne$ ratios are observably in excess of the atmospheric $^{20}Ne/^{22}Ne$ ratio of 9.81. This is notable as ^{20}Ne is a primordial noble gas isotope, with no substantive production routes within the crust.

To explore this aspect further, the concentrations of these isotopes observed in the porewater of each core with respect to its distance along the horizontal borehole are represented in Figures 2.7a, 2.7b, and 2.7c.

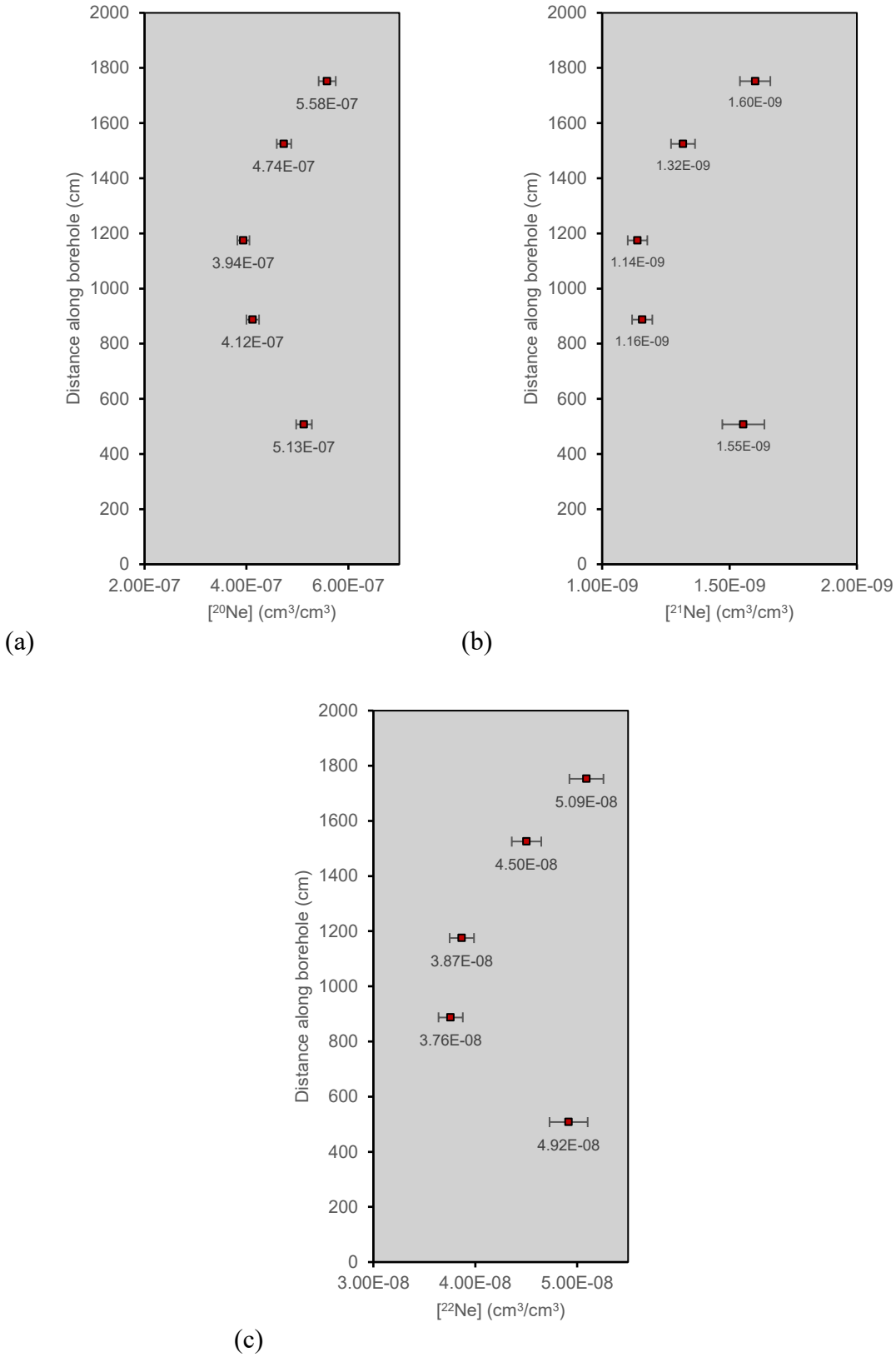

Figure 2.7a, Figure 2.7b, and Figure 2.7c: Concentration plot of ^{20}Ne (2.7a), ^{21}Ne (2.7b), and ^{22}Ne (2.7c) in samples within the sampled headspace with respect to their core distance along the horizontal borehole.

The mean concentration of ^{20}Ne is approximately $4.70 \times 10^{-7} \pm 6.13 \times 10^{-8}$ cm^3/cm^3. In relation to the air concentration of ^{20}Ne (1.65×10^{-5} cm^3/cm^3), the mean sample concentration represents approximately 3% of this. Meanwhile, the mean concentration of ^{21}Ne is approximately $1.35 \times 10^{-9} \pm 1.93 \times 10^{-10}$ cm^3/cm^3. Relative to air, the observed mean sample concentration is approximately 3% of the air concentration (4.87×10^{-8} cm^3/cm^3). Finally, the mean concentration of ^{22}Ne is approximately $4.43 \times 10^{-8} \pm 5.38 \times 10^{-9}$ cm^3/cm^3. Comparative to the air concentration (1.68×10^{-6} cm^3/cm^3), the observed mean sample concentration is again approximately 3% representative of these concentrations.

In summary, all neon isotopes analysed as part of this study exhibit a mean sample concentration approximately 3% of what would be expected within the atmosphere, however the $^{20}Ne/^{22}Ne$ ratio does not indicate any crustal components and instead suggests some potential external contribution or relative enrichment of ^{20}Ne, or fractional depletion/loss of ^{22}Ne due to the $^{20}Ne/^{22}Ne$ of each sample being significantly above the atmospheric ratio of 9.81. This will be discussed further in section 2.4.

2.3.3 Argon

Three stable argon isotopes (^{36}Ar, ^{38}Ar, and ^{40}Ar) were analysed as part of this study. Notably, the $^{40}Ar/^{36}Ar$ ratio is extremely useful, as ^{40}Ar is produced in meaningful quantities within the crust via radioactive decay (see Chapter 1), whereas ^{36}Ar is a non-radiogenic noble gas isotope (Ballentine and Burnard, 2002; Ozima and Podosek, 2002; Warr et al., 2018) and thus should remain at ASW or near-ASW concentrations within the crust. The $^{40}Ar/^{36}Ar$ ratio by sample with respect to core distance along the horizontally drilled borehole is represented in Figure

2.8.

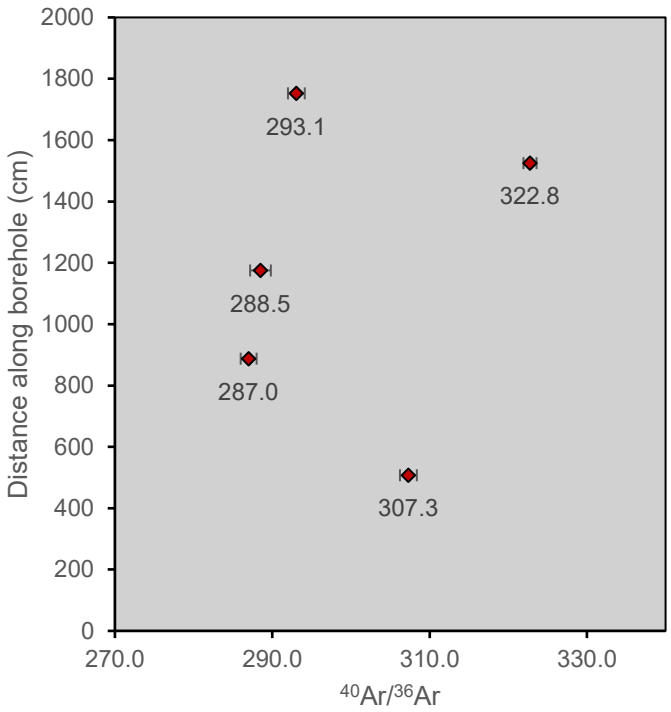

Figure 2.8: $^{40}Ar/^{36}Ar$ plot of samples with respect to their core distance along the horizontal borehole. Note the atmospheric $^{40}Ar/^{36}Ar$ ratio is 295.5 (Ballentine and Burnard, 2002; Warr er al., 2018).

Despite the mean $^{40}Ar/^{36}Ar$ ratio of these samples being approximately 299.7,above the atmospheric $^{40}Ar/^{36}Ar$ ratio of 295.5 (Ballentine and Burnard, 2002; Warr et al., 2018), as would be expected in a system with significant ^{40}Ar production, interestingly, three of the core samples exhibit a $^{40}Ar/^{36}Ar$ ratio below the atmospheric standard (samples at depths 887.5, 1175, and 1752.5 cm, respectively). Again, as observed with the case of neon, this indicated the presence of isotopic fractionation in these samples which is discussed in section 2.4.8.

As for the concentrations of these argon isotopes within the sampled headspace, these are represented in Figures 2.9a, 2.9b, and 2.9c.

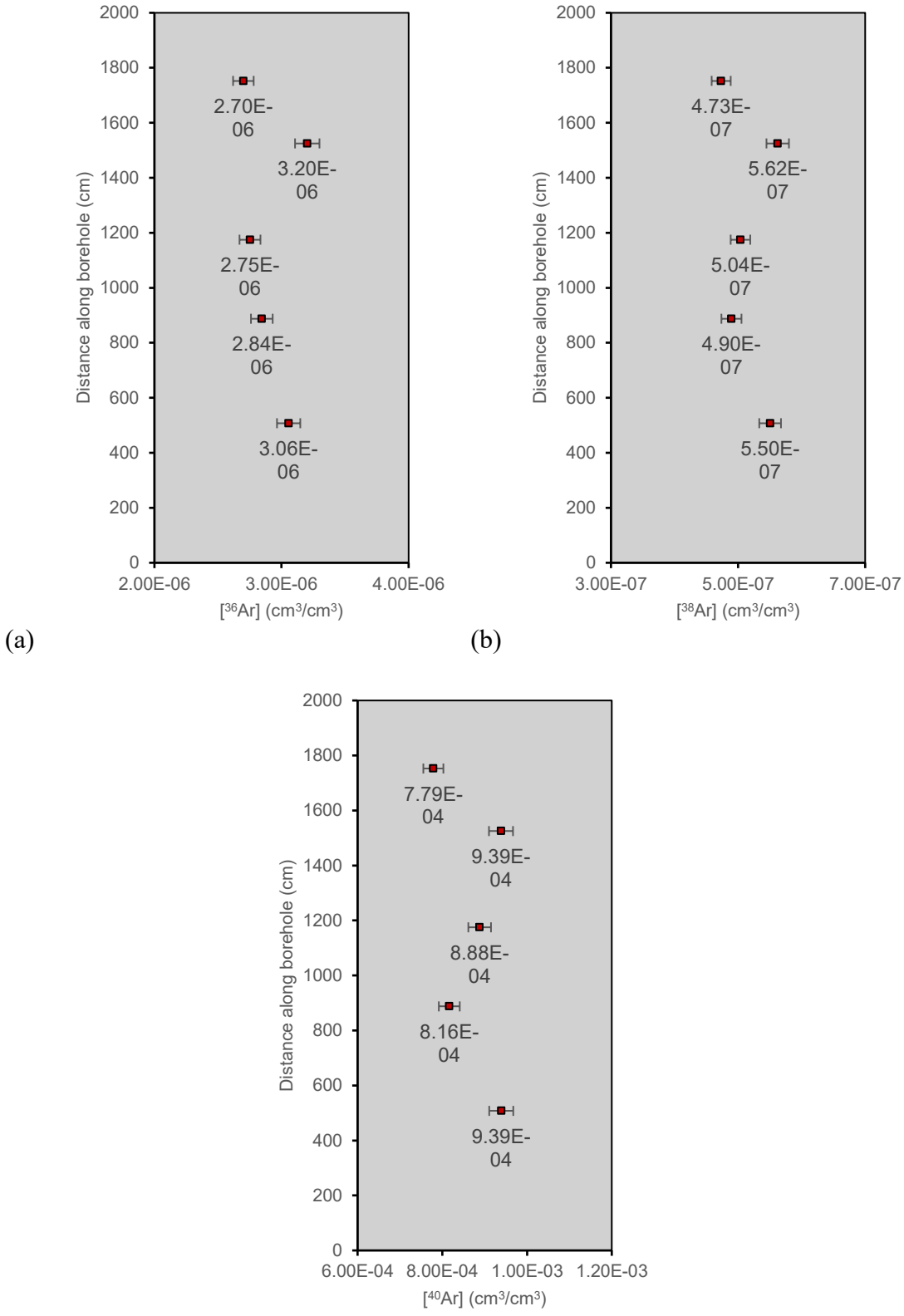

Figure 2.9a, Figure 2.9b, and Figure 2.9c: Concentration plot of ^{36}Ar (2.9a), ^{38}Ar (2.9b), and ^{40}Ar (2.9c) in samples within the sampled headspace with respect to their core distance along the horizontal borehole.

The mean concentration of ^{36}Ar is approximately $2.91 \times 10^{-6} \pm 1.90 \times 10^{-7}$ cm^3/cm^3, which is approximately 9% of the air concentration of ^{36}Ar (3.14×10^{-5} cm^3/cm^3). Meanwhile, the mean concentration of ^{38}Ar is approximately $5.16 \times 10^{-7} \pm 3.46 \times 10^{-8}$ cm^3/cm^3. Relative to air, this is representative of approximately 9% of the ^{38}Ar air concentration (5.90×10^{-6} cm^3/cm^3).Finally, the mean concentration of ^{40}Ar is approximately $8.72 \times 10^{-4} \pm 6.47 \times 10^{-5}$ cm^3/cm^3. Much like with the latter argon isotopes also, the mean sample concentration represents approximately 9% of the air concentration of ^{40}Ar, which is approximately 9.30×10^{-3} cm^3/cm^3.

2.4 Discussion

This chapter will evaluate the different approaches to reconstructing the initial porewater noble gas content prior to degassing in order to delineate the best practices approach for core porewater noble gas analysis. The first approach estimates porewater noble gas content based on the concentrations of noble gases within the headspace, and the porosity of the OPA material – "The Porosity Approach". The second approach estimates porewater noble gas content based on the concentrations of noble gases within the headspace and the total water content measured in a matching OPA material core – "The Water Mass Approach". Lastly, the porewater noble gas content is estimated based on the ^{20}Ne content of the samples, and the ^{20}Ne concentration in ASW – "The ASW Approach". These three approaches are outlined below sequentially, then the normalized values are presented (within Table 2.2), and finally compared, contrasted, and otherwise evaluated in terms of their strengths and potential limitations in deriving the initial porewater noble gas concentrations.

2.4.1 The Porosity Approach

As a brief overview, this approach uses the calculated noble gas volumes in the headspace and normalizes relative to the water content calculated from the mean porosity of the OPA material

(which is characterised as very homogeneous) to estimate the noble gas content in the porewaters. To perform this calculation, it is necessary to know 1. the total amount of each noble gas isotope within the headspace of the cylinder, and 2. the associated volume of the porewater within the core.

For the total amount of each noble gas isotope within the headspace, a series of calculations are required to convert the noble gas concentrations reported in Table C.1 (Appendix C, cm^3 per cm^3 of headspace gas). The first stage was to calculate how much headspace gas was initially in the copper tube aliquot, prior to its expansion during the analysis. For this, two sets of calculations were needed: firstly, to calculate the total amount of noble gases in the measured aliquot (i.e., the calibrated volume component), and secondly, to calculate how much this measured aliquot volume represented of the entire sample. To calculate the total amount of noble gases in the measured aliquot, first for each sample, the pressures taken were multiplied by the amount of the gas inlet (in cm^3) to the extraction line (G_{inlet}) from the copper tube to calculate the total cm^3 of gas. This was then multiplied by the reported gas concentrations in cm^3/cm^3 (C_{NG}) to calculate the volume of noble gases which were analysed from the aliquot (V_{NG}). See equation 1.

$$V_{NG} = C_{NG} \times G_{inlet} \quad (1)$$

Next, the relative proportion that the analysed aliquot represented of the entire copper tube sample was calculated. As outlined in section 2.2.2, the gas was initially expanded from the copper tube of volume 1.05 cm^3. The expanded volume ($V_{expanded}$) therefore represented a total volume comprising the copper tube inletting device ($V_{extractor}$), bellows ($V_{bellows}$), and the previously mentioned extraction line inlet section (of calibrated volume, $V_{calibrated}$). See equation 2.

$$V_{expanded} = V_{extractor} + V_{bellows} + V_{calibrated} \quad (2)$$

Where $V_{expanded}$ is equal to 94.31 cm^3, which represents approximately 54.65% of the total expanded volume, see equation 3:

$$f_{analysed} = \frac{V_{calibrated}}{V_{expanded}} = 0.5465 \text{ (3)}$$

Since only this fraction was analysed upon closing the inlet valve, a correction was applied to V_{NG} to extrapolate the total amount of gas originally present in the copper tube, such that $f_{analysed}$ = 1. Therefore, V_{NGtot} (the total concentration of noble gas within the copper tube) is calculated by equation 4:

$$V_{NGtot} = \frac{V_{NG}}{f_{analysed}} \text{ (4)}$$

This represents the initial total amount of noble gas in the 1.05cm^3 copper tube prior to expansion. This can then be used to calculate the total noble gas content of the headspace within the stainless-steel cylinder as follows. First, the headspace volume was determined by summing the stainless-steel cylinder headspace minus the volume occupied by the core itself (V_{SS}) and the copper tube volume (see section 2.2.2). The copper tube, once the top end was crimped, had a length of 25.5 cm, corresponding to a volume of 4.82 cm^3 (V_{Cu}). The total headspace volume ($V_{headspace}$) was thus calculated (to the nearest cm^3) via equation 5:

$$V_{headspace} = V_{SS} + V_{Cu} = 1164\ cm^3 \text{ (5)}$$

This could then be used in equation 6 to derive the initial total noble gas content in the headspace ($C_{headspace}$) prior to sampling being carried out:

$$C_{headspace} = \frac{V_{headspace}}{V_{Cu}} \times V_{NGtot} \text{ (6)}$$

The total headspace concentrations of noble gases within these stainless-steel cylinder samples are provided in Table C.2, in Appendix C, whereby $C_{headspace}$ is simply divided by $V_{headspace}$ to determine headspace-normalized concentrations of each isotope. To reconstruct the initial

porewater concentration of noble gases, the porewater volume of the OPA core is required. For this, a mean porosity of 10.14% was used, based on the mean OPA porosity of the silty-shaly facies, as determined by Pearson et al., (2003). Therefore, the volume of porewater, and hence porewater mass, can be estimated through the known dimensions of the cuboid-shaped cores, see equation 7:

$$V_{PW} = \varphi \times V_{core} \quad (7)$$

Whereby V_{PW} represents the porewater volume, φ represents the mean OPA core porosity, and V_{core} represents the volume of the cubed OPA cores. Subsequently, the porewater mass can be calculated using equation 8, by multiplying the porewater volume (V_{PW}) by the density of the porewater (ρ_{water}).

$$m_{PW} = V_{PW} \times \rho_{water} \quad (8)$$

In this case, the environment of deposition (and preceding OPA lithification) was a shallow marine setting (Hostettler et al., 2017; Bossart et al., 2017), and hence a more saline environment. Therefore, the density of porewater was estimated to be 1.02 g/cm^3. As a result, the estimated homogeneous porewater mass in this case is approximately 0.069 kg. To estimate the noble gas content of the porewater, the noble gas contents ($C_{headspace}$) were divided by the calculated porewater mass (m_{PW}).

With respect to assumptions made with this approach, the following four are made: (1) that the mean porosity is homogeneous across the OPA formation (based on other experiments conducted on similar cores), and is in line with a recent report (NAGRA, 2024); (2) the assumption that the pore space within the cores are fully saturated with porewater; (3) all noble gases have outgassed completely from the rock core into the porewater and (4) all porewaters have fully degassed into the stainless-steel cylinder headspace. We can assume that (2) is true,

since the OPA was deposited in a marine setting, and for (3) and (4), our samples far exceeded the recommended relaxation time of four weeks, as recommended by Rübel et al. (2002).

2.4.2 The Water Mass Approach

As with the previous section, the Water Mass Approach takes the headspace noble gas content ($C_{headspace}$), as processed in the preceding chapter, and divides this by an experimentally derived water content (mean water contents of 91.98 ± 4.91 g), rather than an estimated water content that assumes a homogeneous, macroscopic porosity throughout the OPA and a fixed water density (i.e., the Porosity Approach). To achieve this, the water content of the series of OPA cores were determined by project partners at Hydroisotop GmbH. What follows is a brief description of which will be discussed in more detail in the upcoming PC-D technical report. First, each core was placed in a crystallization dish and weighed. Next, the cores were baked at 105°C until a stabilised mass is reached. Weighing was carried out weekly until the sample weight remained constant for at least 14 days. The water contents, related to the wet weight of the rock, were calculated via equation 9:

$$m_{PW} = m_{wet} - m_{dry} \quad (9)$$

Where m_{PW} is the water content determined by m_{dry} (the dry mass of the OPA core) and m_{wet} (the wet mass of the OPA core). As with the previous approach, the porewater concentration was then calculated by dividing the total amount of noble gases within the headspace by the mass of water, as determined by this approach.

The primary assumption this approach makes is that all water mass lost during the baking process is porewater, and not for example water constituent within clay minerals (Heller-Kallai, 1997). This approach also again relies upon the assumptions as before, that all porewater noble

gases have (1) outgassed completely from the rock core into the porewater and (2) have fully degassed into the stainless-steel cylinder headspace.

This approach yielded varying porewater mass values ranging from approximately 0.086 kg to 0.098 kg, almost double the estimated porewater mass. The implications of this will be discussed within section 2.4.5.

2.4.3 The ASW Approach

The final approach to normalising the concentrations of porewater noble gas to the OPA porewater is to instead reconstruct porewater based upon an assumed concentration of ^{20}Ne in air-saturated water (ASW) following previously published methodology (e.g., Holland et al., 2013; Warr et al., 2022). For this approach, it is assumed that all ^{20}Ne measured in the headspace was initially derived from ASW. Therefore, by taking both this anticipated ^{20}Ne concentration and the concentrations of all other noble gases in the headspace relative to ^{20}Ne, the noble gas content of the porewater can be calculated. For this approach, seawater at 10°C was selected as ASW with a corresponding ^{20}Ne concentration of 1.50×10^{-4} cm^{3}STP/kg$_{PW}$. This was combined with the relative abundances of noble gases in the headspace as follows in equation 10:

$$^{i}X_{porewater} = \frac{^{i}X}{^{20}Ne_{headspace}} \times {}^{20}Ne_{ASW} \quad (10)$$

Where $^{i}X_{porewater}$ represents the concentration of a noble gas within the OPA porewater (cm^{3}STP/cm^3), ^{i}X represents the concentration of a noble gas within the sampled headspace, $^{20}Ne_{headspace}$ is the ^{20}Ne concentration within the sampled headspace, and finally $^{20}Ne_{ASW}$ is the concentration of ^{20}Ne within ASW. This approach relies on the principle that there is a single source of ^{20}Ne (i.e., ASW), with no addition from the crust on the basis that it is a non-radiogenic noble gas (Ballentine and Burnard, 2002). As with the first two approaches,

additional assumptions must be made when estimating the noble gas content of porewaters using this approach. Firstly, the ^{20}Ne concentration in ASW is highly dependent upon various conditions, such as salinity and temperature (Ballentine et al., 2002). Therefore, this approach is highly sensitive to the value of ASW selected for this normalization approach and so must be tailored to the site being characterised. In this case, Mont Terri was initially deposited in a shallow marine setting (Hostettler et al., 2017; Bossart et al., 2017), thus the most appropriate ASW selected here would be that of seawater at 10°C in line with other noble gas-based studies (Holland et al., 2013; Barry et al., 2018). In addition to the assumption that the values are ASW-like, this approach also assumes no mixing or external secondary source of ^{20}Ne is present (e.g., air) and that the initial ^{20}Ne content of the porewaters has been preserved since deposition. Additionally, and as with the prior two approaches, this too relies upon the assumptions that that all noble gases have (1) outgassed completely from the rock core into the porewater and (2) porewaters have fully degassed into the stainless-steel cylinder headspace.

2.4.4 Resulting concentrations by each approach

The overall resulting concentrations of each noble gas isotope (He-Ar) based on the three outlined approaches to normalize to the OPA porewater are represented in Table 2.2, overleaf:

Table 2.2: The concentrations of each noble gas isotope by normalization approach in cm^3STP/kg_{PW}

Sample	^{20}Ne (ASW) / ^{20}Ne (Measured)	Porosity Approach	Water Mass Approach	ASW Approach	Porosity Approach	Water Mass Approach	ASW Approach	Porosity Approach	Water Mass Approach	ASW Approach	Porosity Approach	Water Mass Approach	ASW Approach
		^{3}He			^{4}He			^{20}Ne			^{21}Ne		
1	1.43E+04	1.87E-08	1.48E-08	1.31E-08	1.25E-01	9.87E-02	8.76E-02	2.15E-04	1.69E-04	1.50E-04	6.52E-07	5.14E-07	4.78E-07
2	1.97E+04	1.43E-08	1.11E-08	1.25E-08	9.64E-02	7.46E-02	8.39E-02	1.73E-04	1.34E-04	1.50E-04	4.85E-07	3.76E-07	4.90E-07
3	1.64E+04	1.39E-08	1.12E-08	1.26E-08	8.21E-02	6.64E-02	7.47E-02	1.65E-04	1.34E-04	1.50E-04	4.78E-07	3.87E-07	4.01E-07
4	1.31E+04	1.65E-08	1.18E-08	1.25E-08	9.46E-02	6.74E-02	7.16E-02	1.99E-04	1.42E-04	1.50E-04	5.53E-07	3.94E-07	3.70E-07
5	1.16E+04	1.19E-08	8.49E-09	7.67E-09	1.19E-01	8.49E-02	7.67E-02	2.34E-04	1.66E-04	1.50E-04	6.71E-07	4.77E-07	4.00E-07
M	1.50E+04	1.51E-08	1.15E-08	1.17E-08	1.04E-01	7.84E-02	7.89E-02	1.97E-04	1.49E-04	1.50E-04	5.68E-07	4.39E-07	4.28E-07
		^{22}Ne			^{36}Ar			^{38}Ar			^{36}Ar		
1	1.43E+04	2.06E-05	1.62E-05	1.44E-05	1.28E-03	1.01E-03	8.96E-04	2.31E-04	1.82E-04	1.61E-04	3.94E-01	3.10E-01	2.75E-01
2	1.97E+04	1.58E-05	1.22E-05	1.37E-05	1.19E-03	9.24E-04	1.04E-03	2.05E-04	1.59E-04	1.97E-04	3.42E-01	2.65E-01	2.98E-01
3	1.64E+04	1.62E-05	1.31E-05	1.48E-05	1.15E-03	9.34E-04	1.05E-03	2.11E-04	1.71E-04	1.69E-04	3.73E-01	3.01E-01	3.39E-01
4	1.31E+04	1.89E-05	1.35E-05	1.43E-05	1.34E-03	9.57E-04	1.02E-03	2.36E-04	1.68E-04	1.51E-04	3.94E-01	2.81E-01	2.98E-01
5	1.16E+04	2.14E-05	1.52E-05	1.37E-05	1.13E-03	8.05E-04	7.27E-04	1.99E-04	1.41E-04	1.13E-04	3.27E-01	2.32E-01	2.10E-01
M	1.50E+04	1.86E-05	1.40E-05	1.42E-05	1.22E-03	9.26E-04	9.46E-04	2.16E-04	1.64E-04	1.58E-04	3.66E-01	2.78E-01	2.84E-01

Note: The ^{20}Ne (ASW) / ^{20}Ne (Measured) ratio is relative to the ASW of ^{20}Ne at 10°C (seawater) per Porcelli et al. (2002) and the measured ^{20}Ne concentration normalized to the stainless-steel cylinder headspace volume, under the assumption of full core degassing. The mean sample reconstructed porewater concentration by approach is represented in the row denoted "M". All headspace-normalized concentrations in cm^3STP/cm^3 are represented within Table C.2, Appendix C. The Water Mass Approach is normalized to the water masses obtained by Hydroisotop GmbH, as to be included in the upcoming PC-D technical report. These values are not obtained from the University of Ottawa cores, but from adjacent cores within the same borehole of the same volume and dimensions.

2.4.5 Comparison of reconstructed porewater values

Generally, there are some trends that can be observed between the reconstructed porewater concentrations by normalization approach. The Porosity Approach consistently has the most elevated reconstructed porewater concentrations of all noble gas isotopes analysed as part of this study, whereas the Water Mass Approach consistently has the lowest reconstructed porewater concentrations, for all isotopes. The mean reconstructed concentration per isotope by normalization approach is denoted in the row "M". It is observed that on average, the reconstructed porewater concentration via the Porosity Approach are typically 1.32 (^{3}He, ^{4}He, ^{36}Ar, ^{38}Ar, and ^{40}Ar) to 1.96 (^{20}Ne, ^{21}Ne, and ^{22}Ne) times greater than those obtained via the Water Mass Approach. And in a similar vein, the mean reconstructed porewater concentrations via the Porosity Approach are typically 1.29 (^{3}He) to 1.37 (^{38}Ar) times greater than those obtained via the ASW Approach.

2.4.6 Evaluation of approaches

Each of the three approaches presented here and proposed as part of the PC-D project by the University of Ottawa and collaborators have both their advantages and limitations. What follows is a review of the outlined techniques for this MSc project, focusing exclusively on data generated by the University of Ottawa with a view to examine each approach, its strengths and weaknesses, and subsequently evaluating which approach is most effective for applications in these settings and to the OPA specifically. These findings will be discussed and used to generate a final PC-D report involving data from all project partners involved in this project (University of Ottawa, Hydroisotop GmbH, and BGR), however the latter two collaborators' data will not be included in this thesis.

Firstly, the Porosity Approach, by which an estimate of the porewater is ascertained by assuming full saturation of a homogenous, known porosity, relies on a variety of assumptions. For example, the main assumption is that porosity is homogenous throughout the OPA.

Notably, the borehole of which was sampled for this project, was selected specifically due to the known homogenous nature of the OPA (NAGRA, 2024), however it is difficult to quantify this and extrapolate to the entire lithological unit. Several factors that are not considered in this case are the potential for smaller scale variabilities of primary and secondary porosity, tortuosity, and interconnectedness of the pore spaces, which may result in the true porewater content at the sample scale being more variable than the consistent estimate that is assumed here. By assuming that the porosity, and hence the porewater mass, is consistent throughout all five cores, small scale variabilities may be ignored. This may be a significant issue, particularly in other settings where documented porosity could be substantially more variable, e.g., granitic basement rocks (Higgins et al., 2025).

Second, the Water Mass Approach, by which the porewater content is experimentally derived by baking the cores over a period and observing the decrease in mass, relies on the assumption that all mass lost is entirely porewater. Comparatively to the estimate made in the former approach, this experimentally derived porewater mass is approximately double, so taking the porosity estimate at face value here, such a broad deviation in values could indicate that some of this water mass loss could be due to the evaporation of interlayer water from clays, and water from constituent clay minerals and/or potentially the loss of other volatile components (Heller-Kalai, 1997). Consequently, this approach is highly dependent on the distribution of water within a lithology, and how readily it can be volatilised via heating. Comparing this approach to the former, in some hypothetical scenario whereby the same volume of noble gases are dissolved within approximately double the volume of water, the apparent concentration via this approach would be approximately half that of the apparent concentration via the former approach. And should this additional volume of water be attributed to clay mineral contributions, this could result in considerable underestimates of porewater noble gas concentrations, as there is no way to ascertain whether noble gases reside within the clay

interlayer water specifically. Additionally, while this approach considers such factors as secondary porosity, tortuosity, and interconnectedness of pore spaces more so than the former approach, baking alone cannot guarantee that all of the water attributed to these factors will be "baked out" within such short timescales, and so it is possible that some porewater may remain trapped. As a result, in cases where connectivity and permeability are lower, even when porosity is relatively high, less of the experimentally derived water content can be readily extracted and therefore attributed to porewater. The effect of this would be to underestimate the water content which would artificially increase the apparent porewater concentration of noble gases (i.e., smaller volume in which the same amount of noble gases are dissolved within).

Lastly, the ASW Approach provides a simpler, yet effective alternative, whereby the volume (and hence the mass) of the porewater does not need to be ascertained, sidestepping the issues flagged above. Such approach already has sufficient precedent, used in various noble gas geochemistry literature (Holland et al., 2013; Warr et al., 2018; 2022; Heard et al., 2018). This removes an element of uncertainty from the study, by instead normalising all concentrations relative to a non-radiogenic noble gas (^{20}Ne) concentration within the porewater. The offset between the ASW concentration of ^{20}Ne in cm^3/cm^3 and the measured concentration within the porewater can be applied to the concentrations of each other isotope such that their concentrations can also be normalized to porewater mass, without requiring an accurate estimate of porewater content, a clear positive contrast to the two former approaches. However, while one element of uncertainty is removed, another is acquired, as the ASW concentration of ^{20}Ne, and any other noble gas isotope, is highly dependent on salinity and temperature, so selecting an appropriate value for this becomes extremely important, and prior literature on site characterisation, geological history, and depositional environment of Mont Terri must be referred to. For example, using the ASW concentrations derived by Kipfer et al. (2002) to

compare the ^{20}Ne concentration normalised to ASW at 10°C (seawater), and the ^{20}Ne concentration normalised to ASW at 20°C (freshwater, Lake Baikal), the latter is 7.3% greater than the former, so the selected ASW value based on appropriate conditions is significant. Furthermore, this normalization approach also relies upon the assumption that there is no excess neon contribution or any other secondary noble gas source, nor any mass-dependent isotopic fractionation of samples, which it is believed that the University of Ottawa samples underwent based on the neon and argon isotopic data (see section 2.4.8)

2.4.7 Importance of selecting an appropriate normalization technique

Selecting an appropriate normalization technique is an important factor to consider, as there may be implications upon further work and conclusions drawn based on the noble gas concentrations calculated with each approach. As explained at length in Chapter 1, noble gases are frequently used as an age-dating tool for groundwaters and other crustal fluids. Therefore, when ^{4}He and ^{40}Ar concentrations are used to determine production rates, alongside the concentration of source radionuclides, the associated production rate and hence radiogenic ages of ^{4}He and ^{40}Ar are affected.

To illustrate the importance of this, the production rates of ^{4}He and ^{40}Ar were calculated for the OPA material using each of the three approaches outlined in this section, following the steps outlined in Ballentine and Burnard (2002), and utilizing average source radionuclide concentrations and OPA density, as reported in Pearson et al. (2003) and Orellana et al. (2022), respectively. These production rates were then used to calculate estimated residence times for the porewater within the OPA material, under the assumption that ^{4}He and ^{40}Ar enter the water phase instantaneously upon production (i.e., a release coefficient of 100%). This was carried out by normalising the concentrations of ^{4}He, ^{36}Ar, and ^{40}Ar using each of the three approaches outlined in this section. The ^{36}Ar concentration was multiplied by the atmospheric ratio of

$^{40}Ar/^{36}Ar$ (295.5), and thus the result of this was termed $^{40}Ar_{initial}$, and is assumed to be the starting concentration of ^{40}Ar prior to any radiogenic ingrowth. Then, the normalized concentrations of ^{40}Ar were termed $^{40}Ar_{total}$, and the following calculation was carried out to calculate the argon excess ($^{40}Ar_{excess}$), from which the ^{40}Ar residence time estimate was calculated in equation 11:

$$^{40}Ar_{total} - {}^{40}Ar_{initial} = {}^{40}Ar_{excess} \quad (11)$$

This process was not carried out for ^{4}He, as the starting concentration of ^{4}He relative to radiogenic ingrowth is considered negligible and therefore has no bearing to residence time estimations.

Table 2.3: The residence time estimation in years by concentration of ^{4}He and ^{40}Ar by normalization approach

	^{4}He Residence Time (yrs)			**^{40}Ar Residence Time (yrs)**		
	Porosity Approach	Water Mass Approach	ASW Approach	Porosity Approach	Water Mass Approach	ASW Approach
1	4.70E+06	3.70E+06	3.29E+06	5.04E+06	3.97E+06	3.53E+06
2	3.62E+06	2.80E+06	3.15E+06	-	-	-
3	3.08E+06	2.49E+06	2.80E+06	1.05E+07	8.49E+06	9.55E+06
4	3.55E+06	2.53E+06	2.69E+06	-	-	-
5	4.48E+06	3.18E+06	2.88E+06	-	-	-

These residence times based upon the three different normalization approaches are represented in Table 2.3. Notably, there are only estimates for two of the samples from the ^{40}Ar excess across each normalization approach, as the $^{40}Ar/^{36}Ar$ ratio is below the atmospheric ratio of 295.5 in the case of the other three samples, indicating no ^{40}Ar excess to calculate the porewater residence time from (see section 2.4.8). The mean ^{4}He residence time estimates are approximately 3.88 Ma, 2.94 Ma, and 2.96 Ma for the Porosity Approach, Water Mass Approach, and ASW Approach, respectively. Notably, there is a closer agreement between the

Water Mass Approach and ASW Approach estimates, however the Porosity Approach indicates a slightly greater residence time based on ^{4}He, just over 30% greater than the estimates for the Water Mass Approach and ASW approaches. In terms of agreement between the ^{4}He and ^{40}Ar residence time estimates, sample 1 exhibits good agreement between the residence time for each approach, with the ^{40}Ar residence time being consistently 7.362% greater than its ^{4}He counterpart for each of the three approaches. However, sample 3 exhibits a far greater disparity between the age estimates, with the ^{40}Ar residence time being over 3 times greater than its ^{4}He counterpart. Not only does this indicate the importance of determining an appropriate normalization approach for the use of noble gas concentrations as age tracers, but also it demonstrates that these estimates are simply estimates, and to be more accurate (or more accurately determine which tracers may be more/less reliable than others), multiple different age tracers should be used in conjunction with one another.

2.4.8 Additional considerations and potential caveats

Beyond the method-specific advantages and disadvantages listed in section 2.4.5, additional considerations that need to be evaluated and assessed for in all three techniques include: the assumption that no significant degassing occurred during sampling, the cores have fully degassed all their noble gas content into the porewater and headspace, and that the headspace prior to sampling contains a single noble gas component (i.e., it is exclusively derived from what was originally held in the porewater, and there is no other contribution from other phases such as mineral lattices, or residual air contamination).

Evaluating the first point, regarding no significant degassing during sampling, it is important to briefly recap the sampling procedure, as detailed in section 1.7. Samples were obtained from the horizontal borehole, then subsequently sealed in two layers of PVC, then a final Al-foil bag which was then vacuum-pumped. The samples were then sent to BGR and Hydroisotop GmbH,

where they were then unbagged, cubed, and flushed with nitrogen before being finally sealed within the stainless-steel cylinders which were then vacuum-pumped. The potential issue with this approach here is the time elapsed between each stage of sample collection and preparation, and the amount of time in which the cores were exposed, or inside a container with low integrity for the encapsulation of noble gases. Between the start of borehole drilling, and samples being bagged within the Al-foil bags, the time elapsed varied between 25 and 59 minutes, and then additional time elapsed between these sample being unbagged, cubed, flushed with nitrogen, and evacuated within the stainless-steel cylinders. This secondary exposure to the atmosphere varied between 12 and 17 minutes for the University of Ottawa samples. Evidently, the time in which the samples were exposed to atmosphere was kept as short as realistically possible; however, it is still an unknown as to whether even this minor amount of time could have risked some the cores degassing some of their noble gases. Additionally, the long-term integrity of the Al-foil bags is also an uncertainty but will be examined within Chapter 3.

As for the assumption that all noble gases have fully degassed into the cylinder headspace, this is something else which must be considered. As previously mentioned, the stainless-steel cylinders were left for an extended period (i.e., samples were prepared between September 7th-9th, 2021, but were not analysed at UQAM-GEOTOP until December 2024, meaning there was over a 3-year period for degassing to occur. While the controls on this are loosely understood, through experiments carried out within Rübel et al. (2002) which determined that a 4-week relaxation time to permit full degassing of all noble gases was appropriate, it is possible that this may not be a "one-size fits all" approach, and consequently it cannot be easily ascertained whether degassing periods significantly longer than this might be required to fully degas a core sample. Torgersen et al. (2004) posits that diffusive processes from cores is highly dependent on physico-chemical conditions which are highly lithology-specific and consider aspects such as porosity, carbon content, tortuosity and interconnectedness of pore space, and that diffusion

of lighter noble gases (such as Ne) occurs at a faster rate than their heavier counterparts (e.g., Xe).

However, while this remains uncertain in this project, the time for degassing for the samples sent to the University of Ottawa was considerably longer than either two project partners involved in the PC-D project. Consequently, this will be able to be evaluated more fully in the final PC-D technical report.

Addressing the final point, that the noble gases are representative of the porewater, and there are no other contributions from other phases, fractionation processes, or residual air contamination, the evidence here suggests that the University of Ottawa core samples may have undergone mass fractionation effects. This is based on both the neon and argon isotopes, as the porewater noble gas $^{20}Ne/^{22}Ne$ and $^{40}Ar/^{36}Ar$ ratios both suggest a significant loss of ^{40}Ar and ^{22}Ne, or a significant gain of ^{36}Ar and ^{20}Ne relative to each other, to drive the $^{20}Ne/^{22}Ne$ ratio considerably above air (9.81) and simultaneously bring the $^{40}Ar/^{36}Ar$ ratio to below the atmospheric value of 295.5 in 3 of the 5 samples. To investigate this further, the ratios of $^{20}Ne/^{22}Ne$ and $^{38}Ar/^{36}Ar$ are plotted together, along with a mass fractionation line, following the same process as in Zhou et al. (2005), in Figure 2.11. This figure, and the plotted mass fractionation line, indicates that the neon and argon isotopic signatures are consistent with mass-dependent fractionation, suggesting a secondary process has occurred during or post-sampling. Additionally, a plot of ^{20}Ne and ^{36}Ar (in cm^3/cm^3) in the headspace has been plotted. It is important to specify that these concentrations are the "headspace-normalized" concentrations, whereby the noble gas amounts within the headspace ($C_{headspace}$) are divided by the headspace volume ($V_{headspace}$), and are not the raw sampled headspace concentrations, as described in section 2.3. It is then possible to observe these concentrations of ^{20}Ne and ^{36}Ar in relation to one another (see Table C.2, Appendix C). These non-radiogenic noble gas isotopes are then plotted alongside the corresponding ASW and air concentrations (also normalized to

what would be expected in the headspace, via a volume expansion from the pore space to the headspace), there appears to be some mixing between some air-like component, and the ASW-like original concentrations. This is depicted in Figure 2.12, whereby the sample concentrations plot on a mixing line between ASW concentrations and air concentrations, indicating some mixing between the expected ASW-like concentrations and air-like concentrations that would indicate some minor air contribution. From these two figures, it can be observed that the samples here are simultaneously indicating that the neon and argon may have undergone mass fractionation, while also entraining a modest air component. In light of this, the working hypothesis that the University of Ottawa samples have undergone some form of mass-dependent fractionation of some residual air component, perhaps an artefact of pumping and flushing during initial sample preparation when samples were placed within the stainless-steel cylinders directly after cubing.

To investigate this further, the trend of each isotope is plotted relative to the mixing line from ASW to air concentrations (Figure 2.12) and quantified as a percentage of air-like concentrations, depicted in Figure 2.13. This allows for the estimation of the percentage of air present within the samples that could have potentially been introduced during the flushing and pumping procedure. For instance, if we were to take the atmospheric pressure of approximately 1013 mbar and consider the mean final pumping pressure of each stainless-steel cylinder during preparation (25 mbar). As a simple back-of-the-envelope calculation (12), one would expect:

$$\frac{25\ mbar}{1013\ mbar} = 0.0247\ mbar \quad (12)$$

0.0247 mbar of air remaining within the stainless-steel cylinder. As the cylinder was pumped (and flushed with nitrogen) twice, we can multiply this by itself, thus resulting in a final (approximate) 0.000610 mbar remaining within the cylinder. And this would result in an approximate 0.061% of residual air remaining as a percentage, which is consistent with the

percentage trend towards air-like concentrations of ^{20}Ne and ^{36}Ar, as demonstrated in Figure 2.12, overleaf. However, while the data generated in this project indicates the presence of a fractionated air component, it is noteworthy that the project collaborators did not observe the same phenomenon within their own samples. Consequently, the exact source of, and process responsible for, the potential mass-dependent fractionation effects in these samples presently remain an open question.

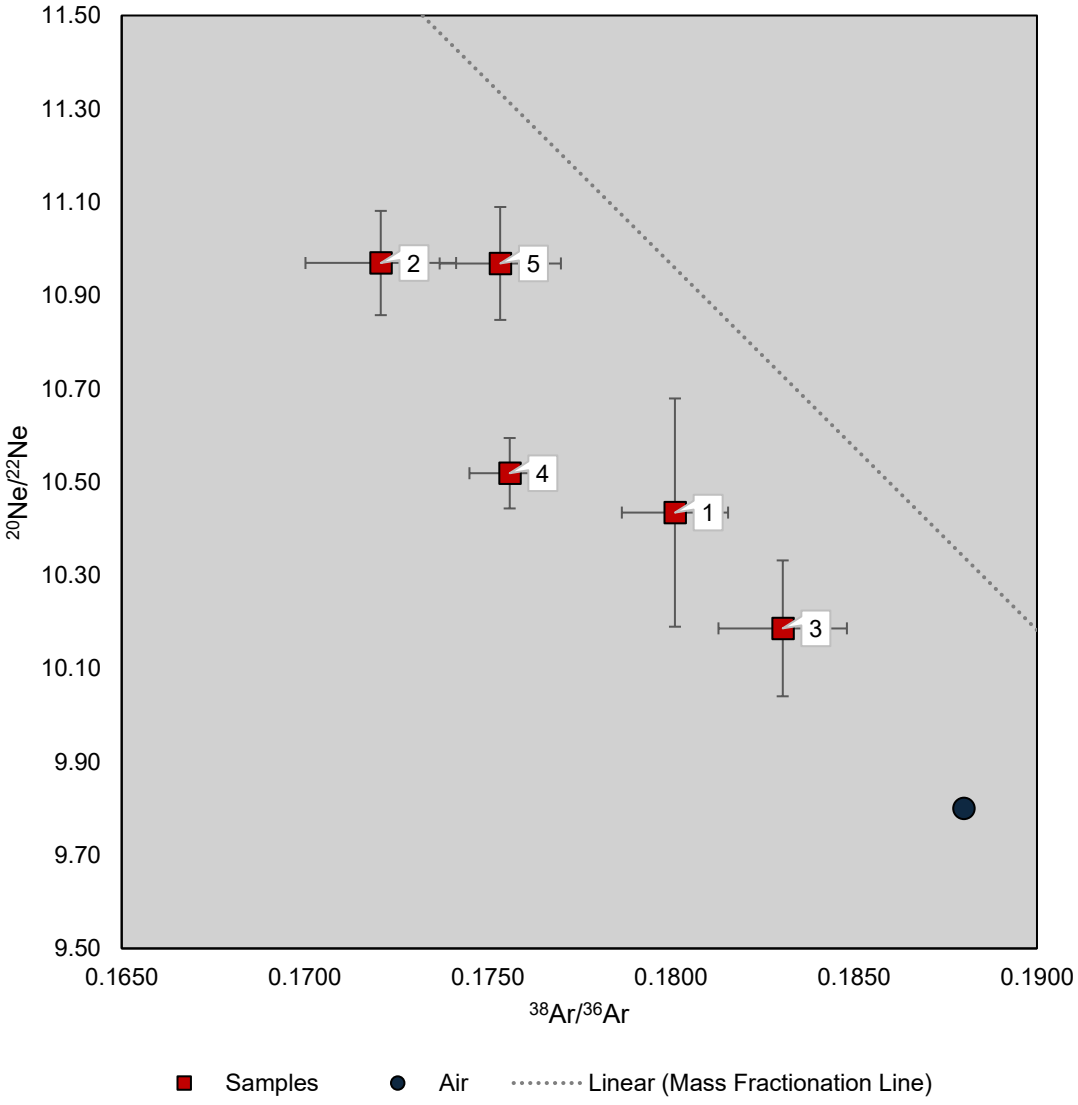

Figure 2.11: $^{20}Ne/^{22}Ne$ versus $^{38}Ar/^{36}Ar$ plot of samples (with sample numbers labelled) plotted against the Mass Fractionation Line of air using the method by Zhou et al. (2005).

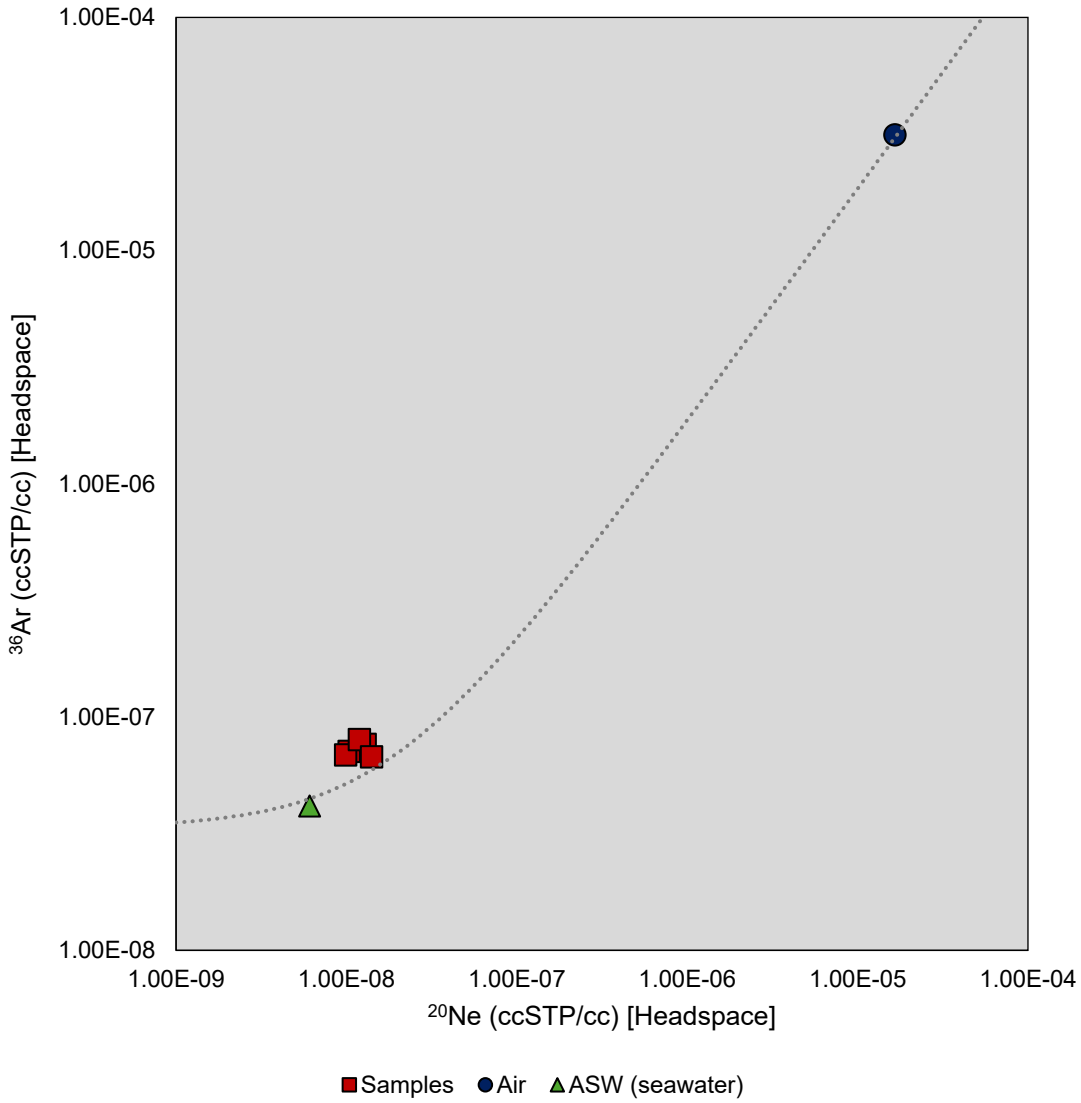

Figure 2.12: Plot of sample concentrations of ^{20}Ne and ^{36}Ar (normalized to the total headspace volume) against a linear mixing line between air and ASW (concentrations also normalized to the headspace volume, ASW concentration assumes that initial concentrations of ^{20}Ne and ^{36}Ar within the porewater are ASW and outgassed into the cylinder headspace volume.

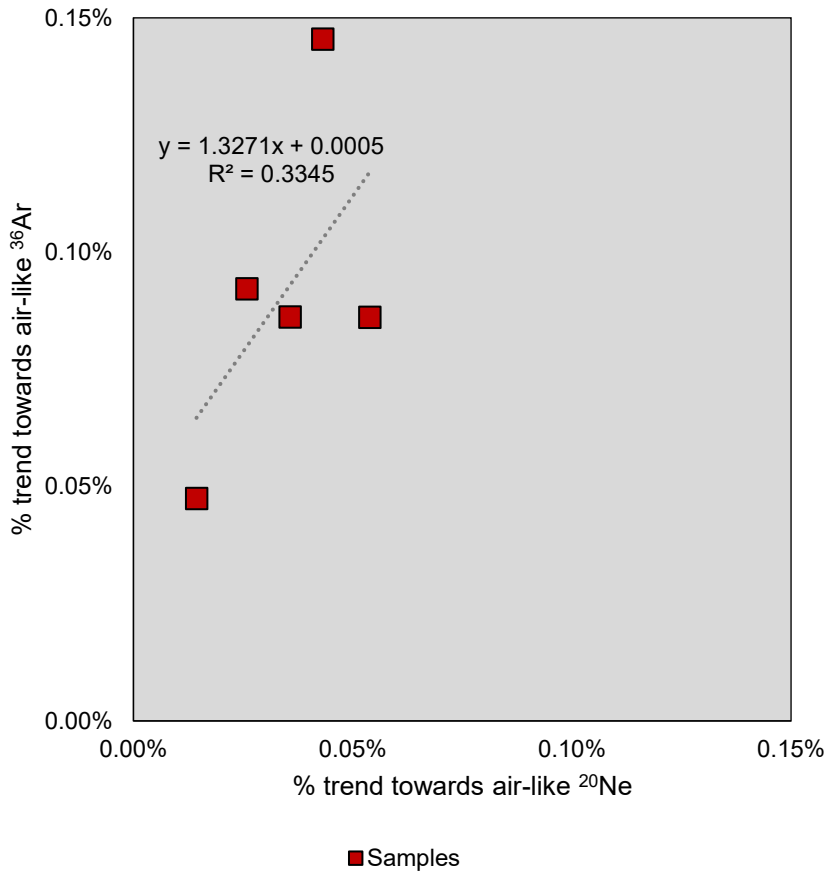

Figure 2.13: Plot of how sample concentrations of ^{20}Ne and ^{36}Ar trend towards air-like values based upon the sample progression along the ASW-air mixing line, per Figure 2.12.

2.5 Summary

Overall, each normalization approach has its strengths and weaknesses. Two of the approaches (The Porosity Approach and The Water Mass Approach) rely heavily on ascertaining a close estimate to the volume (and hence mass) of porewater within each core, yet the third approach (The ASW Approach) is able to eliminate this step, minimising a potential limitation in quantifying the uncertainty associated with the data processing in this instance. Additionally, there is precedent for the use of this normalization approach in a variety of noble gas geochemical datasets (Holland et al., 2013; Warr et al., 2018; 2022; Heard et al., 2018). However, this approach assumes that there is no excess neon, secondary contribution of ^{20}Ne,

or mass-dependent fractionation effects. Evidently, the University of Ottawa samples experienced some combination of these effects, and thus it is less viable that this approach be applied to these samples. An additional consideration that must be made with this approach is which ASW value of ^{20}Ne is most appropriate to use (i.e., freshwater versus seawater, temperature, etc.) Fortunately, this can be reliably estimated here through the depositional and geological history of the setting (Hostettler et al., 2017; Bossart et al., 2017), though in other, less well-characterized settings, this may prove more problematic/less certain.

While this approach is the one that would be recommended for most core-sample-derived porewater noble gas geochemical data, it would not be appropriate to use this normalization in the case of the University of Ottawa samples given the presence of a non-ASW noble gas component. Likewise, if there was a way to experimentally ascertain the total porewater mass of each core (and be able to definitively attribute this water content to only the pore space, and not secondary porosity, or mineral-constituent water, then the Water Mass Approach may be the most precise. However, where secondary hydrated minerals are abundant, and/or permeability is low, significant over- and underestimates of porewater noble gas concentrations may occur, respectively. Both are typical characteristics of clays, and so in this type of setting, the Water Mass Approach may likewise introduce considerable uncertainty. Consequently, the Porosity Approach is perhaps the most appropriate for these samples given these additional considerations, though that requires more accurate constraints on the porosity on the local scale. This could potentially be further evaluated either through measuring porosity on individual samples, or adjacent off cuts.

Of course, each normalization approach also relies heavily upon two assumptions: that (1) all noble gases, including those of radiogenic nature, are present within the porewater phase (i.e., a release coefficient of 100%), and (2) all the porewater noble gases fully degas into the stainless-steel cylinder headspace. While there is no way to be certain of the first assumption,

the second assumption is backed up by scientific literature, such as in Rübel et al. (2002), which determined the relaxation time in order to quantitively extract helium from samples sealed within a similar encapsulation (brass, as opposed to stainless-steel) was approximately 5-6 days, with up to five times higher relaxation times for the heavier noble gases. Rübel et al. (2002), allocated a four-week period for samples to fully outgas – significantly less than the ~3-year period of the University of Ottawa samples. It is possible that this could be ground-truthed within further work, such as perhaps unsealing the stainless-steel cylinders, then following the same sample preparation procedure (i.e., nitrogen flushing and vacuum pumping the cylinders) once more, as outlined in section 1.7, and repeating this experiment again after a prolonged period of time (i.e., 6 months to a year) to further test this assumption that the porewater noble gases had previously fully degassed into the headspace. The hypothesis of this experiment would be to measure negligible concentrations of all noble gases.

2.6 References

Ballentine, C. J., Burgess, R., & Marty, B. (2002). Tracing Fluid Origin, Transport and Interaction in the Crust. *Reviews in Mineralogy and Geochemistry*, *47*(1), 539–614. https://doi.org/10.2138/RMG.2002.47.13

Ballentine, C. J., & Burnard, P. G. (2002). *Production, Release and Transport of Noble Gases in the Continental Crust* (Vol. 47, Issue 1, pp. 481–538). https://doi.org/10.2138/rmg.2002.47.12Barry, P. H., Lawson, M., Meurer, W. P., Cheng, A., & Ballentine, C. J. (2018). Noble Gases in Deepwater Oils of the U.S. Gulf of Mexico. *Geochemistry, Geophysics, Geosystems*, *19*(11), 4218–4235. https://doi.org/10.1029/2018GC007654

Bossart, P., Bernier, F., Birkholzer, J., Bruggeman, C., Connolly, P., Dewonck, S., Fukaya, M., Herfort, M., Jensen, M., Matray, J. M., Mayor, J. C., Moeri, A., Oyama, T., Schuster, K., Shigeta, N., Vietor, T., & Wieczorek, K. (2017). Mont Terri rock laboratory, 20 years of research: introduction, site characteristics and overview of experiments. *Swiss Journal of Geosciences*, *110*(1), 3–22. https://doi.org/10.1007/S00015-016-0236-1/FIGURES/8

Bossart, P., & Thury, M. (2007). Research in the Mont Terri Rock laboratory: Quo vadis? *Physics and Chemistry of the Earth, Parts A/B/C*, *32*(1–7), 19–31. https://doi.org/10.1016/J.PCE.2006.04.031

Heller-Kallai, L. (1997). The nature of clay volatiles and condensates and the effect on their environment. *Journal of Thermal Analysis 1997 50:1*, *50*(1), 145–156. https://doi.org/10.1007/BF01979557

Higgins, P. M., Song, M., Warr, O., & Sherwood Lollar, B. (2025). Natural H2 and Sulfate Production via Radiolysis in Low Porosity and Permeability Crystalline Rocks. *Journal of Geophysical Research: Biogeosciences*, *130*(6), e2025JG008863. https://doi.org/10.1029/2025JG008863

Holland, G., Lollar, B. S., Li, L., Lacrampe-Couloume, G., Slater, G. F., & Ballentine, C. J. (2013). Deep fracture fluids isolated in the crust since the Precambrian era. *Nature*, *497*(7449), 357–360. https://doi.org/10.1038/NATURE12127;SUBJMETA=209,2151,704;KWRD=GEOCHEMISTRY

Hostettler, B., Reisdorf, A., Jaeggi, D., Deplazes, G., Bläsi, H., Morard, A., Feist-Burkhardt, S., Waltschew, A., Dietze, V., & Menkveld-Gfeller, U. (2017). Litho- and biostratigraphy of the Opalinus Clay and bounding formations in the Mont Terri rock

laboratory (Switzerland). *Swiss Journal of Geosciences*, *110*. https://doi.org/10.1007/s00015-016-0250-3

Kambale Kavyavu, W., Pinti, D. L., Kambale Simisi, B., & Tedesco, D. (2025). Sources of helium and associated heat in hydrothermal fluids from the central western branch of the East African Rift System (Democratic Republic of Congo and Burundi). *Journal of Volcanology and Geothermal Research*, *468*, 108464. https://doi.org/10.1016/J.JVOLGEORES.2025.108464

NAGRA. (2024). *Geosynthesis of Northern Switzerland (NTB 24-17)*. https://www.drbg.ch/rbg-gtl/zentrale-referenzberichte/geosynthesis-of-northern-switzerland-ntb-24-17/5-key-characteristics-of-the-host-rock-and-clay-mineral-rich-confining-units-as-geological-barriers-ntb-24-17/2738-5-10-overall-conclusions-on-key-characteristics-of-the-host-rock-and-confining-units-ntb-24-17

Orellana, L. F., Nussbaum, C., Grafulha, L., Henry, P., & Violay, M. (2022). Physical characterization of fault rocks within the Opalinus Clay formation. *Scientific Reports*, *12*(1), 1–13. https://doi.org/10.1038/S41598-022-08236-7;SUBJMETA

Ozima, M., & Podosek, F. A. (2001). Noble Gases in the Earth. *Noble Gas Geochemistry*, 217–252. https://doi.org/10.1017/CBO9780511545986.009

Kipfer, R., Aeschbach-Hertig, W., Peeters, F., & Stute, M. (2002). Noble Gases in Lakes and Ground Waters. *Reviews in Mineralogy and Geochemistry*, *47*(1), 615–700. https://doi.org/10.2138/RMG.2002.47.14

Poblete-González, C., Grelet, T., Tardani, D., Pinti, D., Sanchez-Alfaro, P., Álvarez-Amado, F., Tassara, S., Robidoux, P., Pérez-Flores, P., Aron, F., Berlo, K., & Taussi, M. (2025). Volcano-tectonic controls on magma residence time in arc crusts: Insights

from noble gas geochemistry in the Andean Southern Volcanic Zone. *Earth and Planetary Science Letters*, *661*, 119352. https://doi.org/10.1016/J.EPSL.2025.119352

Pearson, F. J., Arcos, D., Bath, A., Boisson, J.-Y., Fernández, M., Gäbler, H.-E., Gaucher, E., Gautschi, A., Griffault, L., Hernán, P., & Waber, H. N. (2003). *Mont Terri Project - Geochemistry of Water in the Opalinus Clay Formation at the Mont Terri Rock Laboratory*. https://www.mont-terri.ch/en/publication?id=K6Xbk7M26IDf

Porcelli, D., Ballentine, C., Chris, J., & Wieler, R. (2002). *Noble Gases in Geochemistry and Cosmochemistry*. De Gruyter.

Rübel, A. P., Sonntag, C., Lippmann, J., Pearson, F. J., & Gautschi, A. (2002). Solute transport in formations of very low permeability: profiles of stable isotope and dissolved noble gas contents of pore water in the Opalinus Clay, Mont Terri, Switzerland. *Geochimica et Cosmochimica Acta*, *66*(8), 1311–1321. https://doi.org/10.1016/S0016-7037(01)00859-6

Stuart, F. M., Burnard, P. G., Taylor, R. P., & Turner, G. (1995). Resolving mantle and crustal contributions to ancient hydrothermal fluids: He□Ar isotopes in fluid inclusions from Dae Hwa W□Mo mineralisation, South Korea. *Geochimica et Cosmochimica Acta*, *59*(22), 4663–4673. https://doi.org/10.1016/0016-7037(95)00300-2

Warr, O., Rochelle, C. A., Masters, A., & Ballentine, C. J. (2015). Determining noble gas partitioning within a CO2–H2O system at elevated temperatures and pressures. *Geochimica et Cosmochimica Acta*, *159*, 112–125. https://doi.org/10.1016/J.GCA.2015.03.003

Warr, O., Sherwood Lollar, B., Fellowes, J., Sutcliffe, C. N., McDermott, J. M., Holland, G., Mabry, J. C., & Ballentine, C. J. (2018). Tracing ancient hydrogeological fracture

network age and compartmentalisation using noble gases. *Geochimica et Cosmochimica Acta*, *222*, 340–362. https://doi.org/10.1016/J.GCA.2017.10.022

Zhou, Z., Ballentine, C. J., Kipfer, R., Schoell, M., & Thibodeaux, S. (2005). Noble gas tracing of groundwater/coalbed methane interaction in the San Juan Basin, USA. *Geochimica et Cosmochimica Acta*, *69*(23), 5413–5428. https://doi.org/10.1016/J.GCA.2005.06.027

Zuo, E., Lapp, A., Jautzy, J. J., & Clark, I. D. (2022). Crustal Noble Gas Isotopic Characteristics in Low-Permeability Ordovician Sedimentary Rock, Eastern Flank of the Michigan Basin. *ACS Earth and Space Chemistry*, *6*(1), 189–196. https://doi.org/10.1021/ACSEARTHSPACECHEM.1C00346

CHAPTER 3: COMPARING NOBLE GAS EXTRACTION FROM ARGILLACEOUS ROCK POREWATER USING STAINLESS-STEEL CYLINDER AND PE/Al-FOIL BAG CONTAINMENT METHODS

3.1 Introduction

A secondary aim of the project was to investigate the sample preparation and containment methods for porewater-based noble gases from solid samples. Reliability and reproducibility in the effective and efficient extraction of these noble gases is essential for a range of environmental applications, not strictly limited to DGR assessment (Greene et al., 2008; Lu et al., 2014; Heard et al., 2018; Warr et al., 2022). In the natural environment, noble gases are chemically inert and present at only trace concentrations, while also being relatively insoluble in (pore)waters (e.g., Smith and Kennedy, 1983) and thus, their measurement requires robust and reproducible sample collection, storage, and handling techniques that minimize atmospheric contamination, diffusion losses, and isotopic fractionation.

Traditionally, the industry-standard approach to containment of solid cores for subsequent noble gas porewater studies has relied on steel or brass-cylinder encapsulation, a technique that provides mechanically robust containment and low gas permeability (Osenbrück et al., 1998; Rübel et al., 2002; Bensenouci et al., 2011; Zuo et al., 2022). However, this technique is logistically and sometimes financially demanding in terms of equipment, handling, and transport. To address this, more recent advances in alternative containment strategies have considered employing laminated polymer-aluminium (PE/Al) foil bags (Zuo et al., 2022). These lightweight, flexible enclosures promise greater ease of field deployment and reduced operational costs, though questions remain regarding their efficacy in preserving porewater noble gases with the same fidelity as stainless-steel cylinders, particularly over extended storage times or under variable environmental conditions. Figure 3.1 illustrates these

containment methods, with the PE/Al-foil bag containment to the left, and the stainless-steel cylinder containment to the right.

Figure 3.1: Photograph of the PE/Al-foil bag encapsulation approach (left) versus the traditional stainless-steel cylinder encapsulation approach (right).

This study compares noble gas extraction outcomes from argillaceous porewater obtained from cores sampled from near-adjacent intervals at the BPCD-1 borehole drilled into Gallery 08 of the Mont Terri rock laboratory (see Section 1.7) that were encapsulated using both containment methods. By evaluating differences in recovery efficiency, susceptibility to contamination, and isotopic fractionation effects, this comparison aims to clarify the trade-offs between established and emerging sampling and storage techniques and to assess the suitability of PE/Al-foil bags as a practical low-cost alternative for hydrogeological and geochemical investigations.

3.2 Materials and Methods

3.2.1 Ascertaining a headspace within the Al-foil bags

The samples investigated as part of this second project were the 5 remaining cores that were left "as-is" inside of the laminated OPP/PE/Foil/PE Mil PRF-131K Class 1 vapour-barrier Al-foil bags (see section 1.7). Each of these samples initially weighed between 2.60 and 9.18 kg upon receipt from Mont Terri. It was observed that even after ~3 years of time elapsed from initial on-site sample preparation, these samples still appeared to be very tightly vacuum-sealed, with very little headspace to sample and analyse. In order to promote additional outgassing to increase the potential headspace inside of the bag that would be able to be sampled, the cores were gently heated for six weeks at 40°C. Prior to this, the core bag volumes were determined via a water displacement inside of a clear Perspex tank. Sufficient water to be able to fully submerge each core sample was added to the tank, and the water level was recorded. Each core was then added in turn, displacing the water to an increased level within the tank. The water level reached by displacing each core was recorded and using a graduated 50 mL measuring cylinder calibrated to ~2.5% error, the volume of each core was determined by cumulatively recording the volume of water input to reach the marked water level from the core displacement. This process was carried out three times, and a mean was calculated. The relative standard error (RSE) varied between 0.27% and 2.47%. After the cores were baked for six weeks, this process was carried out once more. In this instance, the RSE varied between 0.66% and 2.31%. Based on this, the baking process was overall successful in promoting additional outgassing of porewater gas, as the mean increase in porewater gas ranged from 158.33 to 303.33 mL, see Table 3.1 for the headspace increase and total headspace within each bag.

Table 3.1: PE/Al-foil bag headspace increase determined by water displacement experiments

Sample	Before baking (40°C, 6 weeks)						After baking (40°C, 6 weeks)						
	Vol_1 (cm^3)	Vol_2 (cm^3)	Vol_3 (cm^3)	Mean (cm^3)	SD (cm^3)	RSE %	Vol_1 (cm^3)	Vol_2 (cm^3)	Vol_3 (cm^3)	Mean (cm^3)	SD (cm^3)	RSE %	Mean Out (cm^3)
1	1170	1150	1135	1152	14.34	1.24	1305	1325	1300	1310	10.80	0.82	158.33
2	1370	1420	1430	1407	26.25	1.87	1550	1600	1640	1597	36.82	2.31	190
3	4050	4070	4075	4065	10.80	0.27	4330	4375	4400	4368	28.96	0.66	303.33
4	2200	2260	2270	2243	30.91	1.38	2380	2440	2425	2415	25.50	1.06	171.67
5	1690	1770	1790	1750	43.20	2.47	1960	2010	1990	1987	20.55	1.03	236.67

Note: Volumes are to the nearest cm^3.

3.2.2 Preparation for sample analysis

Once each Al-foil bag had a headspace volume that could be extracted and analysed, the bags were prepared for analysis. In this instance, sample analysis was able to be carried out at the University of Ottawa using the newly-commissioned noble gas extraction and purification line (hereby referred to as the "extraction line" or simply "the line") and Helix-MC Plus mass spectrometer, the same instrument used at UQAM-GEOTOP, however the purification and extraction process of noble gas samples, standards, and blank was carried out slightly differently (see Chapter 2, sections 2.2.2 to 2.2.6). Of note, these samples were run during the final stages of technique development, and due to the lack of historic standards, these samples were ascribed a higher associated uncertainty than usual to reflect this. In terms of how these samples were prepared, the exterior of each bag was cleaned with acetone, then subsequently, two butyl septa of diameter 10 mm were "sandwiched" together with butyl caulking, then adhered to each bag with butyl caulking. Afterwards, 8 hours was given for this caulking to fully dry.

For sample archival purposes, it was decided that during the extraction of each bag's headspace, this would also be done using a method adapted from the one described in section

2.2.2. In this instance, the same length (33 cm) of ¼” refrigeration-grade copper tubing was cut, with 7.5 cm excess length at both ends, with triplicate 6 cm intervals in the centre for sub-sampling the headspace via crimping during extraction. Each end of excess tubing was bent such that one side was 45 degrees, and the other was 60 degrees, as it was expected that this would provide flexibility in the way we could set up the core headspace extraction. The copper tubing was connected to a 1/16” stainless-steel capillary tubing which was connected at the other end to a stainless-steel type-K needle. The alternate end of the copper tubing was attached the soft-seal KF sample inlet fitting on the extraction line, all while the sample inlet was isolated from the vacuum pumps. This setup therefore provided a means to effectively and efficiently extract the samples while simultaneously allowing for pristine sample aliquots to be taken for future analysis at a time when analytical uncertainty could be reduced further. Figure 3.2 demonstrates this setup.

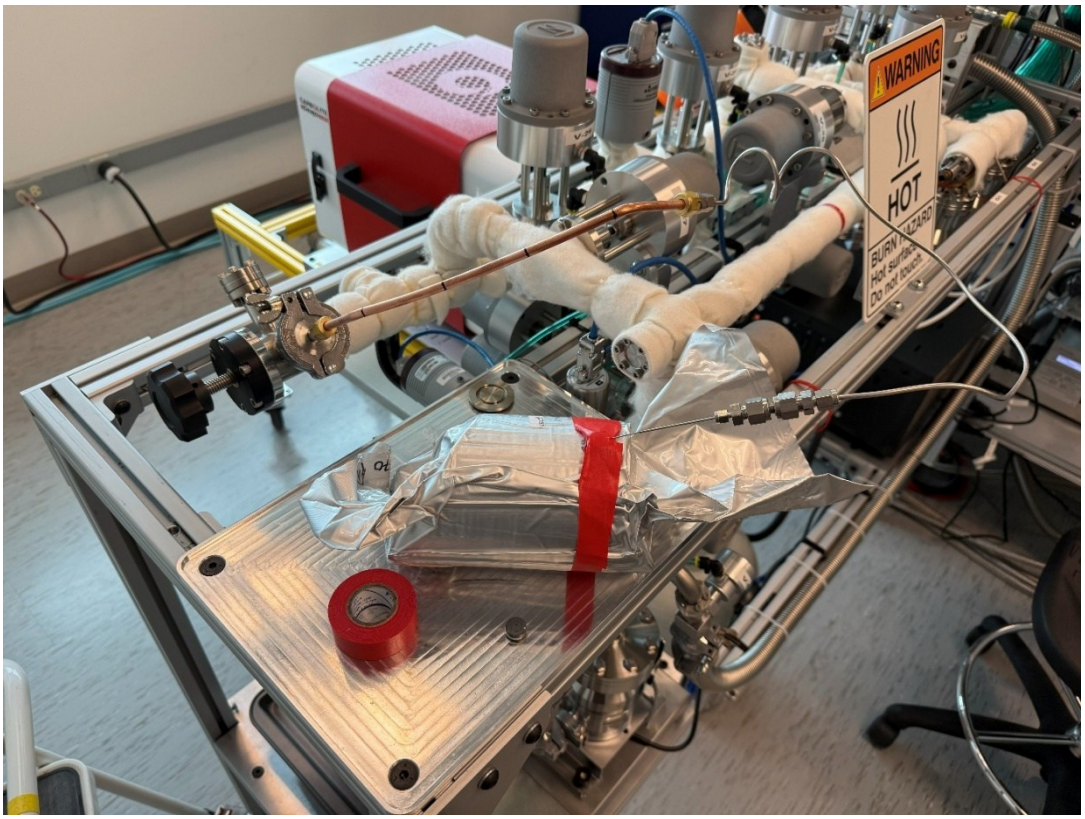

Figure 3.2: Photograph demonstrating the inletting setup to the noble gas extraction line. The PE/Al-foil bagged-core was pierced through the butyl septa by the Type-K needle (pictured).

The copper tube aliquoting setup (i.e., Chapter 2, section 2.2.2) permitted future sampling at a time when analytical uncertainty can be reduced further.

The afternoon prior to sample analysis, the Type-K needle was inserted into the butyl septa (but not the foil bag) and held in place with tape. Then the sample inlet was opened to the roughing pump (then subsequently the turbo pump, once the inlet pressure decreased below 1 torr). The inlet was left pumping on the turbo pump overnight, such that a baseline vacuum of $<5 \times 10^{-6}$ torr or below could be reached the following morning.

As with the stainless-steel cylinders in section 2.2.2, the sample inlet was leak-checked the following morning by observing the pressure rise once the turbo pump was shut off. Provided the rate of this pressure rise was steady, reached a plateau, and the pressure did not exceed 1×10^{-4} torr, the system was considered sufficiently leak-tight. Where needed, and where the vacuum was elevated due to the presence of moisture, a heat gun on a low setting was used on the extraction setup to promote evaporation and pumping until baseline levels were reached. The sample inlet was then isolated from the turbo pump, and the pressure prior to the sample being inlet was noted. Next, the Type-K needle was fully inserted through the butyl septa to pierce the Al-foil bag and the interior PVC layers to sample the headspace. This occasionally took multiple attempts as the needles were prone to bending and/or not successfully passing through the septa and Al-foil bag. There was initially difficulty in doing this, as the Type K needle was sometimes a little flimsy. If the Type-K needle was exposed to air (after being vacuum pumped to baseline), it was inserted back into the septa, placed on the roughing pump (them subsequently the turbo) back to baseline. Once the Type-K needle was successfully fully inserted into the bag, 5 minutes equilibration time was given for the headspace to expand into the inlet. This longer period of equilibration time was chosen due to the narrow width of the needle and capillary tubing, and high volume of gas entering the system. Once expansion was

complete, an aliquot of gas sample was then isolated in the calibrated volume, and pressure readings were taken with a calibrated 0-1000 torr MKS 626D Capacitance Manometer.

Afterwards, the sample was expanded to an Inconel finger containing Ti-sponge, inserted into a Carbolite furnace at 950°C for 30 minutes to remove all active gases in the sample. The furnace was then retracted, and the Inconel finger and Ti-sponge were left to cool to room temperature for 20 minutes. Subsequently, the sample was then expanded to two SEAS Z200 Getters (one hot at 200°C and one held at room temperature) to remove any final trace contaminants for 15 minutes. After this stage, the sample was then expanded to a cryogenic water trap held at 165 K to remove water vapour. Immediately following this, a small aliquot of purified sample was stored within a sub-section of the manifold after 2 minutes equilibration time, for subsequent Ar analysis. Next, the sample was then frozen onto dual cryogenic traps, first, a stainless-steel (SS) held at 5 K to isolate and remove Ar for 20 minutes, then the sample was introduced to the second trap comprised of activated charcoal (ACT) held at 5 K, for trapping both He and Ne for ~45 minutes (depending on ramp rate of the heater). Once trapping was complete, the cryogenic traps were isolated from the extraction line. The manifold section (except for the sub-section in which the Ar aliquot is stored behind a valve) is opened to the turbo pump, such that prior to Ar being released from this sub-section, the pressure in the manifold has returned to baseline and any residual noble gas component was removed.

3.2.3 Helium Analysis

At this stage, the ACT temperature is raised to 28 K for 10 minutes to enable the release of He from the trap. The Helix-MC cup setting is then switched to He in advance for additional stability of the Helix-MC magnet. Once He was released from the cryogenic trap, the sample was diluted using volume sections on the extraction line until concentrations were at measurable values, per the pressure reading on the Spinning Rotor Gauge (SRG). Subsequently, the He aliquot was inlet to the mass spectrometer with 1 minute equilibration

time, and following this peak-centring was run for both ^{4}He and ^{3}He, whereby ^{4}He was run on the Faraday (H2) and ^{3}He was run on the axial CDD multiplier. Once peak-centred, and peaks noted, the He aliquot was run for 30 measurement cycles. During this analysis, excess sample within the cryogenic section of the extraction line was pumped away, first on the turbo pump, and then on the ion getter pump. The ACT is then isolated and the temperature set to 60 K for subsequent Ne release.

3.2.4 Neon Analysis

After He was successfully analysed, the remaining sample within the mass spectrometer was pumped away on the ion getter pump. The cup-setting on the Helix-MC Plus Mass Spectrometer then changed to Ne, and much like with He, appropriate volume splits (within known calibrated volumes) were carried out, per the reading on the SRG. The Helix-MC was then isolated, and the valve on the ACT was opened to expand Ne (with 1 minute equilibration time). Much like with He, once Ne was expanded into the cryogenic section of the extraction line, a pressure reading was taken on the SRG, and the sample was diluted using volumes on the line until concentrations were at measurable values. 1 minute equilibration time was allotted to inlet the Ne aliquot into the mass spectrometer. Ne ran with automatic peak centring, for 40 measurement cycles, with ^{20}Ne, ^{21}Ne, and ^{22}Ne ran on the Faraday L2, axial, and H2, respectively. At this stage, the cryogenic section of the extraction line was then placed back under turbo pump vacuum, then ion getter pump once the pressure reached the turbo pump baseline ($<1 \times 10^{-6}$ torr or below). Once all Ne had been measured, the excess Ne was ion pumped from the mass spectrometer.

3.2.5 Argon Analysis

The manifold section was isolated from the turbo pump, then the valve isolating the Ar within the small sub-section of the manifold was opened to permit equilibration of Ar into the manifold for 1 minute. After this point, the cryogenic section of the extraction line was then

isolated from vacuum, and the Ar aliquot was further expanded into this section, where the SRG is housed. The pressure reading was then taken from the SRG, and like with He and Ne, appropriate volume splits were made. In this case, given the high Ar contents within these samples it was appropriate to carry out the volume splits using the large-volume manifold section. This was done by isolating the manifold from the cryogenic section, then opening the manifold to the turbo pump. Then, the manifold section was isolated again and re-equilibrated with the cryogenic section for 1 minute. This was repeated until the pressure on the SRG was approximately 5×10^{-5} torr or below (i.e., below the limit of measurement for Ar). Once this pressure was reached, the mass spectrometer was opened to inlet the Ar aliquot.

Like with helium, manual peak centring was run for argon, with ^{36}Ar run on the axial Faraday initially, then was peak jumped for ^{36}Ar to be run on the Faraday L2, ^{38}Ar on the axial, and ^{40}Ar on the Faraday H2, for 40 measurement cycles. After this was successfully completed, the excess argon was pumped from the mass spectrometer, and the extraction line was prepared for the next sample and/or standard.

3.2.6 Blank correction and normalization to air standards

As with the samples run at UQAM (Chapter 2), procedural blanks and standards were run for normalization and background corrections. The procedural blank is represented below in Table 3.2 as a percentage of each measured sample concentration.

Table 3.2: Procedural blanks represented as a percentage of each measured sample concentration.

Sample	^{3}He	^{4}He	^{20}Ne	^{21}Ne	^{22}Ne	^{36}Ar	^{38}Ar	^{40}Ar
UO_1_Al	0.00%	0.00%	1.42%	1.24%	1.41%	0.00%	0.00%	0.05%
UO_2_Al	0.00%	0.00%	0.61%	0.53%	0.60%	0.00%	0.00%	0.07%
UO_3_Al	0.00%	0.00%	0.62%	0.54%	0.61%	0.00%	0.00%	0.02%
UO_4_Al	0.00%	0.00%	1.29%	1.12%	1.28%	0.00%	0.00%	0.10%
UO_5_Al	0.00%	0.00%	1.33%	1.16%	1.32%	0.00%	0.00%	0.08%

These blanks and standards followed the same protocols as detailed here. All samples were normalized to the air standard as per convention. As mentioned previously, these samples were run during the final stages of technique development and due to the lack of historic standards, these samples were ascribed a higher associated uncertainty than usual to reflect this. Consequently, the following results and discussion represent preliminary data which will be revisited once analytical uncertainty is reduced.

3.2.7 Error propagation

Much like the samples encapsulated within the traditional stainless-steel cylinders, errors were propagated using the standard addition in quadrature method, identical to the approach taken in Warr et al. (2015). Uncertainties associated with the air standard raw counts, sample raw counts, inlet baratron gauge (for both samples and standards), and SRG gauge (for both samples and standards), were propagated in this method. As briefly explained, these samples were run during the final stages of technique development for the newly-commissioned noble gas extraction line and Helix-MC Plus Mass Spectrometer, and as a result, many of the standards run during this project were "jumpy", and deviated to a large extent from known, published air concentrations in some cases. As a result, the four standards run on September 25th, 29th (2025) and October 13th, 15th (2025) were treated as samples and normalized to the standard run on October 21st. The percentage deviation from the published air concentrations (in cm^3STP/cm^3, via Porcelli et al., 2002) was treated as an uncertainty, and noted for each concentration, and the highest uncertainty per noble gas from each of the five standards run was taken, then rounded up to the nearest whole number. This uncertainty was treated as an additional error to be included in the standard addition in quadrature method and was propagated throughout the samples. These additional uncertainties were quantified as 55%, 10%, and 18% for helium, neon, and argon, respectively. The reason behind this phenomenon is not fully understood, however it is possible that it could be attributed to potential human error, or perhaps a valve

not fully actuating during the automated procedure. Generally, these additional uncertainties are in line with one another elementally, leading to the suspicion that it was perhaps an accidental volume expansion in the extraction line during the purification process. These uncertainties per isotope are represented in Table 3.3.

Table 3.3: Additional uncertainties ascertained by normalising earlier standards relative to the October 21st standard that were factored into the error propagation

Stnd	^{3}He	^{4}He	^{20}Ne	^{21}Ne	^{22}Ne	^{36}Ar	^{38}Ar	^{40}Ar
Sep 25	54.74%	10.51%	8.39%	9.22%	9.93%	0.32%	0.12%	0.30%
Sep 26	4.63%	2.63%	3.09%	4.21%	5.31%	15.34%	3.53%	5.24%
Oct 13	6.73%	11.14%	0.59%	0.87%	1.43%	17.26%	16.59%	15.89%
Oct 15	22.03%	42.86%	0.40%	0.68%	1.24%	17.10%	16.42%	15.73%
Final	55%		10%			18%		

3.3 Results

Blank-corrected and air-normalized concentrations were calculated in cm^3/cm^3 of sampled headspace gas at Standard Temperature and Pressure (STP) and these were then normalized to the OPA porewater via the ASW approach (see section 2.4.3) and are given in Table 3.4. Due to the uncertainties associated with determining a headspace, the ASW approach was utilised. For context and comparison, atmospheric concentrations and ASW concentrations are included alongside the data. These ASW values are considered indicative of the initial porewater concentrations, following the methodologies described by Holland et al. (2013), Warr et al. (2018, 2022), and Heard et al. (2018). All ASW and air concentrations within this section are derived from Porcelli et al. (2002) unless stated otherwise, and ASW concentrations are relative to seawater at 10°C. Additionally, the common noble gas isotopic ratios that will be examined within this chapter are shown in Table 3.5. The raw concentrations of these noble gases within the sampled headspace prior to normalization to the OPA porewater are represented in Table D.1 within Appendix D. In this section, each of the concentrations of ^{3}He, ^{4}He, ^{20}Ne, ^{21}Ne,

^{22}Ne, ^{36}Ar, ^{38}Ar, and ^{40}Ar, and the corresponding ratios between these noble gas isotopes will be outlined in turn.

Table 3.4: Concentrations normalized to the OPA porewater based on the ASW Approach, represented in cm^3STP/kg_{PW} obtained from the PE/Al-foil bag sample headspace

	^{3}He	±	^{4}He	±	^{20}Ne	±	^{21}Ne	±	^{22}Ne	±	^{36}Ar	±	^{38}Ar	±	^{40}Ar	±
UO_1_Al	1.92E-11	1.05E-11	2.97E-05	1.64E-05	1.50E-04	1.51E-05	4.43E-07	4.45E-08	1.51E-05	1.52E-06	6.09E-05	1.10E-05	1.14E-05	2.06E-06	1.80E-02	3.25E-03
UO_2_Al	3.19E-11	1.75E-11	8.84E-05	4.86E-05	1.50E-04	1.51E-05	4.43E-07	4.45E-08	1.53E-05	1.53E-06	3.69E-05	6.65E-06	7.08E-06	1.28E-06	1.14E-02	2.06E-03
UO_3_Al	1.45E-11	7.99E-12	7.23E-06	3.98E-06	1.50E-04	1.51E-05	4.41E-07	4.44E-08	1.51E-05	1.52E-06	6.03E-05	1.09E-05	1.13E-05	2.04E-06	1.76E-02	3.17E-03
UO_4_Al	2.20E-11	1.21E-11	1.31E-05	7.23E-06	1.50E-04	1.51E-05	4.44E-07	4.47E-08	1.52E-05	1.53E-06	5.99E-05	1.08E-05	1.16E-05	2.09E-06	1.87E-02	3.38E-03
UO_5_Al	1.36E-10	7.47E-11	6.48E-04	3.56E-04	1.50E-04	1.51E-05	4.43E-07	4.46E-08	1.52E-05	1.53E-06	6.14E-05	1.11E-05	1.18E-05	2.13E-06	1.90E-02	3.44E-03
Air	7.34E-12	-	5.24E-06	-	1.65E-05	-	4.87E-08	-	1.68E-06	-	3.14E-05	-	5.90E-06	-	9.30E-03	-
ASW	5.45E-14	-	3.90E-08	-	1.50E-04	-	4.46E-10	-	1.53E-08	-	1.03E-06	-	1.93E-07	-	3.05E-04	-

Note: There is an additional uncertainty associated with the "jumpy" air standards and lack of historical data for the newly commissioned noble gas extraction line and Helix-MC Mass Spectrometer, as explained. Only blank correction and air standards normalization have been applied to this data. This data is representative of the bag headspace volume, and not the porewater of the OPA core within the PE/Al-foil bag.

Table 3.5: The common noble gas isotopic ratios obtained from sampling the PE/Al-foil bag sample headspace

	R/R_a	±	$^{20}Ne/^{22}Ne$	±	$^{38}Ar/36Ar$	±	$^{40}Ar/^{36}Ar$	±	$^{20}Ne/^{36}Ar$	±
UO_1_Al	0.46	0.005	9.95	0.23	0.19	0.002	296.08	2.22	2.47	0.51
UO_2_Al	0.26	0.004	9.86	0.25	0.19	0.002	310.00	2.84	4.08	0.84
UO_3_Al	1.44	0.010	9.94	0.22	0.19	0.001	291.44	1.96	2.49	0.52
UO_4_Al	1.20	0.012	9.90	0.24	0.19	0.002	313.07	2.67	2.51	0.52
UO_5_Al	0.15	0.004	9.89	0.24	0.19	0.005	309.39	8.09	2.45	0.51
Air	1	-	9.81	-	0.188	-	295.5	-	0.52	-

Note: The uncertainty for the $^{20}Ne/^{36}Ar$ isotopic ratio is greater than the other ratios represented here due to having to account for the additional error introduced by the "jumpy" standards. These additional uncertainties are generally in-proportion between isotopes of the same noble gas, so are able to be neglected for the other ratios here.

3.3.1 Helium

As explained in section 2.3.1, the most pivotal metric to examine in any noble gas geochemistry study involving the measurement of helium isotopes, is the R/R_a ratio. To reiterate, this metric is representative of the sample $^3He/^4He$ ratio relative to the atmospheric $^3He/^4He$ ratio (1.399×10^{-6}, per Porcelli et al., 2002) and if our samples exhibited an atmospheric $^3He/^4He$ signature, we would expect an R/R_a equal to 1. Figure 3.3 represents the R/R_a metric within the headspace of the 5 cores encapsulated within the PE/Al-foil bags, alongside the R/R_a for the near-identical samples from the stainless-steel (SS) cylinders.

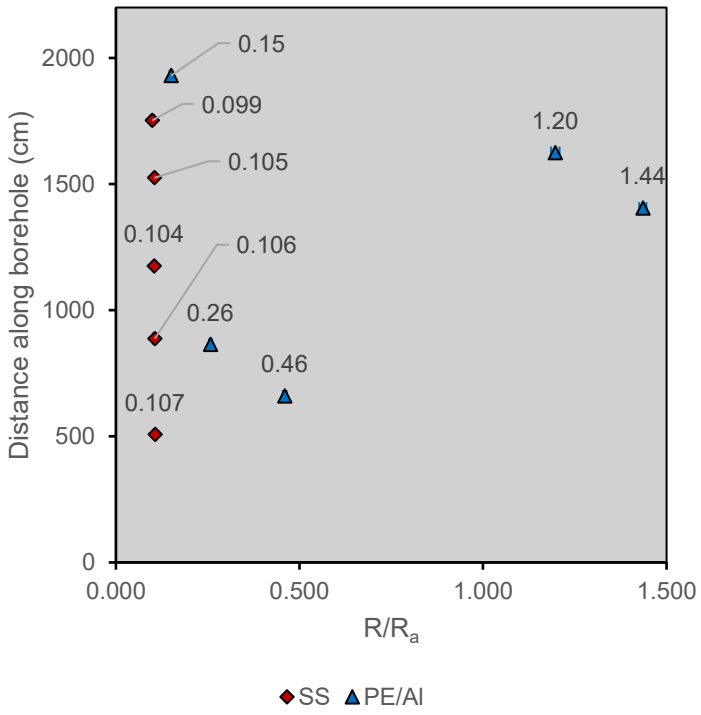

Figure 3.3: Plot of R/Ra values within the PE/Al-foil bag-encapsulated samples with respect to their distance along the horizontal borehole. These ratios are plotted alongside the corresponding ratios from the stainless-steel cylinder encapsulated samples (SS).

The range of R/R_a values for the PE/Al-foil bag samples ranges from 0.15 to 1.44, with a mean of 0.7 ± 0.52, exhibiting far less agreement than the SS-encapsulated samples. Generally, the samples exhibit an R/R_a below the atmospheric value of 1, however, two of these samples (3

and 4, at depths 1405 and 1625 cm, respectively) do not have uncertainties overlap with their SS-encapsulated sample counterparts and have an R/R_a value of approximately 1.44 and 1.2, respectively.

As for the concentrations of ^{3}He and ^{4}He, these are represented in Figures 3.4a and 3.4b and are plotted against their SS-encapsulated counterparts (also normalized to ^{20}Ne at ASW of seawater at 10°C). In terms of ^{3}He, the mean normalized concentration is $4.48 \times 10^{-11} \pm 4.61 \times 10^{-11}$ cm^3/kg_{PW}. Relative to air, the mean normalized ^{3}He concentration is 6.28 times greater than the air concentration (7.34×10^{-12} cm^3/kg_{PW}), indicating potential minor thermal neutron capture of ^{6}Li within the crustal environment sampled (Ballentine and Burnard, 2002). Relative to the mean normalized ^{3}He concentration within the SS-encapsulated sample porewater (1.43×10^{-8} cm^3/kg_{PW}), the mean normalized ^{3}He concentration within PE/Al-foil bag-encapsulated sample porewater represents approximately 0.318% of this value.

Whereas, in terms of ^{4}He, the mean normalized concentration is $1.57 \times 10^{-4} \pm 2.47 \times 10^{-4}$ cm^3/kg_{PW}. Relative to air, the mean normalized ^{4}He concentration is 47.11 times greater than the air concentration (5.24×10^{-6} cm^3/kg_{PW}), thus potentially indicating a significant radiogenic component of ^{4}He (Ballentine and Burnard, 2002). Relative to the mean normalized ^{4}He concentration within the SS-encapsulated sample porewater (9.65×10^{-2} cm^3/kg_{PW}), the mean normalized ^{4}He concentration within PE/Al-foil bag-encapsulated sample porewater represents approximately 0.163% of this value.

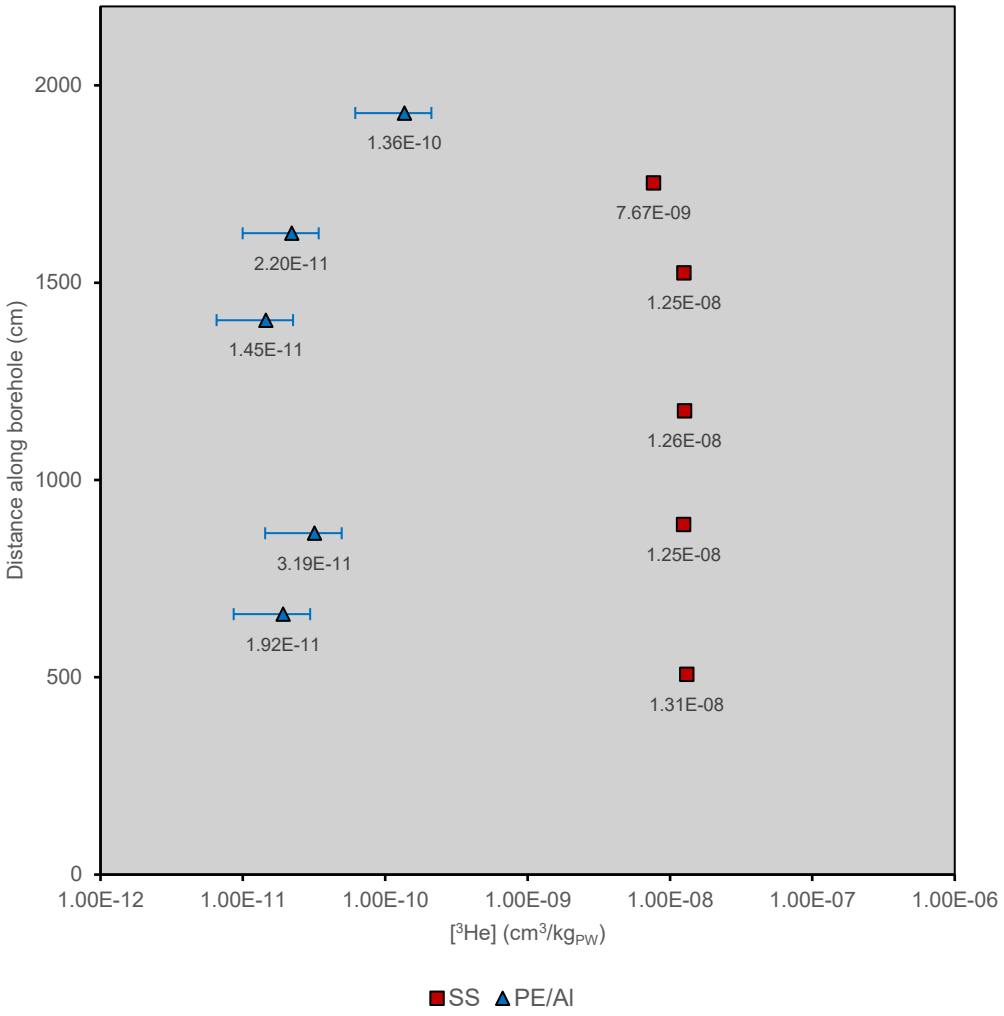

Figure 3.4a: Plot of normalized ^{3}He concentrations within the PE/Al-foil bag-encapsulated sample porewater with respect to their distance along the horizontal borehole. These concentrations are plotted alongside the corresponding concentrations from the stainless-steel cylinder encapsulated samples (SS).

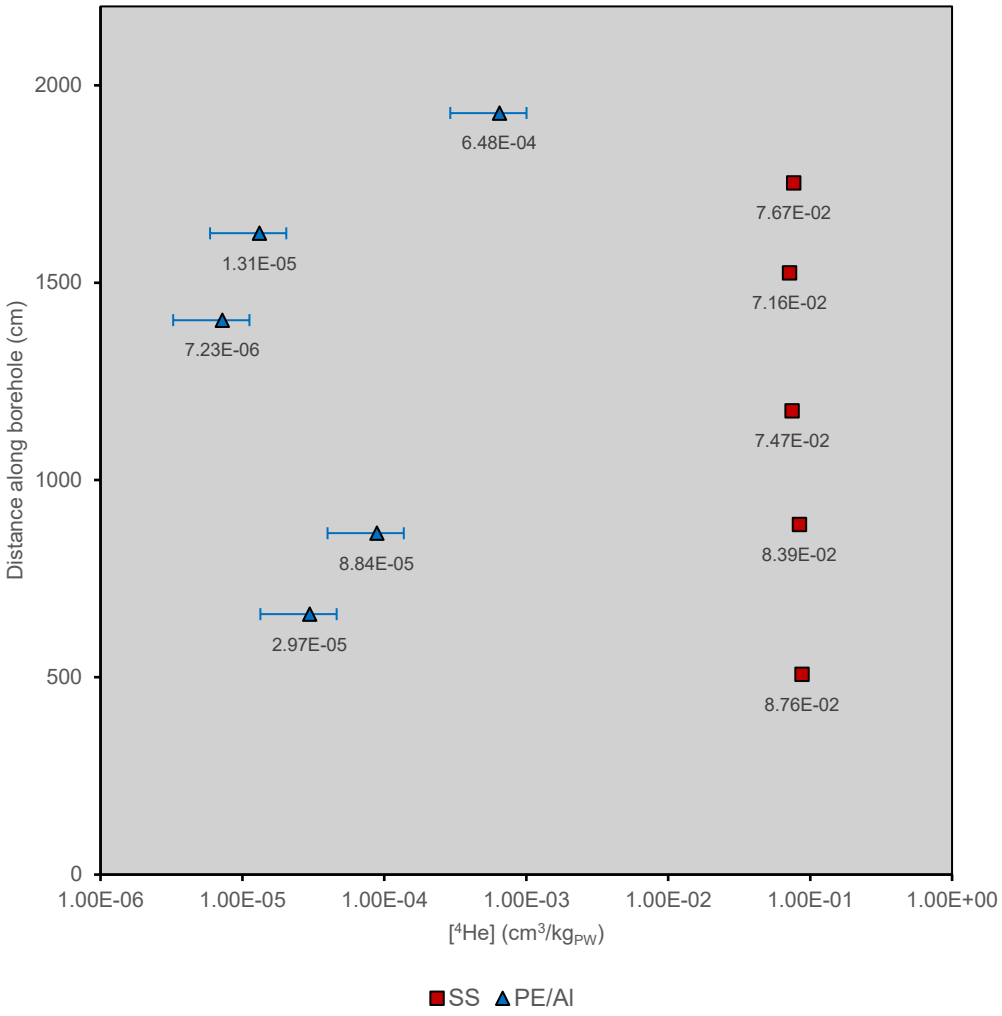

Figure 3.4b: Plot of normalized ^{4}He concentrations within the PE/Al-foil bag-encapsulated sample porewater with respect to their distance along the horizontal borehole. These concentrations are plotted alongside the corresponding concentrations from the stainless-steel cylinder encapsulated samples (SS).

3.3.2 Neon

Figure 3.5 demonstrates this $^{20}Ne/^{22}Ne$ ratio for these PE/Al-foil bag samples, and their SS-encapsulated counterparts alongside each other, with respect to their distance along the horizontal borehole.

The $^{20}Ne/^{22}Ne$ ratio for the PE/Al-foil bag samples ranges from 9.86 to 9.95, and has a mean of 9.91 ± 0.03, demonstrating a closer agreement between one another than the SS-

encapsulated samples. In addition to this, these PE/Al-foil bag samples demonstrate isotopic signatures more closely aligned with the atmospheric value of 9.81, as the error bars extend below this atmospheric value.

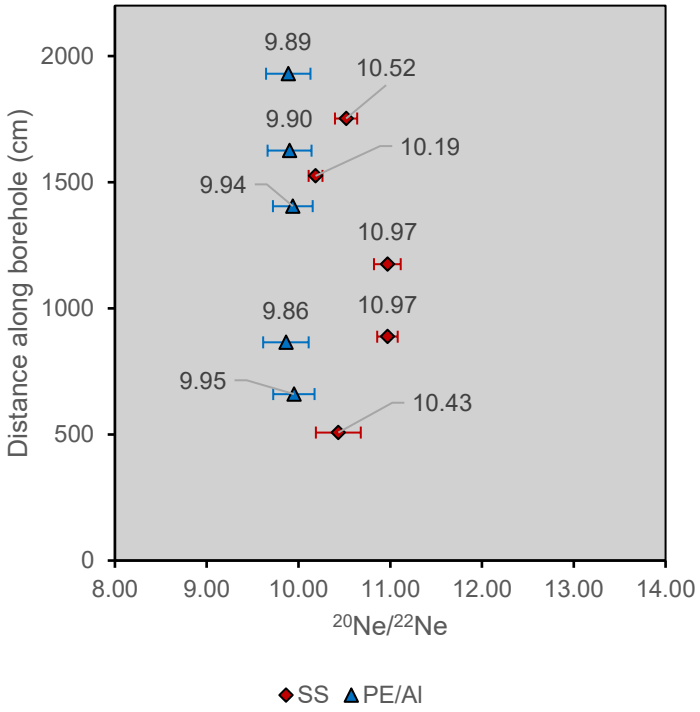

Figure 3.5: Plot of $^{20}Ne/^{22}Ne$ values within the PE/Al-foil bag-encapsulated samples with respect to their distance along the horizontal borehole. Note the atmospheric ratio of 9.81 (Porcelli et al., 2002). These ratios are plotted alongside the corresponding ratios from the stainless-steel cylinder encapsulated samples (SS).

The concentration of ^{20}Ne within the porewater of the PE/Al-foil encapsulated cores was not plotted, as via the ASW Approach, it is assumed that the porewater concentrations are equal to ASW of seawater at 10°C. As for the concentrations of ^{21}Ne, and ^{22}Ne, these are represented in Figures 3.6a, and 3.6b, and are plotted against their SS-encapsulated counterparts (also normalized to ^{20}Ne at ASW of seawater at 10°C). In terms of ^{20}Ne, since the ASW Approach has been utilised to normalize the ^{20}Ne concentrations to the value of ^{20}Ne at ASW (of seawater at 10°C), the assumption that all ^{20}Ne within the porewater of the

OPA is this ASW value (1.50×10^{-4} cm^3/kg_{PW}). Relative to ^{20}Ne within air (1.65×10^{-5} cm^3/kg_{PW}), the ASW concentration is 9.15 times greater than this.

As for ^{21}Ne, the mean normalized concentration is approximately $4.43 \times 10^{-7} \pm 9.98 \times 10^{-10}$ cm^3/kg_{PW}. Relative to air, the observed mean normalized concentration is approximately 2.05% of the air concentration (4.87×10^{-8} cm^3/kg_{PW}). Relative to the mean normalized ^{21}Ne concentration within the SS-encapsulated sample porewater (5.23×10^{-7} cm^3/kg_{PW}), the mean normalized ^{21}Ne concentration within PE/Al-foil bag-encapsulated sample porewater is approximately 18.17% greater.

Finally, for ^{22}Ne, the mean normalized concentration is approximately $1.52 \times 10^{-5} \pm 4.89 \times 10^{-8}$ cm^3/kg_{PW}. Comparative to the air concentration (1.68×10^{-6} cm^3/kg_{PW} [3]), the observed mean normalized concentration is approximately 2.92% representative of this. Relative to the mean normalized ^{22}Ne concentration within the SS-encapsulated sample porewater (1.73×10^{-5} cm^3/kg_{PW}), the mean normalized ^{22}Ne concentration within PE/Al-foil bag-encapsulated sample porewater is approximately 14.24% greater.

In summary, all neon isotopes analysed as part of this study exhibit a mean sample concentration close to the approximate 3% of what would be expected within the atmosphere (in comparison to the SS-encapsulated samples), however the $^{20}Ne/^{22}Ne$ ratio in this case is closely aligned with the atmospheric value of 9.81.

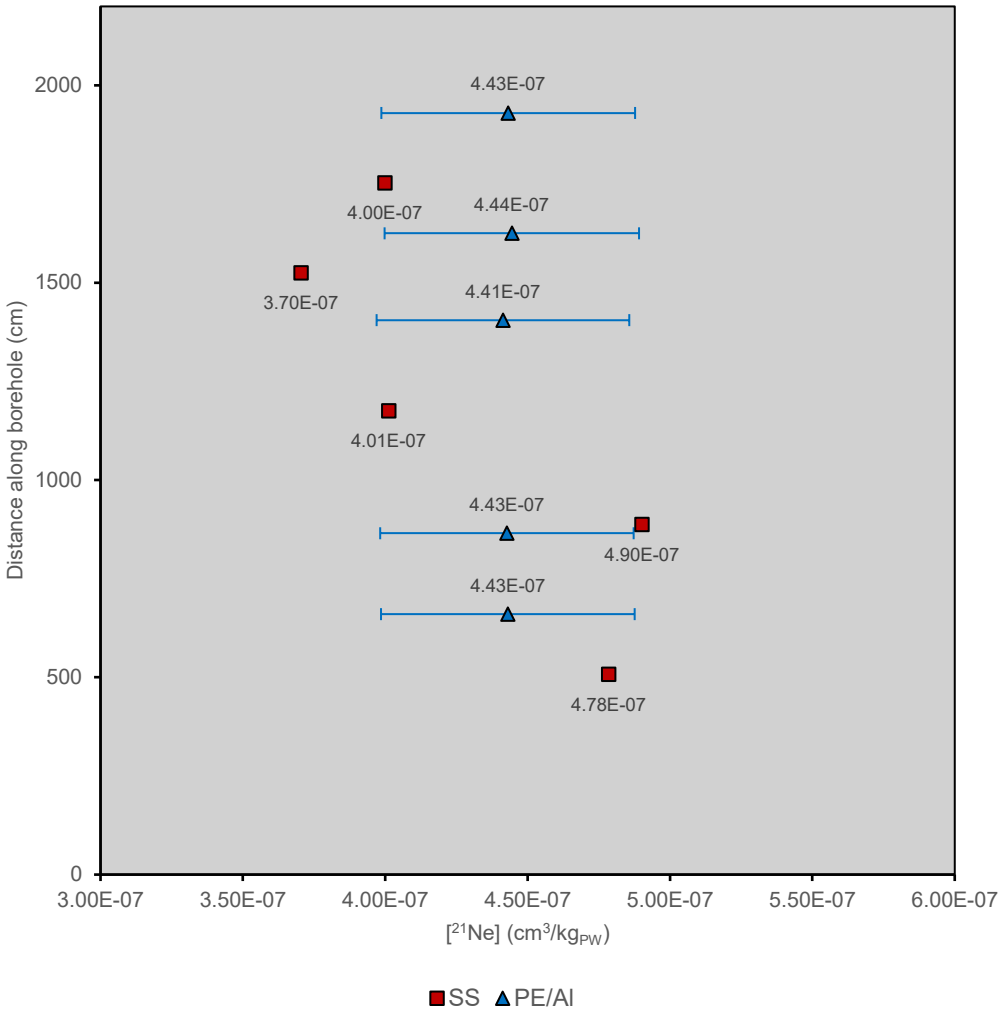

Figure 3.6a: Plot of normalized ^{21}Ne concentrations within the PE/Al-foil bag-encapsulated sample porewater with respect to their distance along the horizontal borehole. These concentrations are plotted alongside the corresponding concentrations from the stainless-steel cylinder encapsulated samples (SS).

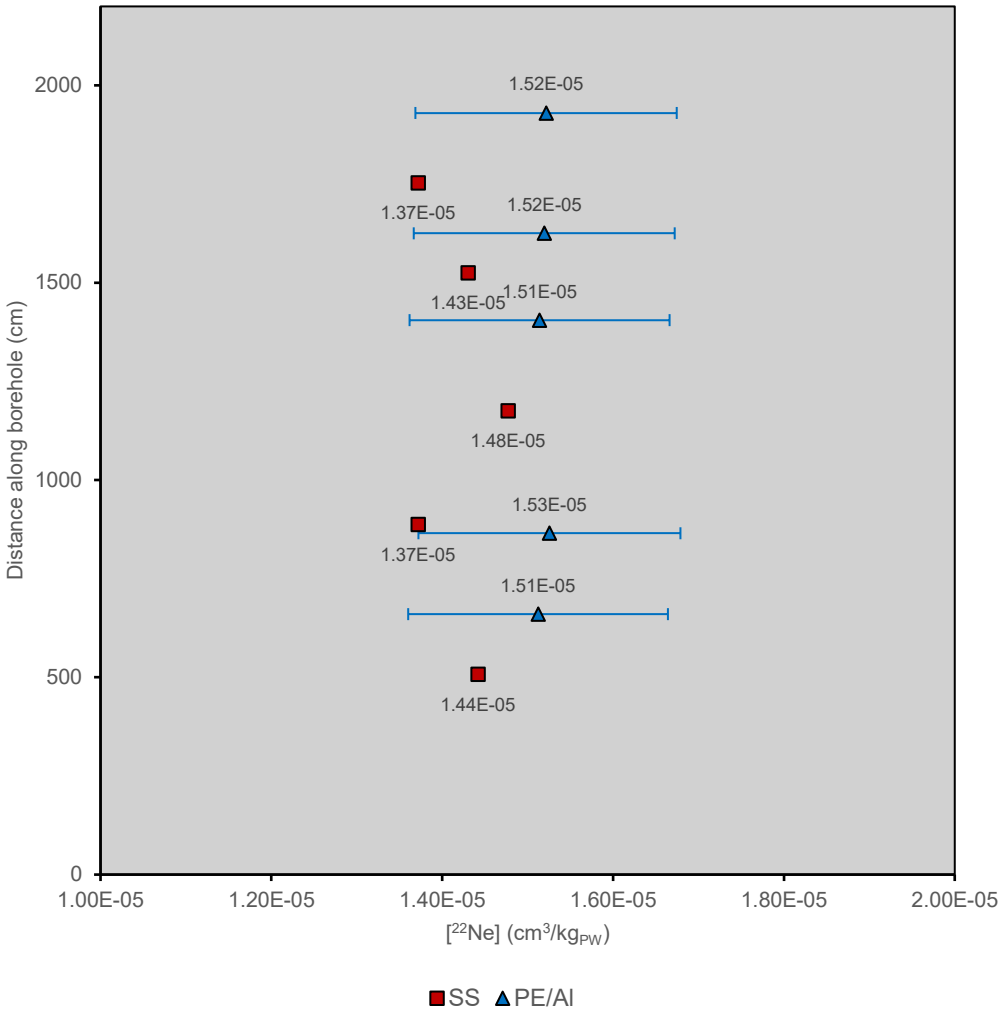

Figure 3.6b: Plot of normalized ^{22}Ne concentrations within the PE/Al-foil bag-encapsulated sample porewater with respect to their distance along the horizontal borehole. These concentrations are plotted alongside the corresponding concentrations from the stainless-steel cylinder encapsulated samples (SS).

3.3.3 Argon

The $^{40}Ar/^{36}Ar$ ratio for the PE/Al-foil bag samples ranges from 291.44 (sample 3, depth 1405 cm) to 313.07 (sample 4, depth 1625 cm), and between these five samples, the mean is 303.99 ± 8.58. All samples, with the exception of sample 3, are above the atmospheric ratio of 295.5, although sample 1 does have an error range that overlaps with this atmospheric value (Porcelli et al., 2002). These ratios with respect to distance along the horizontal borehole are represented in Figure 3.7.

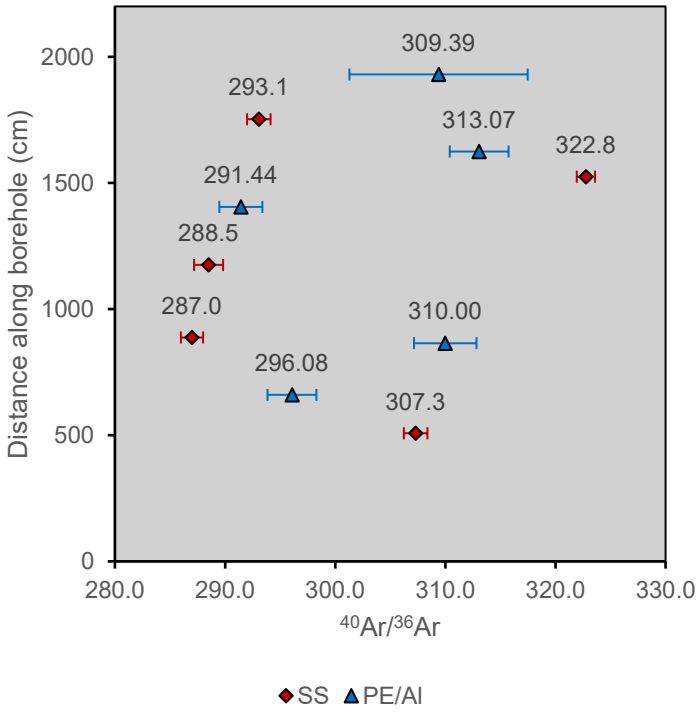

Figure 3.7: Plot of $^{40}Ar/^{36}Ar$ values within the PE/Al-foil bag-encapsulated samples with respect to their distance along the horizontal borehole. Note the atmospheric ratio is 295.5 (Porcelli et al., 2002). These ratios are plotted alongside the corresponding ratios from the stainless-steel cylinder encapsulated samples (SS).

As for the concentrations of ^{36}Ar, ^{38}Ar, and ^{40}Ar, these are represented in Figures 3.8a, 3.8b, and 3.8c, and are plotted against their SS-encapsulated counterparts (also normalized to ^{20}Ne at ASW of seawater at 10°C). In terms of ^{36}Ar, the mean normalized concentration is approximately $5.59 \times 10^{-5} \pm 9.52 \times 10^{-6}$ cm^3/kg_{PW}, which is approximately 30.29% of the air concentration of ^{36}Ar (3.14×10^{-5} cm^3/kg_{PW}). Relative to the mean normalized ^{36}Ar concentration within the SS-encapsulated sample porewater (1.16×10^{-3} cm^3/kg_{PW}), the mean normalized ^{36}Ar concentration within PE/Al-foil bag-encapsulated sample porewater represents approximately 4.831% of this value.

Whereas, with ^{38}Ar, the mean normalized concentration is approximately $1.06 \times 10^{-5} \pm 1.78 \times 10^{-6}$ cm^3/ kg_{PW}. Relative to air, this is also representative of approximately 30.16% of the ^{38}Ar

air concentration (5.90×10^{-6} cm^3/kg_{PW}). Relative to the mean normalized ^{38}Ar concentration within the SS-encapsulated sample porewater (1.93×10^{-4} cm^3/kg_{PW}), the mean normalized ^{38}Ar concentration within PE/Al-foil bag-encapsulated sample porewater represents approximately 5.493% of this value.

Finally, for ^{40}Ar, the mean normalized concentration is approximately $1.70 \times 10^{-2} \pm 2.81 \times 10^{-3}$ cm^3/kg_{PW}. Much like with the latter argon isotopes also, the mean sample concentration represents approximately 30.2% of the air concentration of ^{40}Ar, which is 9.30×10^{-3} cm^3/kg_{PW}. Relative to the mean normalized ^{40}Ar concentration within the SS-encapsulated sample porewater (3.47×10^{-1} cm^3/kg_{PW}), the mean normalized ^{40}Ar concentration within PE/Al-foil bag-encapsulated sample porewater represents approximately 34.744% of this value.

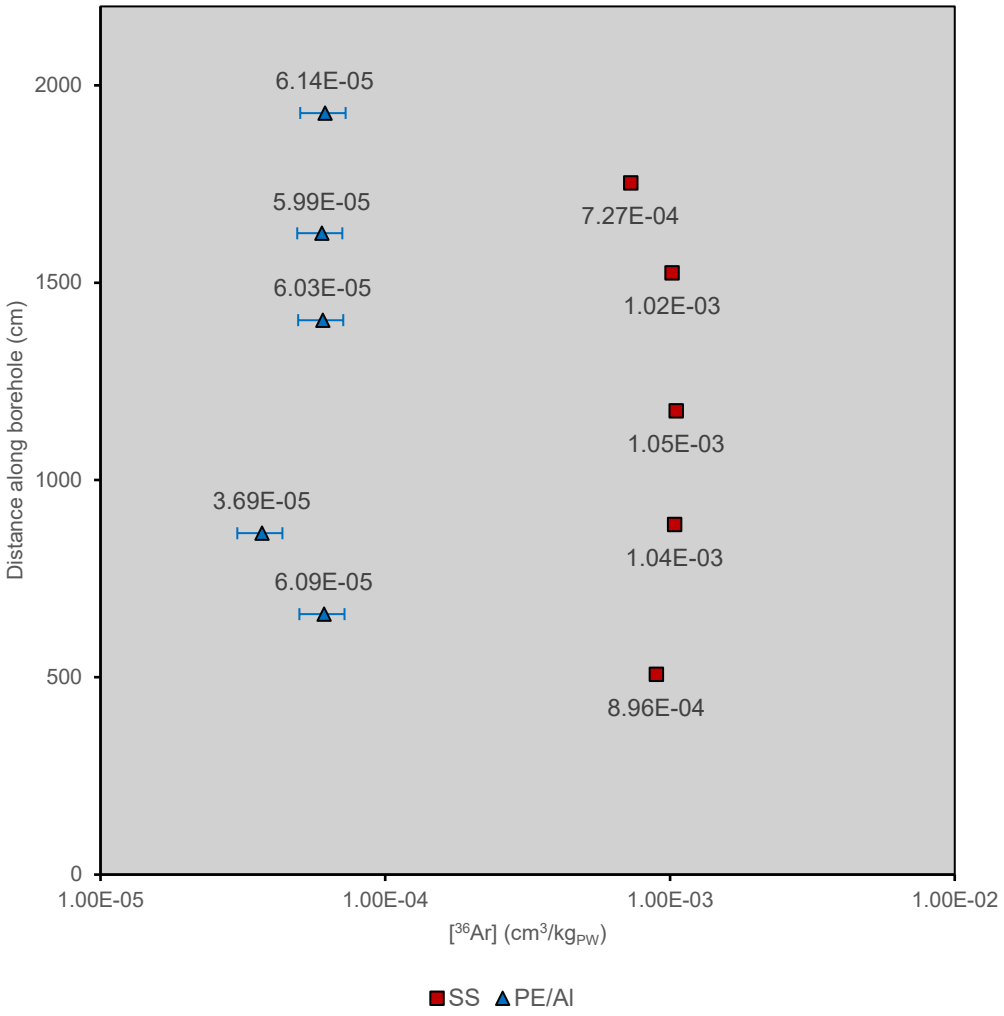

Figure 3.8a: Plot of normalized ^{36}Ar concentrations within the PE/Al-foil bag-encapsulated sample porewater with respect to their distance along the horizontal borehole. These concentrations are plotted alongside the corresponding concentrations from the stainless-steel cylinder encapsulated samples (SS).

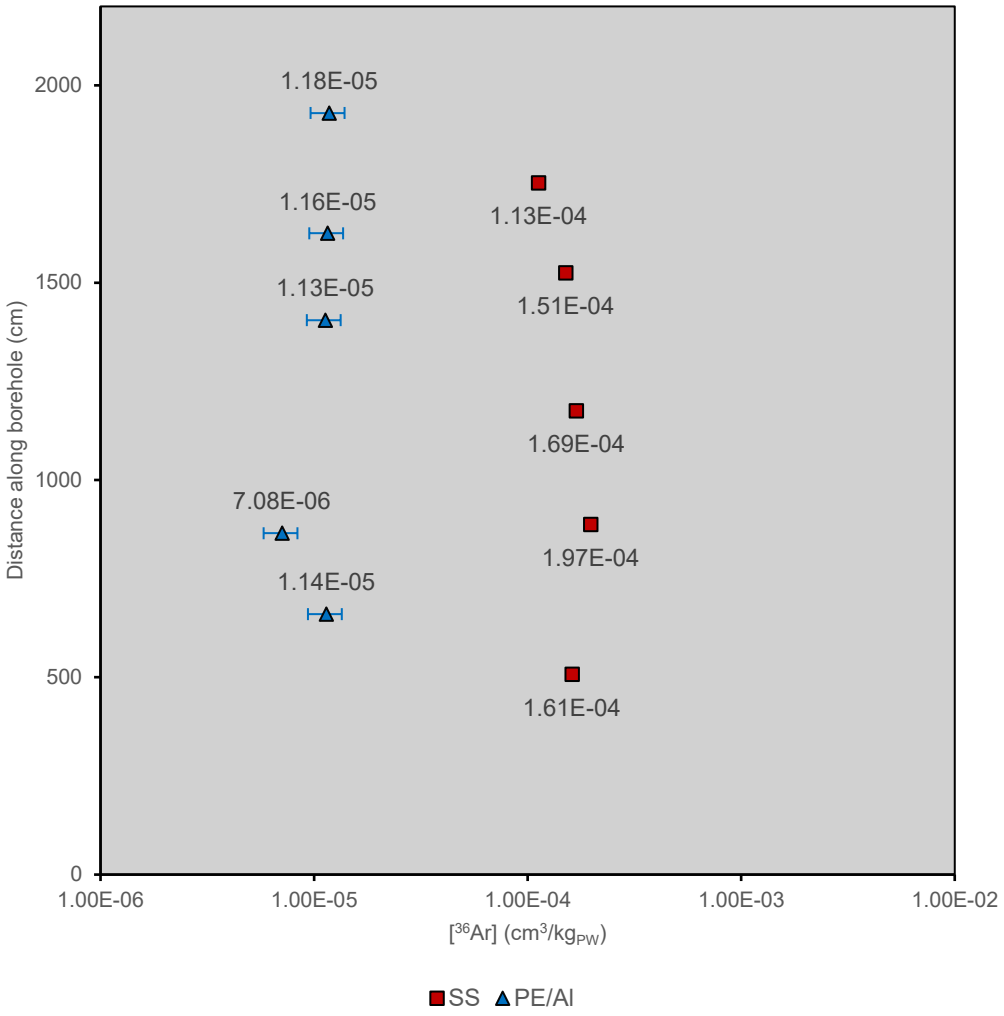

Figure 3.8b: Plot of normalized ^{38}Ar concentrations within the PE/Al-foil bag-encapsulated sample porewater with respect to their distance along the horizontal borehole. These concentrations are plotted alongside the corresponding concentrations from the stainless-steel cylinder encapsulated samples (SS).

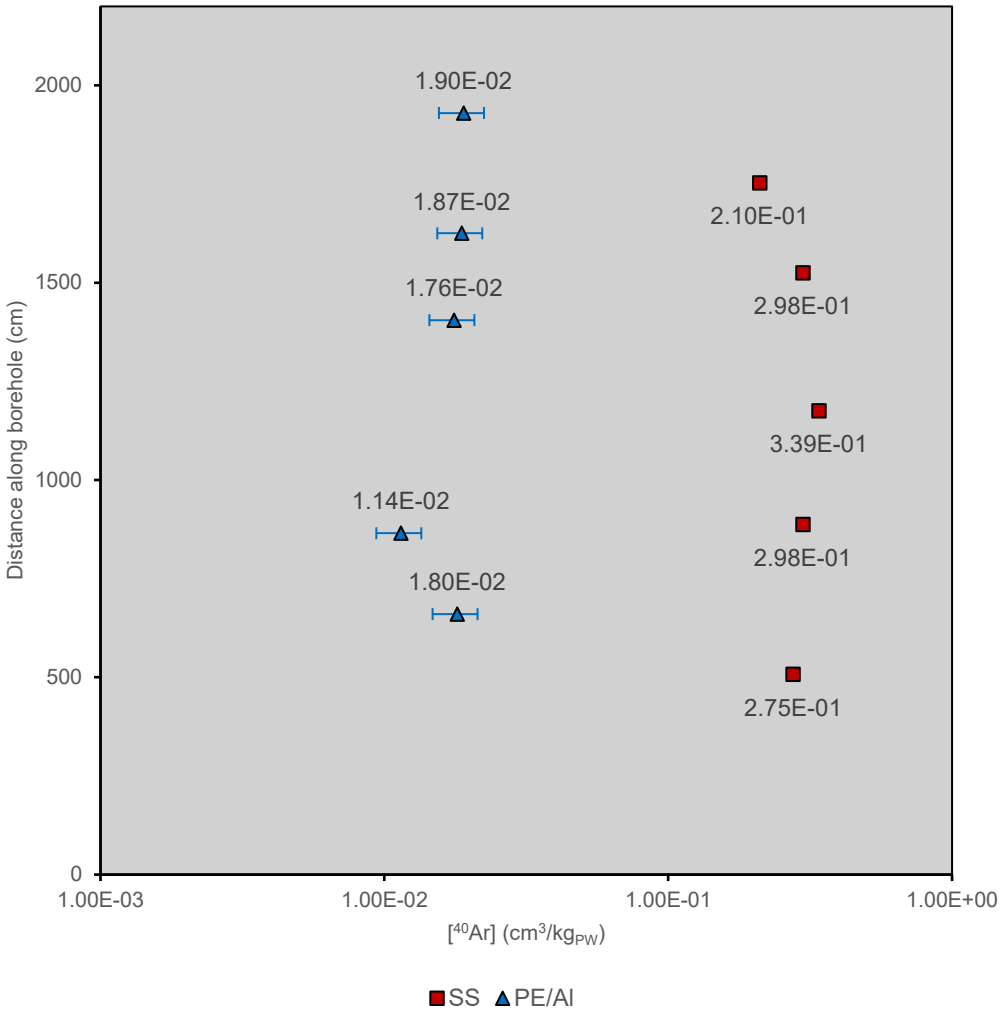

Figure 3.8c: Plot of normalized ^{40}Ar concentrations within the PE/Al-foil bag-encapsulated sample porewater with respect to their distance along the horizontal borehole. These concentrations are plotted alongside the corresponding concentrations from the stainless-steel cylinder encapsulated samples (SS).

3.4 Discussion

3.4.1 Air contamination

During data processing, it was noted that the R/R_a value for two of the samples was elevated to beyond the value expected for air. Typically, an R/R_a value beyond the value of air (1) often suggests that there is some mantle contribution of helium. However, The Mont Terri site is well-characterized (Rübel et al., 2002, Bossart and Thury, 2007; Bossart et al., 2017), so it is highly unlikely that there could be any mantle contributions that would push the R/R_a

ratio above the atmospheric signature (Hilton et al., 1999; Ballentine and Burnard, 2002; Jackson et al., 2007). As an alternative explanation, it is plausible that this elevated R/R_a value does simply represent what was initially an air-like signature, which was affected by some fractionation effect (as to be discussed in section 3.4.3). Isotopic mass-dependent fractionation has not been observed between the neon and argon isotopes, however there is a 25% difference in mass between ^3He and ^4He, thus following the logic as described within Torgersen et al. (2004), whereby lighter noble gases diffuse out of sedimentary rocks preferentially under elevated temperatures (with the absolute rate dependent on the physico-chemical structure of the host rock). Consequently, it is entirely possible that this R/R_a value simply reflects what could have been air (or even to some degree crustal with an air component), had the cores not been baked at 40°C for six weeks.

3.4.2 Sampling and extraction difficulties

As briefly outlined within section 3.2.2, this method of sample encapsulation within the PE/Al-foil bags presented additional challenges during the sampling and extraction process, which likely contributed to the potential (though unconfirmed) air contamination associated with two of the samples.

Firstly, and most notably, upon receipt of the bagged samples it was noticed that they were still rather tightly vacuum-sealed, with no headspace of note, with the exception of sample 3 (UO_3_Al) which was the longest core section (30 cm). In addition, when these samples were prepared, they were sealed within two interior layers of PVC, prior to being sealed within the PE/Al-foil bags. This proved difficult for the extraction procedure that had to be undertaken, as there was virtually no headspace for the Type-K needle to pierce into, and the opaque nature of the bags made it very difficult to positively identify whether the PVC layers were punctured by the needle.

Secondly, the Type-K needles proved to be a challenge in their own right. These needles were customized to be able to be connected to the Swagelok 1/6” stainless-steel capillary tubing and were designed not to core the septa and butyl caulk, and in turn, plug the needle preventing sampling of the apparent low volume of interior gases within the bag headspace. Thus, only a limited quantity of these were engineered for this experiment. The issue here is that it was very difficult to be able to support and guide the relatively thin needle while inserting it through the thick septa and butyl to puncture the bag, as the needle was often not strong enough to be able to withstand the resistance of these layers, causing bending, and in some cases, breaking. In this experiment, all 4 of the Type-K needles within the laboratory were spent as part of this process, which given the custom nature of these, could prove costly and time-consuming.

3.4.3 The $^{20}Ne/^{36}Ar$ ratio

During data processing, it was noted that for all samples the $^{20}Ne/^{36}Ar$ ratio was extremely elevated and well above the expected ASW and air ratio (0.15 and 0.52 (Porcelli et al., 2002), respectively), which represents the range that one would typically expect since both isotopes are primordial. This ratio (for the PE/Al-foil bag samples) is plotted with respect to the distance of each sample along the horizontal borehole within Figure 3.9. Notably, all 5 samples plot well above this ASW/air value range, even despite the additional error in analysis as outlined in previous sections, which has been propagated into this metric. This indicates that there is some external and consistent contribution of ^{20}Ne, or loss of ^{36}Ar through some suspected elemental mass-fractionation process. Unlike the samples examined within Chapter 2, with the exception of perhaps the helium isotopic ratios, these samples only appear to demonstrate this consistent elemental fractionation, rather than any form of isotopic mass fractionation in the heavier noble gases (i.e., Ne, Ar) whereby a Mass Fractionation Line (per the methodology outlined in Zhou et al., 2005) can be plotted. Currently, it is

suspected that the baking process (by which the cores were baked at 40°C for six weeks) to promote outgassing and headspace formation may have either resulted in, or contributed to, this observed mass fractionation effect. Therefore, promoting the preferential outgassing of the lighter Ne relative to the heavier Ar, whereby the rates of which are a complex function of temperature, lithology, structure, and geochemical composition (Torgersen et al., 2004). This leads one to believe that not enough time had elapsed between the sample collection and analysis for the cores to fully degas into the PE/Al-foil bag prior to the analysis.

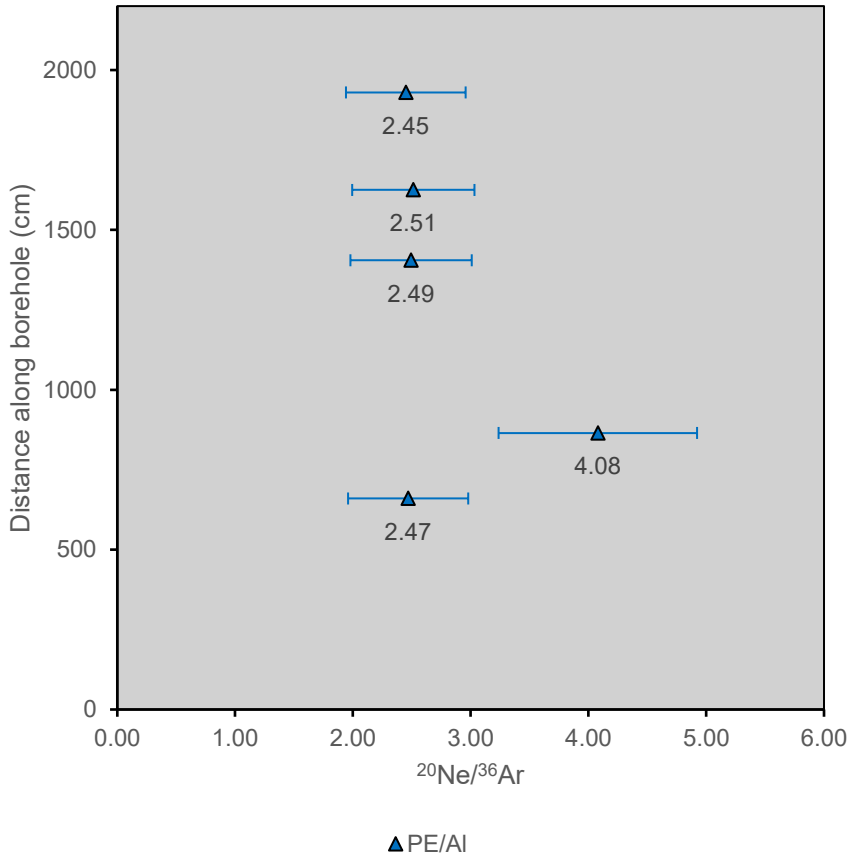

Figure 3.9: Plot of $^{20}Ne/^{36}Ar$ values within the PE/Al-foil bag-encapsulated samples with respect to their distance along the horizontal borehole. Note the atmospheric ratio is 0.52 (Porcelli et al., 2002).

Ultimately, this means that none of the normalization approaches outlined in Chapter 2 can truly be ideal in this scenario, since both the Porosity Approach and the Water Mass Approach

require a reliably determined headspace volume, and the ASW Approach relies on the assumption that there is no mass-dependent fractionation effects of ^{20}Ne, and that the primordial isotopes ^{20}Ne and ^{36}Ar remain at expected ASW concentrations. This again demonstrates the difficulty of sampling cores encapsulated within PE/Al-foil bags, particularly argillaceous cores, in this manner.

3.4.4 Future work

As explained throughout this chapter, there have been numerous challenges with the extraction and analysis of noble gases from PE/Al-foil bags. As an upcoming section within the PC-D report (either as an addendum, or to be included in the main body, depending on date of submission), these samples will be reanalysed utilizing the additional reserved copper tube aliquots prepared during the sampling process at a later date when there have been many more additional air standards run using the newly-commissioned noble gas extraction line and Helix-MC Plus mass spectrometer. It is hoped that this would provide further clarity and accuracy with respect to the isotopic concentrations and potential fractionation associated with these samples.

In terms of lessons learned by conducting this experiment, it would be presently recommended to not exclusively sample cores in this way, until such a time that a methodology can be further evaluated and standardised to ensure reproducible results. This experiment has demonstrated that despite the low-quality results obtained through difficulties with instrumentation, as previously detailed, information and insights can still be gathered simply from the isotopic ratios alone, should the cost of sampling with stainless-steel encapsulation outweigh the need for accurate porewater concentrations. If sampling and extracting noble gases from cores this way is an essential, then in that case it would be recommended to bake the cores for a longer period, beyond the six-week period used within this experiment, as to allow all noble gases to fully outgas into the bag and create a headspace. Alternatively, introducing an artificial

headspace at the time of sampling (e.g., with a highly pure inert gas, such as nitrogen), may allow for more efficient and effective degassing, in line with their stainless-steel counterparts. Or, it could also be suggested that leaving the cores at room temperature for an even more extended period to completely eliminate this risk of baking the cores driving a mass-dependent fractionation effect. In that regard, Zuo et al., (2022) demonstrated that at room temperature, an outgassing time of approximately 7-11 years may be required to generate a headspace, a timescale that presently may preclude reasonable turnaround times required for ongoing DGR prospecting and research.

3.5 References

Ballentine, C. J., & Burnard, P. G. (2002). *Production, Release and Transport of Noble Gases in the Continental Crust* (Vol. 47, Issue 1, pp. 481–538). https://doi.org/10.2138/rmg.2002.47.12

Bensenouci, F., Michelot, J. L., Matray, J. M., Savoye, S., Lavielle, B., Thomas, B., & Dick, P. (2011). A profile of helium-4 concentration in pore-water for assessing the transport phenomena through an argillaceous formation (Tournemire, France). *Physics and Chemistry of the Earth, Parts A/B/C*, *36*(17–18), 1521–1530. https://doi.org/10.1016/J.PCE.2011.10.016

Bossart, P., Burrus, F., Jaeggi, D., & Nussbaum, C. (2017). The Mont Terri rock laboratory. In X.-T. Feng (Ed.), *Rock Mechanics and Engineering* (1st ed., Vol. 2, pp. 469–510). CRC Press. https://doi.org/10.1201/9781315364254-26

Bossart, P., & Thury, M. (2007). Research in the Mont Terri Rock laboratory: Quo vadis? *Physics and Chemistry of the Earth, Parts A/B/C*, *32*(1–7), 19–31. https://doi.org/10.1016/J.PCE.2006.04.031

Greene, S., Battye, N., Clark, I., Kotzer, T., & Bottomley, D. (2008). Canadian Shield brine from the Con Mine, Yellowknife, NT, Canada: Noble gas evidence for an evaporated Palaeozoic seawater origin mixed with glacial meltwater and Holocene recharge. *Geochimica et Cosmochimica Acta*, *72*(16), 4008–4019. https://doi.org/10.1016/J.GCA.2008.05.058

Heard, A. W., Warr, O., Borgonie, G., Linage, B., Kuloyo, O., Fellowes, J. W., Magnabosco, C., Lau, M. C. Y., Erasmus, M., Cason, E. D., van Heerden, E., Kieft, T. L., Mabry, J. C., Onstott, T. C., Sherwood Lollar, B., & Ballentine, C. J. (2018). South African crustal fracture fluids preserve paleometeoric water signatures for up to tens of millions of years. *Chemical Geology*, *493*, 379–395. https://doi.org/10.1016/J.CHEMGEO.2018.06.011

Hilton, D. R., Grönvold, K., Macpherson, C. G., & Castillo, P. R. (1999). Extreme 3He/4He ratios in northwest Iceland: constraining the common component in mantle plumes. *Earth and Planetary Science Letters*, *173*(1–2), 53–60. https://doi.org/10.1016/S0012-821X(99)00215-0

Jackson, M. G., Kurz, M. D., Hart, S. R., & Workman, R. K. (2007). New Samoan lavas from Ofu Island reveal a hemispherically heterogeneous high 3He/4He mantle. *Earth and Planetary Science Letters*, *264*(3–4), 360–374. https://doi.org/10.1016/J.EPSL.2007.09.023

Lu, Z. T., Schlosser, P., Smethie, W. M., Sturchio, N. C., Fischer, T. P., Kennedy, B. M., Purtschert, R., Severinghaus, J. P., Solomon, D. K., Tanhua, T., & Yokochi, R. (2014). Tracer applications of noble gas radionuclides in the geosciences. *Earth-Science Reviews*, *138*, 196–214. https://doi.org/10.1016/J.EARSCIREV.2013.09.002

Osenbrück, K., Lippmann, J., & Sonntag, C. (1998). Dating very old pore waters in impermeable rocks by noble gas isotopes. *Geochimica et Cosmochimica Acta*, *62*(18), 3041–3045. https://doi.org/10.1016/S0016-7037(98)00198-7

Ozima, M., & Podosek, F. A. (2001). Noble Gases in the Earth. *Noble Gas Geochemistry*, 217–252. https://doi.org/10.1017/CBO9780511545986.009

Rübel, A. P., Sonntag, C., Lippmann, J., Pearson, F. J., & Gautschi, A. (2002). Solute transport in formations of very low permeability: profiles of stable isotope and dissolved noble gas contents of pore water in the Opalinus Clay, Mont Terri, Switzerland. *Geochimica et Cosmochimica Acta*, *66*(8), 1311–1321. https://doi.org/10.1016/S0016-7037(01)00859-6

Smith, S. P., & Kennedy, B. M. (1983). The solubility of noble gases in water and in NaCl brine. *Geochimica et Cosmochimica Acta*, *47*(3), 503–515. https://doi.org/10.1016/0016-7037(83)90273-9

Torgersen, T., Kennedy, B. M., & van Soest, M. C. (2004). Diffusive separation of noble gases and noble gas abundance patterns in sedimentary rocks. *Earth and Planetary Science Letters*, *226*(3–4), 477–489. https://doi.org/10.1016/J.EPSL.2004.07.030

Warr, O., Ballentine, C. J., Onstott, T. C., Nisson, D. M., Kieft, T. L., Hillegonds, D. J., & Sherwood Lollar, B. (2022). 86Kr excess and other noble gases identify a billion-year-old radiogenically-enriched groundwater system. *Nature Communications*, *13*(1), 1–9. https://doi.org/10.1038/S41467-022-31412-2;TECHMETA

Warr, O., Rochelle, C. A., Masters, A., & Ballentine, C. J. (2015). Determining noble gas partitioning within a CO2–H2O system at elevated temperatures and pressures. *Geochimica et Cosmochimica Acta*, *159*, 112–125. https://doi.org/10.1016/J.GCA.2015.03.003

Warr, O., Sherwood Lollar, B., Fellowes, J., Sutcliffe, C. N., McDermott, J. M., Holland, G., Mabry, J. C., & Ballentine, C. J. (2018). Tracing ancient hydrogeological fracture network age and compartmentalisation using noble gases. *Geochimica et Cosmochimica Acta*, *222*, 340–362. https://doi.org/10.1016/J.GCA.2017.10.022

Zhou, Z., Ballentine, C. J., Kipfer, R., Schoell, M., & Thibodeaux, S. (2005). Noble gas tracing of groundwater/coalbed methane interaction in the San Juan Basin, USA. *Geochimica et Cosmochimica Acta*, *69*(23), 5413–5428. https://doi.org/10.1016/J.GCA.2005.06.027

Zuo, E., Lapp, A., Jautzy, J. J., & Clark, I. D. (2022). Crustal Noble Gas Isotopic Characteristics in Low-Permeability Ordovician Sedimentary Rock, Eastern Flank of the Michigan Basin. *ACS Earth and Space Chemistry*, *6*(1), 189–196. https://doi.org/10.1021/ACSEARTHSPACECHEM.1C00346

CHAPTER 4: CONCLUSIONS AND FURTHER WORK

In recent years, the safe long-term storage of nuclear waste into geological formations has proven to be a key area of ongoing research, and also of strong interest to the public. The development of nuclear energy, particularly within Canada, is an essential in order to sustain the energy requirements of current and future generations. The use of noble gases are increasingly being considered as tracers for evaluating the (bio)geochemical and physical processes of interest and relevance to Deep Geological Repositories (DGRs), however, there are significant challenges in the development of these tracers in order for them to become commonplace in such site characterisations.

The purpose of this research was to develop and evaluate methodologies and approaches to both extract and quantify the isotopic noble gases within the porewater of the Opalinus Clay (OPA) formation in Switzerland, a potential analogue for argillaceous DGRs (Bossart and Thury, 2008). The first study included here focuses primarily on the traditional stainless-steel cylinder encapsulation of these cores, whereby the headspace within these cylinders is sampled for its noble gases. This study engages heavily with three proposed techniques to normalize these noble gases sampled from the headspace to the porewater of the OPA and subsequently determines that each approach relies heavily on a number of assumptions. Typically, normalizing based on the "ASW Approach" would be the preferred approach for most solid-phase samples of this type, since this would rely on the fewest number of assumptions to be made. However, in instances where additional processes may have occurred (e.g., modest degrees of mass-dependent isotopic fractionation effects, such as those observed in the University of Ottawa samples) this approach may not be optimal. Instead, other straightforward approaches may be preferred that do not make assumptions on the initial noble gas content of the fluids. Specifically, since the Opalinus Clay is a homogeneous analogue (Bossart and Thury, 2008) for argillaceous-type DGR settings, the "Porosity

Approach" which estimated noble gas porewater content based on average porosities for this lithology was deemed the next-best solution.

As a secondary study included here, an alternative encapsulation technique, identical to the technique used in Zuo et al. (2021), was evaluated against the standard approach. In this alternative sampling technique, samples are stored within vacuum-sealed PE/Al-foil bags, as opposed to the traditional stainless-steel cylinders. This study required the development of new techniques in the sampling and extraction of the headspace gas from these bags. In particular, a new technique was developed to generate sufficient headspace to sample, as it was evident that very little headspace had degassed from the cores in the ~4 years between on-site sample preparation and in-laboratory sampling and extraction. Consequently, these cores were gently baked at 40°C for six weeks to promote outgassing to successfully create a headspace to sample. However, this study found that this may have inadvertently caused isotopic fractionation of helium isotopes, and elemental fractionation of neon and argon, as demonstrated by the $^{20}Ne/^{36}Ar$ ratio which consistently plotted well above the corresponding air and ASW ratios.

In sum, these studies illustrate the lessons learned through sampling solid-phase argillaceous core samples for their porewater noble gases, including the considerations that must be made, and potential variability within their results. Further work would be recommended to outline a more definitive best-practice approach at each stage of the process of this analysis, from on-site sampling, sample encapsulation and storage, in-laboratory analytical techniques, and effective normalization to the porewater of the core. It is hoped that the upcoming PC-D project technical report may shed further light on this.

4.1 References

Bossart, P., & Thury, M. (2008). Mont Terri Rock Laboratory. Project, Programme 1997 to 2007 and results (Issue 3).

Zuo, E., Lapp, A., Jautzy, J. J., & Clark, I. D. (2022). Crustal Noble Gas Isotopic Characteristics in Low-Permeability Ordovician Sedimentary Rock, Eastern Flank of the Michigan Basin. ACS Earth and Space Chemistry, 6(1), 189–196. https://doi.org/10.1021/ACSEARTHSPACECHEM.1C00346

APPENDIX A: DEPOSITIONAL ENVIRONMENT, LITHOSTRATIGRAPHY, AND FACIES OF THE MONT TERRI REGION

A.1 Depositional Environment

The Opalinus Clay (OPA) was deposited in a shallow marine environment, characterized by an average water depth ranging from 20 to 50 metres. During storms or shift in current patterns, fine sand layers were transported from the mainland and deposited within the clay formation. The northern boundary of this shallow sea was marked by the presence of the Rhenish Slate Mountains, while to the east and south, it was delineated by the Bohemian Massive or the Alemannic Islands. Geographically, the deposition area was marked by a triangular shape spanning between Bern, Munich, and Strasbourg (Wermeille and Bossart, 1999). Given the extensive coverage of this deposition area and homogeneity of the OPA formation, we can reasonably extrapolate the conditions observed at Mont Terri to other regions, including potential Deep Geological Repositories (DGRs) (NAGRA, 2024).

A.2 Lithostatigraphy and Facies

The stratigraphy of the Mont Terri site is most clearly documented within Hostettler et al. (2017). This study examined a vertical borehole (BDB-1) and identified that the site is composed of four primary formations, which will be described in turn from deepest to shallowest, with the following information all from Hostettler et al. (2017) unless otherwise indicated.

First, the Staffeleg formation (247.5 – 236.8 m) occupies stratigraphically the lowermost section of the core. The deepest interval is assigned to the Rietheim Member (247.5-243.28 m) and consists of thinly bedded, brownish-black bituminous silty mudstones. These fine-grained sediments mark the foundation of the stratigraphic succession observed in the borehole. Overlying is the Gross Wolf Member (243.28-236.8 m), characterized by grey clayey marls,

light grey marls, and argillaceous limestones. The top of the Staffelegg Formation is defined by the uppermost occurrence of an argillaceous limestone bed.

Second, the Opalinus clay (OPA) in the BDB-1 core had a thickness of 130.55 m. The OPA can be subdivided into five lithofacies-based subunits arranged from bottom to top, represented in Table A.1.

Table A.1: Lithofacies of the Opalinus Clay formation, their depth intervals, and typical characteristics.

Lithofacies	Depth Interval	Characteristics
Shaly facies 1	236.8 – 190.4 m	Dark grey calcareous, silty-sandy claystones containing mica and pyrite. Numerous calcite lenses from mm-scale to 3 cm in thickness.
Carbonate-rich sandy facies	190.4 – 186.35 m	Dark grey calcareous, silty-sandy claystone layers alternating with fine-grained light-grey calcareous lenses and dm-size layers. Biogenic debris up to 2 cm.
Sandy facies 1	166.35 – 173.7 m	Calcareous with silty-sandy claystones interspersed with light grey, thinly bedded sandstone lenses. Ripple marks and bioturbation structures with lens-like appearance due to compactional deformation.
Shaly facies 2	173.70 – 137.73 m	Dark grey, mostly mica and pyrite containing calcareous silty-sandy claystones.
Sandy facies 2	137.73 – 106.25 m	Calcareous, silty-sandy claystones with numerous light-grey, laminated sandstone lenses. These lenses are often rippled and are lens-shaped due to compaction.

Third, the Passwang Formation extends from 106.25 to 37.07 m within BDB-1. The basal interval (106.25 – 95.4 m) is assigned to the Sissach Member, and includes silty to fine-sandy marls, quartz sands, bio-detrital and ferruginous limestones, and iron oolitic marls, with grey marls interbedded with sandstone lenses varying in quartz and bioclast content. Rust-red limonitic and sandy limestone beds containing limonitic bioclasts and iron ooids also occur,

with the uppermost beds (97.9 – 95.4 m) consisting of iron oolitic limestones with lithoclasts. The overlying interval (76.38 – 57.07 m), which does not correspond to any previously defined members, comprises alternating sandy limestones and marls, with features such as laminated and cross-bedded structures, quartz- and bioclast-rich laminae, and coarse, spiritic, bioclast-bearing limestones with limonitic intraclasts. The upper part of this formation (57.07-37.07 m) includes slab-shaped, fine-sandy, bio-detrital limestones alternating with marls, transitioning upwards into silty to fine-sandy marls with mm-thin sandstone lenses, often enriched in ferruginous dolomite.

Finally, the Hauptrogenstein formation begins at 37.07 m, marked by the first occurrence of oolithic limestone. The entire interval from 37.07 to 0 m belongs to the lower portion of the Hauptrogenstein, commonly referred to as the "Lower Oolitic Series" after Gonzales and Wetzel (1996). The basal section (37.07 – 29.9 m) is composed of grey micrites that are oolithic, oncolithic, and bioclastic in nature. This is overlain by a thicker unit of well-defined, coarse-grained, beige and light-grey calcarenites (29.9 – 13.18 m), in which oncosparites are the dominant lithology. In the subsequent interval (13.18 – 5.1 m), coral-bearing, bioclast-rich marls are present, followed by a return to the oncomicritic and oncosparitic limestones in the uppermost section (5.1 – 0 m) of the core.

A.3 References

Gonzalez, R., & Wetzel, A. (1996). Stratigraphy and paleogeography of the Hauptrogenstein and Klingnau Formations (middle Bajocian to late Bathonian), northern Switzerland. *Eclogae Geologicae Helvetiae: Recueil Périodique de La Société Géologique Suisse= Mitteilungen Der Schweiz. Geologischen Gesellschaft*, *89*(1), 695–720.

Hostettler, B., Reisdorf, A., Jaeggi, D., Deplazes, G., Bläsi, H., Morard, A., Feist-Burkhardt, S., Waltschew, A., Dietze, V., & Menkveld-Gfeller, U. (2017). Litho- and biostratigraphy of the Opalinus Clay and bounding formations in the Mont Terri rock

laboratory (Switzerland). *Swiss Journal of Geosciences*, *110*. https://doi.org/10.1007/s00015-016-0250-3

NAGRA. (2024). *Geosynthesis of Northern Switzerland (NTB 24-17)*. https://www.drbg.ch/rbg-gtl/zentrale-referenzberichte/geosynthesis-of-northern-switzerland-ntb-24-17/5-key-characteristics-of-the-host-rock-and-clay-mineral-rich-confining-units-as-geological-barriers-ntb-24-17/2738-5-10-overall-conclusions-on-key-characteristics-of-the-host-rock-and-confining-units-ntb-24-17

Wermeille, S., & Bossart, P. (1999). *Paleohydrological Study on the Surroundings of the Mont Terri Rock Laboratory* (Issues 99–01).

APPENDIX B: LIST OF OPALINUS CLAY SAMPLES FROM BOREHOLE BPCD-1

Table B.1: List of samples obtained as part of the "PC-D" project for the noble gas characterisation experiments

Sample ID	Drilling Date	Drilling Start	Drilling End	Recovery Time	"Out of Shell" Time	Bagging Time	Depth From (cm)	Depth To (cm)
UO_1_SS	2021/09/07	10:40	10:44	10:54	10:57	11:05	490	525
HI_1_SS*	2021/09/07	10:40	10:44	10:54	10:57	11:05	585	610
BGR_1_SS*	2021/09/07	10:40	10:44	10:54	10:57	11:05	625	640
UO_1_Al	2021/09/07	12:15	12:25	12:38	12:40	12:52	650	670
BGR_2_SS*	2021/09/07	15:11	15:24	15:30	15:34	-	820	830
UO_2_Al	2021/09/07	15:11	15:24	15:30	15:34	-	855	875
UO_2_SS	2021/09/07	15:11	15:24	15:30	15:34	-	875	900
HI_2_SS*	2021/09/07	15:11	15:24	15:30	15:34	-	910	940
UO_3_SS	2021/09/08	09:01	09:08	09:20	09:25	09:30	1160	1190
HI_3_SS*	2021/09/08	09:01	09:08	09:20	09:25	09:30	1210	1240
BGR_3_SS*	2021/09/08	09:01	09:08	09:20	09:25	09:30	1240	1260
UO_3_Al	2021/09/08	11:37	11:43	12:15	12:29	12:26	1390	1420
HI_4_SS*	2021/09/08	11:37	11:43	12:15	12:29	12:26	1480	1510
UO_4_SS	2021/09/08	11:37	11:43	12:15	12:29	12:26	1510	1540
BGR_4_SS*	2021/09/08	11:37	11:43	12:15	12:29	12:26	1560	1580
UO_4_Al	2021/09/08	13:51	13:57	14:32	14:36	14:45	1610	1640
UO_5_SS	2021/09/08	15:08	15:16	15:34	15:39	15:48	1740	1765
BGR_5_SS*	2021/09/08	15:08	15:16	15:34	15:39	15:48	1830	1855
HI_5_SS*	2021/09/08	15:08	15:16	15:34	15:39	15:48	1880	1900
UO_5_Al	2021/09/09	07:58	08:05	08:28	08:32	08:40	1920	1940

Note: Sample containment denoted by suffix at the end of sample ID. Samples contained within the stainless-steel cylinders are denoted by "_SS" suffix, and Al-foil bagged samples denoted by "_Al" suffix. "Out of shell" time refers to the time at which the cores were exposed to atmosphere prior to bagging. BGR and Hydroisotop GmbH samples (marked with a "*") are not investigated as part of this thesis but will be included in the upcoming "PC-D" project technical report.

APPENDIX C: RAW CONCENTRATIONS AND HEADSPACE-NORMALIZED CONCENTRATIONS OF NOBLE GASES WITHIN THE STAINLESS-STEEL CYLINDERS

Table C.1: Isotopic noble gas concentrations (He-Ne-Ar), represented in cm^3STP/cm^3 within the sampled headspace of the stainless-steel cylinder

	^{3}He	±	^{4}He	±	^{20}Ne	±	^{21}Ne	±	^{22}Ne	±	^{36}Ar	±	^{38}Ar	±	^{40}Ar	±
UO_1	4.47E-11	1.96E-12	2.99E-04	8.96E-06	5.13E-07	1.54E-08	1.55E-09	8.25E-11	4.92E-08	1.87E-09	3.06E-06	9.17E-08	5.50E-07	1.71E-08	9.39E-04	2.84E-05
UO_2	3.41E-11	1.69E-12	2.30E-04	6.89E-06	4.12E-07	1.24E-08	1.16E-09	3.97E-11	3.76E-08	1.19E-09	2.84E-06	8.53E-08	4.90E-07	1.58E-08	8.16E-04	2.47E-05
UO_3	3.30E-11	1.51E-12	1.96E-04	5.87E-06	3.94E-07	1.18E-08	1.14E-09	3.84E-11	3.87E-08	1.20E-09	2.75E-06	8.26E-08	5.04E-07	1.54E-08	8.88E-04	2.67E-05
UO_4	3.94E-11	2.28E-12	2.25E-04	6.76E-06	4.74E-07	1.42E-08	1.32E-09	4.71E-11	4.50E-08	1.45E-09	3.20E-06	9.61E-08	5.62E-07	1.77E-08	9.39E-04	2.84E-05
UO_5	2.85E-11	1.19E-12	2.85E-04	8.54E-06	5.58E-07	1.68E-08	1.60E-09	5.97E-11	5.09E-08	1.67E-09	2.70E-06	8.10E-08	4.73E-07	1.50E-08	7.79E-04	2.36E-05
Air	7.34E-12	-	5.24E-06	-	1.65E-05	-	4.87E-08	-	1.68E-06	-	3.14E-05	-	5.90E-06	-	9.30E-03	-
ASW	5.45E-14	-	3.90E-08	-	1.50E-07	-	4.46E-10	-	1.53E-08	-	1.03E-06	-	1.93E-07	-	3.05E-04	-

Table C.2: Isotopic noble gas concentrations (He-Ne-Ar), represented in cm^3STP/cm^3, under the assumption of full core outgassing, and normalized to the headspace volume

	^{3}He	^{4}He	^{20}Ne	^{21}Ne	^{22}Ne	^{36}Ar	^{38}Ar	^{40}Ar
UO_1	1.12E-12	7.49E-06	1.29E-08	3.90E-11	1.23E-09	7.66E-08	1.38E-08	2.35E-05
UO_2	8.55E-13	5.76E-06	1.03E-08	2.90E-11	9.42E-10	7.13E-08	1.23E-08	2.05E-05
UO_3	8.29E-13	4.91E-06	9.88E-09	2.86E-11	9.70E-10	6.90E-08	1.26E-08	2.23E-05
UO_4	9.88E-13	5.65E-06	1.19E-08	3.30E-11	1.13E-09	8.03E-08	1.41E-08	2.35E-05
UO_5	7.14E-13	7.14E-06	1.40E-08	4.01E-11	1.28E-09	6.77E-08	1.19E-08	1.95E-05
Air	2.14E-10	1.53E-04	4.80E-04	1.42E-06	4.90E-05	9.17E-04	1.72E-04	2.71E-01
ASW*	2.20E-15	1.57E-09	6.08E-09	1.80E-11	6.20E-10	4.16E-08	7.82E-09	1.23E-05

Note: All concentrations are at STP conditions. All concentrations here are representative of $C_{headspace}/V_{headspace}$. ASW concentrations (denoted with "*") here represent the concentration within the headspace one would expect if the porewater was at noble gas concentration, then fully degassed into the stainless-steel cylinder headspace. The headspace volume here includes both the stainless-steel cylinder, and attached evacuated copper tube, at length at which tube is crimped for equilibration.

APPENDIX D: RAW CONCENTRATIONS OF NOBLE GASES FROM THE SAMPLED PE/Al-FOIL BAG HEADSPACE

Table D.1: Raw isotopic noble gas concentrations (He-Ne-Ar) obtained from sampling the headspace of the PE/Al-foil bagged samples

	^{3}He	±	^{4}He	±	^{20}Ne	±	^{21}Ne	±	^{22}Ne	±	^{36}Ar	±	^{38}Ar	±	^{40}Ar	±
UO_1	1.18E-11	6.49E-12	1.83E-05	1.01E-05	9.27E-05	9.32E-06	2.73E-07	2.74E-08	9.31E-06	9.36E-07	3.75E-05	6.77E-06	7.04E-06	1.27E-06	1.11E-02	2.00E-03
UO_2	2.02E-11	1.11E-11	5.61E-05	3.09E-05	9.55E-05	9.60E-06	2.81E-07	2.82E-08	9.68E-06	9.73E-07	2.34E-05	4.22E-06	4.49E-06	8.11E-07	7.26E-03	1.31E-03
UO_3	9.15E-12	5.04E-12	4.56E-06	2.51E-06	9.48E-05	9.53E-06	2.78E-07	2.80E-08	9.54E-06	9.59E-07	3.80E-05	6.86E-06	7.11E-06	1.28E-06	1.11E-02	2.00E-03
UO_4	1.13E-11	6.23E-12	6.76E-06	3.72E-06	7.74E-05	7.78E-06	2.29E-07	2.30E-08	7.82E-06	7.86E-07	3.08E-05	5.56E-06	5.96E-06	1.08E-06	9.64E-03	1.74E-03
UO_5	6.47E-11	3.56E-11	3.07E-04	1.69E-04	7.14E-05	7.18E-06	2.10E-07	2.11E-08	7.22E-06	7.26E-07	2.91E-05	5.29E-06	5.58E-06	1.01E-06	9.02E-03	1.63E-03
Air	7.34E-12		5.24E-06		1.65E-05		4.87E-08		1.68E-06		3.14E-05		5.90E-06		9.30E-03	